Summer 2007

Innovative solutions in bridge construction, rehabilitation, and structural health monitoring

Fabio Matta

Department: Civil, Architectural and Environmental Engineering

INNOVATIVE SOLUTIONS IN BRIDGE CONSTRUCTION, REHABILITATION, AND STRUCTURAL HEALTH MONITORING

by

FABIO MATTA

A DISSERTATION

Presented to the Faculty of the Graduate School of the

UNIVERSITY OF MISSOURI-ROLLA

In Partial Fulfillment of the Requirements for the Degree

DOCTOR OF PHILOSOPHY

in

CIVIL ENGINEERING

2007

_____	_____
Dr. Antonio Nanni, Advisor	Dr. Ashraf Ayoub
_____	_____
Dr. Lawrence C. Bank	Dr. Victor Birman
_____	_____
Dr. Lokeswarappa R. Dharani	Dr. Ward N. Marianos, Jr.

PUBLICATION DISSERTATION OPTION

This dissertation has been prepared in the form of a collection of three technical papers that have been submitted for possible publication in archival journals.

The first paper, “Connection of concrete railing post and bridge deck with internal FRP reinforcement,” consisting of pages 12 through 62, was submitted to the ACI Structural Journal.

The second paper, “Externally post-tensioned carbon FRP bar system for deflection control,” consisting of pages 63 through 104, was submitted to Construction and Building Materials (Special Issue on FRP Composites).

The third paper, “Measurement of distributed strain in steel bridge: validation through diagnostic load test,” consisting of pages 105 through 141, was submitted to Structural Health Monitoring.

ABSTRACT

This dissertation includes three technical papers that investigate the development of innovative technologies for bridge construction, rehabilitation, and structural health monitoring, respectively, at different stages of the technology transfer process.

The first paper covers the design and experimental validation of the connection between a railing post and a bridge deck reinforced with fiber reinforced polymer (FRP) bars. Compliance of the connection with mandated strength criteria was demonstrated. The structural response of the railing system was analytically studied, showing that the behavior is consistent with that of crashworthy railings. The design was implemented in an off-system bridge. The second paper introduces a novel system for external post tensioning that uses carbon FRP bars as tendons, and where the anchorages allow attainment of the bar strength. The structural implications of relevant design parameters were analyzed for systems aimed at controlling the deflection of single-span one-way members with arbitrary degree of continuity. The third paper presents the field validation of a distributed strain measurement setup along the steel girders of a continuous highway bridge. The bridge was load tested to assess the performance of a girder that was heat-straightened after falling during erection. It was concluded that the member did not pose serviceability concerns. Distributed measurement proved its potential in overcoming practical and economical limitations of discrete measurement technologies in the field.

The research impact is twofold: first is the introduction of promising innovative technologies in development and implementation projects with the direct involvement of forward-thinking industry partners; second is the demonstration of the validity of these technologies on the basis of a rigorous scientific approach.

ACKNOWLEDGMENTS

I wish to thank my advisor and mentor, Dr. Nanni. For his passion, hard work, and for his uncanny ability to find opportunities and funds for his teams: if I worked so hard, that's also because of the beauty of the projects we've tackled. For his consistency in pinpointing weaknesses when called upon, from which I benefited by improving the quality of my work: I hope to pick such an "efficiency ratio" up someday. I owe a thank you to each of the fine minds who served in my advisory committee: Dr. Ayoub, for fruitful discussions and for serving as lab supervisor; Dr. Birman, for his advice and four brilliant courses; Dr. Dharani, for his true "open-door policy" and two great courses; my friend Dr. Marianos, for his advice and stimulating discussions, and Dr. Bank, of whom I enjoyed the intellectual drive while working together: I hope there will be more. To Jason and Travis: I'm going to miss your cool and skills in the lab and in the field. To many graduate students and visitors, with whom I've shared countless hours in a crowded lab under the patient supervision of Dr. LaBoube, while enjoying the exposure to their ideas, explanations, together with their help and a good time. To Gary, Jeff, Bill, Steve, and Mike for their expert and efficient help with instrumentation and lab equipment. To the CIES ladies Abbie, Cheryl and Gayle, and to Gene and Virginia, for their assistance that made my life easier. I feel fortunate to have worked alongside valuable people outside UMR. Among all: Rich Altice, Glenn Barefoot, Filippo Bastianini, Jim Francka, Doug Gremel, the Hartman crew, Spencer Jones, Ryan Koch, Bruce Nelson, Brian Orr, Tom Ringelstetter, Dan Smith, and the incredible Max Vath. Thanks to all of you. The biggest hug goes to my parents, for their love and support throughout these years of "crazy and most desperate study", as a good italian poet would humbly and vibrantly say.

TABLE OF CONTENTS

Page

PUBLICATION DISSERTATION OPTION iii

ABSTRACT iv

ACKNOWLEDGMENTS v

LIST OF ILLUSTRATIONS x

LIST OF TABLES xiii

SECTION

1. INTRODUCTION 1

    1.1 PROJECT 1: CONSTRUCTION 7

    1.2 PROJECT 2: REHABILITATION 9

    1.3 PROJECT 3: STRUCTURAL HEALTH MONITORING 10

PAPER

1. CONNECTION OF CONCRETE RAILING POST AND BRIDGE DECK WITH INTERNAL FRP REINFORCEMENT 12

    ABSTRACT 12

    INTRODUCTION 14

    RESEARCH OBJECTIVES 17

    EXPERIMENTAL INVESTIGATION 18

        Specimens design 19

        Materials 22

        Test setup and instrumentation 23

    EXPERIMENTAL RESULTS AND DISCUSSION 24

        Structural behavior 24

Analytical modeling of connection response 26

IMPLICATIONS IN STRUCTURAL DESIGN 28

Numerical formulation of post and beam elements 29

Nonlinear finite element analysis of railing 30

IMPACT ON DESIGN GUIDELINES 33

CONCLUSIONS 35

LIST OF SYMBOLS 37

ACKNOWLEDGMENTS 40

REFERENCES 41

2. EXTERNALLY POST-TENSIONED CARBON FRP BAR SYSTEM FOR DEFLECTION CONTROL 64

ABSTRACT 64

INTRODUCTION 66

PRACTICAL SIGNIFICANCE 69

EXTERNALLY POST-TENSIONED CFRP SYSTEM 70

Description 70

Laboratory validation of CFRP bar assembly 73

STRUCTURAL IMPLICATIONS OF EPT SYSTEM CONFIGURATION 73

Structural efficiency and effect of boundary conditions 74

Beam with simple supports 77

Beam with rotational end constraints 77

Post-tensioning forces applied via deviators and selection of bar diameter and number 79

Design of adhesive anchors in concrete 81

SUMMARY 82

LIST OF SYMBOLS 84

ACKNOWLEDGMENTS 87

REFERENCES 88

3. MEASUREMENT OF DISTRIBUTED STRAIN IN STEEL BRIDGE: VALIDATION THROUGH DIAGNOSTIC LOAD TEST 106

ABSTRACT 106

INTRODUCTION 108

BOTDR SENSING PRINCIPLES 111

BRIDGE DESCRIPTION 112

DIAGNOSTIC LOAD TEST 113

Load passes and procedure 113

BOTDR setup 113

ATS setup 115

VALIDATION OF DISTRIBUTED STRAIN MEASUREMENTS 116

STRUCTURAL ASSESSMENT 118

PERFORMANCE OF BOTDR SYSTEM 120

CONCLUSIONS 123

ACKNOWLEDGMENTS 125

REFERENCES 126

SECTION

2. CONCLUSIONS AND RECOMMENDATIONS 143

2.1 BRIDGE CONSTRUCTION 143

2.2 BRIDGE REHABILITATION 145

2.3 BRIDGE STRUCTURAL HEALTH MONITORING 146

APPENDICES

A. MATERIAL AND CONSTRUCTION SPECIFICATIONS FOR GLASS FIBER REINFORCED POLYMER BARS FOR BRIDGE NO. 14802301, GREENE COUNTY, MO 149

B. RAPID CONSTRUCTION OF CONCRETE BRIDGE DECK USING PREFABRICATED FRP REINFORCEMENT 161

C. GEOMETRIC DESIGN OF OPEN-POST RAILING PROFILE FOR BRIDGE NO. 14802301, GREENE COUNTY, MO 174

D. VERIFICATION OF BOUNDARY CONDITIONS OF POST-OVERHANG SUBASSEMBLIES 179

E. GENERALIZED *N*-DOF NONLINEAR FINITE ELEMENT FORMULATION FOR OPEN-POST RAILING SYSTEM 182

F. RAW DATA OF QUASI-STATIC TEST ON POST-DECK CONNECTION SPECIMEN M2 188

G. MODULAR FRAME CONCEPT CART FOR INSPECTION OF SLAB-ON-GIRDER BRIDGE SUPERSTRUCTURE 199

H. RAW DATA FROM DIAGNOSTIC LOAD TEST OF BRIDGE NO. A6358, OSAGE BEACH, MO 216

I. PUBLICATIONS 227

J. PRESENTATIONS 234

BIBLIOGRAPHY 237

VITA 240

LIST OF ILLUSTRATIONS

Figure Page

1.1 General outline of dissertation 6

PAPER 1

1. Prefabricated GFRP stay-in-place deck reinforcement 49
2. Rehabilitation of Bridge No. 14802301 50
3. Reinforcement layout of post-deck connection subassemblies 51
4. Test setup 52
5. Design of Specimen M2 53
6. Flow chart for post-deck connection design controlled by diagonal tension failure at corner 54
7. Load-displacement response 55
8. Close-up of diagonal fracture surface at corner in Specimen M1 56
9. Failure of Specimen M2 57
10. Load-strain response of Specimen M2 58
11. Analytical modeling of horizontal post displacement 59
12. Finite element formulation 60
13. Structural analysis of railing 61
14. Numerical load-displacement response of Bridge No. 1482301 railing 62
15. Design strength of railing at varying opening length L_O 63

PAPER 2

1. Externally post-tensioned CFRP system 94
2. Tensile testing of Ø12.7 mm CFRP bar assembly 95

3. Schematic of single-span member with EPT system 96

4. Schematic of PT force and bending moment components producing maximum uplift 97

5. Efficiency ratio for deflection recovery with respect to D / L_b and a / L for simply supported end condition ($k_\varphi = 0$) 98

6. Effect of boundary conditions and distance of anchors from supports on effective PT moment along L 99

7. Normalized midspan uplift produced by same PT force as function of a / L at different values of rotational stiffness k_φ.....100

8. Efficiency ratio for deflection recovery with respect to D / L_b and a / L for fixed end condition ($k_\varphi = \infty$) 101

9. Plot of PT force applied by engaging deviator as function of D / L_b for different bar diameters 102

10. Ratio ε_{curv} / ε_{fu} as function of radius of curvature of deviator plate in contact with CFRP bar 103

11. Design flowchart for EPT system 104

12. Design of post-installed adhesive anchors in concrete.....105

PAPER 3

1. Schematic of Brillouin frequency shift in FOS subjected to mechanical- or temperature-induced deformation 130

2. Bridge No. A6358 131

3. Diagnostic load test 132

4. Photograph of exterior girder fallen during erection due to high wind..... 133

5. Fiberglass tape with embedded FOSs for strain (S) and temperature (T) measurement.....134

6. BOTDR setup 135

7. ATS setup 136

8. Least squares polynomial fitting of BOTDR curvature profiles along Girder 1, Span 1 at Location I at Passes A, B and D 137

9. Deflection profiles derived from BOTDR measurements and discrete ATS measurements 138

10. Schematic of finite element model of bridge superstructure..... 139

11. Experimental and theoretical strain profiles at Location I along Girder 1, Span 1. 140

12. Experimental and FEA strain profiles along Girder 5..... 141

13. Strain gauge measurements on Girder 2 at Location II..... 142

LIST OF TABLES

Table Page

PAPER 1

1. Reinforcement and flexural capacity of post and deck sections at connection..... 45

2. Properties of GFRP reinforcement..... 46

3. Factored design forces for crash test level TL-2 railing design (AASHTO 2004)..... 47

4. Convergence check of railing FEA for $F_t = \phi R_t$ in load Case A and Case B..... 48

PAPER 2

1. Results of uniaxial tensile tests on Ø12.7 mm CFRP bar assemblies..... 92

2. Dimensional and nondimensional expressions for midspan uplift produced by PT forces and couples in Figure 4 93

SECTION

1. INTRODUCTION

The scientific and technological progress has endowed today's engineers with advanced knowledge base and tools to tackle relevant problems, and improve the well-being of our communities. The utter complexity of a long list of challenges, once portrayed as unsolvable per se, or simply not effectively nor economically treatable, has been and is being turned into successes with sustained frequency.

From the eyes of a civil engineer, the progressive and inevitable deterioration of the transportation infrastructure represents a crucial challenge that still is, at least on a large scale, far from being effectively addressed. Bridges are vital links of this infrastructure, and are with no doubt most sensitive to safety concerns because of the structural and functional deficiencies that accrue from aging and deterioration. Exacerbating factors are the increases in design loads as well as in the levels of traffic, insufficient routine inspection and maintenance, and exposure to aggressive and changing environments. As a result, hundreds of thousands of bridge structures around the world do present safety concerns that the civil engineering community is striving to address.

The engineer who faces a structurally deficient bridge has essentially two alternatives: full or partial reconstruction, which may be required in the worst cases or, when feasible, rehabilitation in the form of either strengthening or repair. The legitimate expectation is that, as a result of the scientific and technological quantum leaps achieved in the very last decades, and in particular in material science, the engineer can enlist a

palette of efficient and modern solutions that respond to the growing demand towards sustainability. That is, from a structural engineering standpoint, innovative materials and technologies would enable to build more durable structures, and to strengthen and repair existing structures while significantly increasing their service life as well as their resiliency to aging and deterioration. Field operations would be faster, easier, and safer. The final product would have a higher quality at a contained or no short-term premium compared with more traditional practices, since budget limitations that affect virtually any country make long-term savings a weak selling point. In addition, the decision making regarding the implementation of such remedies would be based on structural assessment performed with advanced and more effective tools and techniques for health monitoring. The same would hold for inspection and maintenance operations, especially because the substantial increase in traffic on existing life-lines, including bridges, puts a high premium on keeping these facilities in service, and justifies research investments.

On the contrary, the construction industry has been historically slow in assimilating technological innovations, and in turning them into accepted practice for full exploitation. This is the result of a recognized aversion to risk that encompasses primarily owners, engineering firms, and contractors. Two are the fundamental reasons (Nanni 2006): first, the prescriptive nature of design codes and construction specifications, where the objective of ensuring safety as well as open tender processes make incentives to innovation unattractive, if not inconvenient; second, the fee basis on which procurement relies, where profits typically arise from efficient project management and financing, and any financial risks associated with innovation become impractical without incentives. This premise inevitably translates into a lack of research

investments, possibly with the exception of material suppliers, and into a disconnect between researchers and practitioners that constitutes a formidable barrier to innovation.

In this scenario, civil engineering research has the fundamental role of driving innovation through traditional R&D activities, and by truly reaching out and pursuing interaction with industry and owners through systematic technology transfer. Investing research resources (time, funds, scholarship, creativity) is key to disseminate an understanding of the opportunities behind what is perceived essentially as risk, and to increase the familiarity of owners, contractors and designers with advanced technologies that are promising or mature for implementation. Representative examples of this philosophy are offered by the transition from research and development to practice of fiber reinforced polymer (FRP) material systems in a number of applications. The versatility of advanced composites emerges from the unique combination of corrosion resistance, light weight, tailorability of the mechanical properties (Kaw 1997), and compatibility with relatively low-cost applications that belong to the construction sector.

For instance, the use of externally bonded fiber reinforced polymer (FRP) systems for the rehabilitation of reinforced concrete (RC) and prestressed concrete structures (Nanni 1997, Teng et al. 2002) has become a common and frequent practice in about 20 years from the early implementations conducted in Europe (Meier 1987) and Japan (Katsumata et al. 1988). Despite long-term durability needs to be further investigated, and despite of the lack of codes of practice, the rapid (for the construction sector) acceptance of this technology for strengthening, repair, and retrofitting, was prompted by its speed, ease, structural effectiveness and low-cost. In addition, the process was expedited by the introduction of in-situ load testing for validation purposes (Nanni 2006).

Another example that may become a major case study in the future is the use of internal FRP reinforcement in concrete bridge decks in lieu of steel bars (Bradberry 2001, Nanni and Faza 2002). The non-corrosive properties of FRP reinforcement respond to the pressing need of constructing bridges without the risk of premature deterioration from exposure to deicing salts, which are routinely used in cold regions, or harsh environments, such as in coastal regions. Design principles are well established (Nanni 2003, Bank 2006), and guideline documents have been published in North America, Europe, and Japan. A number of field implementations, typically as parts of research projects, have demonstrated the validity of the technology when deformed FRP bars are used (Phelan et al. 2003, Benmokrane et al. 2004, 2006, Mufti et al. 2007). In addition, the lack of ductility of FRP bars in tension is not a primary concern, since flexural failure does not usually govern. While in the United States of America the American Concrete Institute (ACI) Committee 440 has recently published updated design guidelines (ACI 2006), and is currently balloting two documents written in mandatory language that address material and construction specifications, the use of FRP bars in Canada has been codified in Section 16 of the Canadian Highway Bridge Design Code (CAN/CSA 2006). As a result, transition from government-subsidized research projects to actual commercialization is decidedly accelerating, and valuable experience has been already gained by demonstrating the viability of construction management practices where FRP bars are adopted using traditional bid letting processes and competitive bidding from multiple suppliers.

The use of internal FRP reinforcement for concrete stands at the core of the first of three technical papers that constitute the main body of this dissertation, which emerges

from three projects where the development of innovative solutions for bridge construction, rehabilitation, and structural health monitoring, respectively, was investigated at different stages of the technology transfer process. The outline of the dissertation is illustrated in Figure 1.1.

A background binder of this paper-based dissertation is represented by the strict interdependencies between construction or rehabilitation solutions and structural health monitoring for bridge assessment, within the framework of the development and maintenance of a safe and efficient transportation infrastructure. More importantly, from a research standpoint, the significance and originality of this work as a whole reside: first, in the introduction of innovative technologies in each of the aforementioned and closely related fields into development and implementation projects, and with the direct involvement of forward-thinking and naturally business-oriented industry partners; second, in the demonstration of the potential of these technologies on the basis of a rigorous scientific approach, which remains instrumental to a successful transition from the laboratory to the field.

Specific conclusions are reported in each technical paper, including experimental and theoretical results and their implications, as well as design methodologies and recommendations for implementation in design guidelines and codes of practice. The research efforts that are presented herein also enabled to formulate a number of questions that were either partially or not addressed, and to identify further research needs. The final Section of this dissertation summarizes the key conclusions as well as the questions that emerged and that should be addressed. In addition, relevant information that complement the main body of this dissertation are provided in the Appendices, along

with two pertinent papers published in the proceedings of international conferences, and raw data from laboratory testing in PAPER 1, and field testing in PAPER 3.

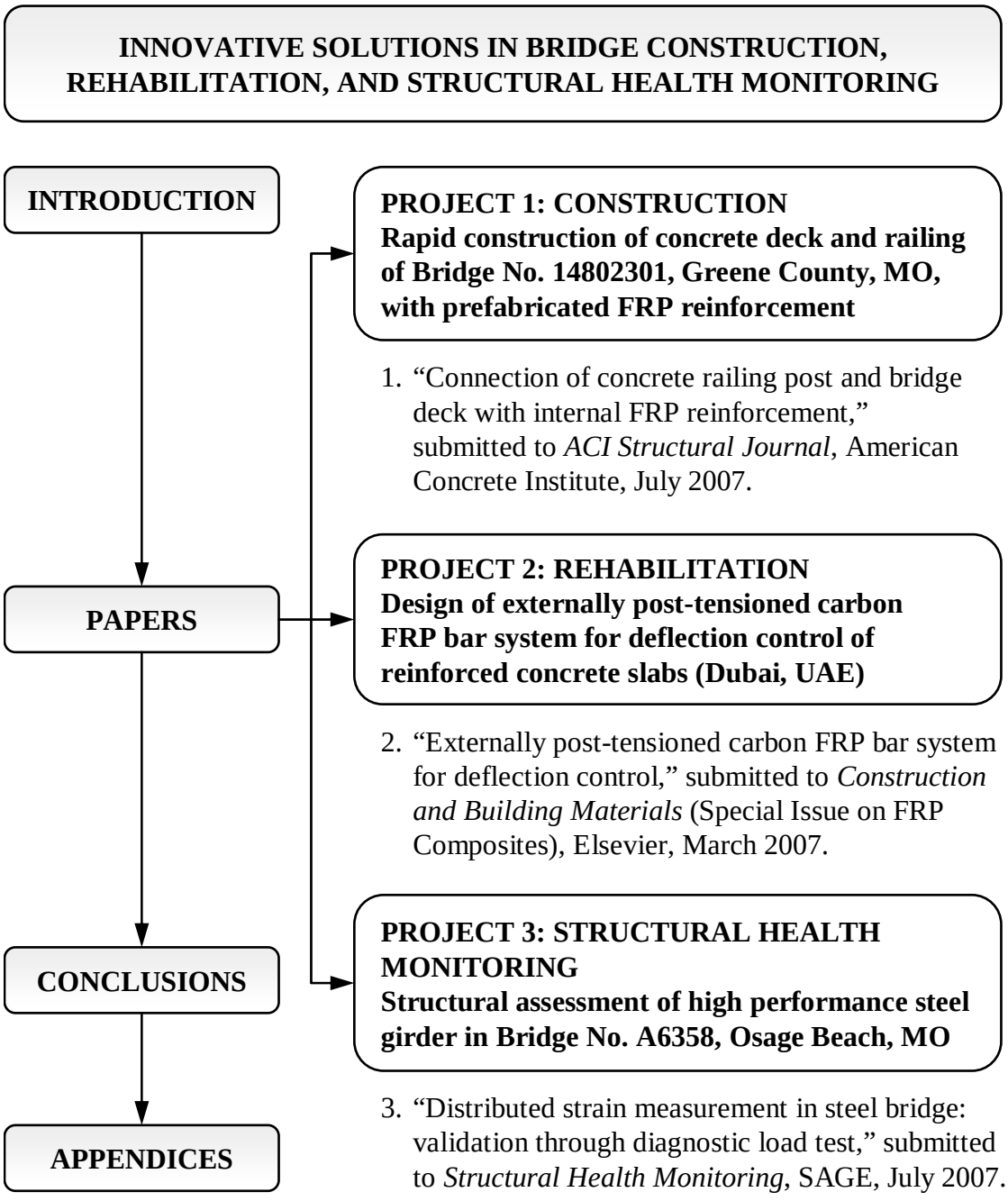

Figure 1.1 – General outline of dissertation.

1.1. PROJECT 1: CONSTRUCTION

The first paper of this dissertation is titled "CONNECTION OF CONCRETE RAILING POST AND BRIDGE DECK WITH INTERNAL FRP REINFORCEMENT," and originates from Project 1. The project was funded by the US Department of Transportation and the University Transportation Center on Advanced Materials and Non-destructive Testing Technologies, and culminated with the accelerated construction of the FRP RC deck and railing of Bridge No. 14802301 in Greene County, Missouri.

The project unfolded in two main stages: first, the development and experimental validation of novel prefabricated glass FRP reinforcement systems for the concrete deck, where a three dimensional pultruded grating was used (Matta et al. 2005, Ringelstetter et al. 2006), and for the open-post railing (Matta and Nanni 2006), where pultruded deformed bars were used; second, the field implementation (Matta et al. 2006). The concepts introduced, which combine the durability of FRP reinforcement with the rapidity and ease of installation of prefabricated systems, and the successful conduction of the project earned the University of Missouri-Rolla recognition as the runner-up for the 2006 C. J. Pankow Award for Innovation by the American Society of Civil Engineers (ASCE) and the Civil Engineering Research Foundation (CERF), together with its partners in the academia (University of Wisconsin-Madison), local and state administration (Greene County Highway Department, MoDOT), and industry, including manufacturers (Strongwell Corp., Hughes Brothers, Inc.), a designer firm (Great River Engineering of Springfield, Inc.) and a contractor (Hartman Construction Co.).

PAPER 1 presented herein focuses on the design and validation of the post-deck connection of the open-post concrete railing, which was the solution preferred by the

owner. Typically, design is based on empirical considerations and analogy with existing systems, preferably those that have been crash tested following the criteria of the NCHRP 350 Report (Ross et al. 1993). In the present case, the Standard Specifications by the American Association of State Highway and Transportation Officials (AASHTO 2002), which were used to design the bridge, required the connection to resist a specified transverse load. The solution implemented was designed to meet the strength requirement on the basis of structural analysis that addresses two relevant aspects. First, the fact that the connection constitutes a discontinuity region where the flexural capacity of the weaker section may not be reached. Yet, the design may be retained due to constructability and cost considerations, provided that the strength is adequate. Second, FRP reinforcement was used instead of steel, which required the design to follow applicable guidelines (ACI 2006). In addition, geometrical compliance between the reinforcement and the deck reinforcing grating had to be ensured in a manner consistent from a constructability standpoint. The design was validated through quasi-static testing of two full-scale post-deck overhang subassemblies.

The second part of the paper aims at analyzing whether the structural response of the railing system, that is, not merely at the component level, had the characteristics of resistance and negligible displacements typical of crashworthy railings (Buth et al. 2003, Jiang et al. 2004, Polivka et al. 2004). The problem was solved by modeling the nonlinear load-displacement response of the connection and the beam elements, and by incorporating them into the nonlinear finite element analysis of the selected post-and-beam frame system. The applied load was simulated by means of the specified equivalent static loads prescribed in the AASHTO LRFD Bridge Design Specifications

(AASHTO 2004), which will soon have to be followed to design new bridges financed with Federal funds.

1.2. PROJECT 2: REHABILITATION

The second paper of this dissertation is titled “EXTERNALLY POST-TENSIONED CARBON FRP BAR SYSTEM FOR DEFLECTION CONTROL,” and originates from Project 2. The project was aimed at developing a corrosion-resistant solution capable of recovering short-term deflection and reducing the long-term deflection of a number of large-size RC slabs in a high-rise building in Dubai, United Arab Emirates. The milestones included: development and validation of a novel carbon FRP (CFRP) bar system for external post-tensioning, in collaboration with Hughes Brothers, Inc.; design of a solution for implementation; and field trial thereof on-site.

In the first part of PAPER 2 presented herein, the CFRP system is introduced. The components and their functioning are described, and the constructability characteristics are illustrated, drawing from installation procedures that do not involve time-consuming operations, nor use of specialized equipment operated by specially trained personnel. The challenge in the use of CFRP tendons is in the development of anchor systems that allow the exploitation of the high tensile strength of the material, typically in excess of 260 ksi (1800 MPa). Tensile tests on tendon-anchor assemblies demonstrated that the CFRP system met this challenge.

In the second part of the paper, the structural implications of relevant geometric and mechanical parameters for the design and analysis of externally post-tensioned systems aimed at controlling the deflection of single-span, one-way members, were

analyzed. The objective was to gain a rational understanding of the influence of system configuration (for example, straight or profiled tendons), geometry, and boundary conditions (for example, degree of rotational constraint), irrespectively of the material used. A procedure for the design of "king-post" systems (that is, with symmetric profiled tendons and a single deviator at midspan) using the proposed CFRP bar-anchor solution was finally presented.

1.3. PROJECT 3: STRUCTURAL HEALTH MONITORING

The third paper of this dissertation is titled "MEASUREMENT OF DISTRIBUTED STRAIN IN STEEL BRIDGE: VALIDATION THROUGH DIAGNOSTIC LOAD TEST," and originates from Project 3. The project was aimed at assessing the structural response of a high performance steel (HPS) highway bridge (No. A6358 in Osage Beach, Missouri) under extreme service loads, which were simulated by means of a diagnostic load test. Focus was on one of the exterior girders that collapsed during erection due to high wind, and was heat-straightened before repositioning.

The project offered a dual opportunity in implementing a fiber optic distributed strain measurement technique under development (Komatsu 2002). First, to validate a distributed strain measurement setup based on spontaneous Brillouin scattering (Brillouin 1922) in the field, thereby allowing to advance the validation process of a technique whose potential on flexural members had been investigated through scaled laboratory experiments only. Second, and following validation, to study the girder response along the entire monitored length in the form of continuous strain profiles, thus overcoming the inherent limitations of discrete measurement techniques. In perspective, such capability

would become valuable in a number of applications: in bridge engineering, the first example that may come to mind is the identification and monitoring of fatigue cracks along tensile and flexural steel members.

PAPER 3 of this dissertation first presents the validation of the measured strains. The strain profiles were converted into deflection profiles, and compared with benchmark measurements performed with a high-precision total station system that is extensively used in practice.

In the second part of the paper, the structural response of the girder is assessed with respect to strain profiles from three-dimensional finite element analysis as may be used for design purposes, and to the limit strain levels mandated by the design specifications used for the bridge (MoDOT 2002), which replicate those of the AASHTO Standard Specifications (AASHTO 2002).

Finally, the performance of the distributed strain measurement setup is discussed.

PAPER 1

CONNECTION OF CONCRETE RAILING POST AND BRIDGE DECK WITH INTERNAL FRP REINFORCEMENT

Fabio Matta[a,*], and Antonio Nanni[b]

[a] Center for Infrastructure Engineering Studies, University of Missouri-Rolla

[b] Dept. of Civil, Architectural and Environmental Engineering, University of Miami

ABSTRACT

The use of fiber reinforced polymer (FRP) reinforcement is a practical alternative to conventional steel bars in concrete bridge decks and safety appurtenances, as it eliminates corrosion of the steel reinforcement. Due to their tailorability and light weight, FRP materials also lend themselves to the development of prefabricated systems that improve constructability and speed of installation. These advantages have been demonstrated in the construction of an off-system bridge, where prefabricated cages of glass FRP bars were used for the open-post railings. This paper presents the results of full-scale static tests on two candidate post-deck connections to assess compliance with specification mandated strength criteria at the component (connection) level. Strength and stiffness

* Graduate Research Assistant. Corresponding author – 220 Engineering Research Laboratory, 1870 Miner Circle, 65409-0710 Rolla, MO, USA. Tel +1 (573) 341-6661, Fax -6215, E-mail: *mattaf@umr.edu*.

until failure are shown to be accurately predictable, which enabled to study structural adequacy at the system (post-and-beam) level under equivalent static load by numerically modeling the nonlinear behavior of the railing, on the basis of well established structural analysis principles of FRP reinforced concrete.

Keywords: Bridge deck; Design; Fiber-reinforced polymer reinforcement; Railing.

INTRODUCTION

The use of fiber reinforced polymer (FRP) reinforcement ideally eliminates the issue of corrosion of concrete bridge decks, which accrues from exposure to deicing salts and harsh environments and affects a large portion of the bridge inventory worldwide. Glass FRP (GFRP) bars are more economical than carbon FRP bars and are a practical alternative to steel reinforcement for non-prestressed bridge decks (Bradberry 2001, Nanni and Faza 2002). A number of field implementations, typically as parts of research projects conducted in North America, have demonstrated the validity of the technology (Phelan *et al.* 2003, Benmokrane *et al.* 2004, 2006). In addition, recent findings from tests performed on concrete cores containing portions of GFRP bars, which were removed from four bridges and a wharf that had operated from 5 to 8 years under aggressive environments, revealed that no degradation occurred upon frequent exposure to wet and dry and freezing and thawing cycles, chlorides from deicing salts or salt water, and concrete alkaline environment (Mufti *et al.* 2007). The demand is strong from the construction industry and practitioners to exploit this technology by developing material and construction specifications, as well as limit-state based design specifications, such as those incorporated in the Canadian Highway Bridge Design Code (CAN/CSA 2006).

Degradation also affects reinforced concrete (RC) railings, and in particular their connection to bridge decks, and may compromise crashworthiness. The development and validation of corrosion-free railings and post connections to FRP RC decks have been addressed in very few research efforts that followed the pioneering development of the hybrid steel-GFRP RC Ontario Bridge Barrier, where carbon FRP grids were used as

flexural reinforcement in the deck and barrier wall, along with stainless steel double-headed tension bars to provide a good anchorage (Maheu and Bakht 1994). The performance of connections between a steel RC barrier and a deck overhang reinforced with GFRP bars in the top mat was investigated through pendulum impact tests on full-scale subassemblies (Trejo *et al.* 2001). The hybrid steel-GFRP specimens attained a maximum load between 3% and 16% smaller than the steel RC counterparts, with larger deformations. Based on the fact that in either configuration the barrier remained attached to the deck without displaying any sign of further movement or instability while inspected, it was concluded that the hybrid configuration granted adequate performance for implementation. In another experimental research (Deitz *et al.* 2004), GFRP, steel and hybrid (that is, having GFRP and steel bars in the top and bottom mat, respectively) RC overhang subassemblies cast with steel RC New Jersey barrier walls were subjected to transverse static loading. All connections met the AASHTO Standard Specifications (AASHTO 2002) criteria, which require the connection to resist a load of 10 kip (44.5 kN) applied at the top of the continuous barrier.

A comprehensive investigation was undertaken to study the behavior of concrete bridge barriers internally reinforced with GFRP bars under static and pendulum impact loads (El-Salakawy *et al.* 2003). The results of full-scale testing, where the GFRP RC subassemblies were designed on a strength equivalency basis with their steel RC counterparts, showed similar behavior at failure, and the former were approved by the Ministry of Transportation of Québec for use in construction. The crashworthiness of an open-post railing internally reinforced with GFRP bars, which was developed for use in

highway bridges, was assessed through two crash tests (Buth *et al.* 2003) as per the NCHRP Report 350 Test Level 3 (TL-3) criteria (Ross *et al.* 1993). The test demanded a 4500 lb pickup truck to impact the railing at a speed of 60 mph and at an angle of 25° with respect to the roadway direction, as typically required on the National Highway System (Mak and Bligh 2002). The first test was failed due to vehicle rollover, which was attributed to the insufficient height of the railing. The second, successful test was performed on a railing having a steel tube bolted on top to increase the height from 27 in. (686 mm) to 30 in. (762 mm). In both cases, the structural performance was acceptable since the railing withstood the impact load, while negligible deflections were reported (Buth *et al.* 2003).

The use of prefabricated GFRP reinforcement was implemented in the reconstruction of the deck and open-post railings of a severely degraded off-system bridge (No. 14802301) in Greene County, Missouri, USA (Matta *et al.* 2006). Prefabricated, light-weight GFRP bar cages were designed for the railings following the ACI 440.1R-03 guidelines (ACI 2003) and the AASHTO Standard Specifications (AASHTO 2002), which were used to design the bridge. The bar cages were used in combination with a deck reinforcement grating made of smooth pultruded profiles, where the load transfer mechanism is produced by mechanically constraining the core concrete rather than bond, and is not explicitly covered in the ACI guidelines (ACI 2003, 2006).

Design principles for FRP RC are well established and reflect the different philosophy with respect to traditional steel RC design (Nanni 1993, 2003), which stems from the

peculiar physical and mechanical properties of FRP materials. The most relevant are the brittle behavior in tension in the fiber (axial) direction, which make over-reinforced sections more desirable; the smaller axial stiffness than steel, which results in greater deflections and crack widths, and in shear design that accounts for reduced aggregate interlock and concrete strength contribution; and the reduced transverse strength and stiffness of the bars, where the properties are resin dominated.

Understanding the structural implications of designing FRP RC deck and railing systems is instrumental to rationally develop safety appurtenances or crash test specimens and, in perspective, to economically screen candidate systems for the assessment of structural and functional performance by means of advanced numerical tools (Bligh *et al.* 2004), with the overarching objective of efficiently validating more durable solutions for implementation.

RESEARCH OBJECTIVES

This research had two objectives. First, to select a GFRP RC post-deck connection design for Bridge No. 14802301 by proof testing two full-scale overhang subassemblies, and assess compliance with specification mandated strength requirements at the component (rail beam and post-deck connection) level (AASHTO 2002). Second, to analytically model the connection response under static loading, and incorporate it into the nonlinear analysis of the railing to verify the strength and stiffness response at the system (post-and-beam) level under equivalent static load, pursuant to the approach of Section 13 (Railings) of the AASHTO LRFD design specifications (AASHTO 2004).

EXPERIMENTAL INVESTIGATION

Two full-scale post-overhang subassemblies were tested under quasi-static loading as part of a research program aimed at developing and implementing a steel-free concrete deck and railing system for the accelerated construction of an off-system bridge (Matta *et al.* 2006).

Large size stay-in-place (SIP) panels with an integrated double-layer grating fabricated from GFRP pultruded I-bars and cross rods were used as the deck reinforcement (Figure 1). GFRP bar cages were used for the open-post railings, producing a GFRP RC version of the required Modified Kansas Corral Rail (MKCR). Open-post railings are constructed by cast-in-place of a continuous rail beam on top of suitably spaced posts, and are often preferred due to aestethics and efficient drainage, along with the stiffness, inertial properties, and low-cost maintenance typical of concrete railings.

Figure 2(a) and Figure 2(b) show the new reinforcement prior to casting and the finished railing, respectively. The original MKCR profile, which performed adequately under crash testing by preventing vehicle snagging and rollover, was improved by increasing the height of the rail beam from 14 in. (356 mm) to 17 in. (432 mm), for a total height of 30 in. (762 mm), to further reduce the risk of rollover (Matta and Nanni 2006). In addition, the original width of intermediate posts and openings L_P and L_O of 3 ft (0.9 m) and 7 ft (2.1 m), respectively, was changed into 4 ft (1.2 m) for both [Figure 2(b)] to be geometrically compatibile with the 8 ft (2.4 m) long SIP panels.

Specimens design

The geometry and reinforcement layout of the post-deck connection in Specimens M1 and M2 are detailed in Figure 3(a) and Figure 3(b), respectively. The latter was implemented in Bridge No. 14802301. Both configurations use two layers of bent No. 5 (16 mm) GFRP bars to connect the post to the 8 ft (2.4 m) by 8 ft (2.4 m), 7 in. (178 mm) thick concrete slab, whose 3 ft (0.9 m) overhang shown in Figure 4 replicates that of the bridge. The slab dimensions and boundary conditions were selected as representative of the continuous deck structure. The posts were cast three days after the slab.

Specimen M1 was designed following ACI 440.1R-03 (ACI 2003) with three main objectives. First, to provide a nominal moment capacity of the 4 ft (1.2 m) by 10 in. (254 mm) post section equal to or greater than that of the steel RC MKCR, which is about 150.0 kip-ft (203.4 kN-m). Second, to provide a nominal moment capacity of the deck section at the connection similar to that away from the connection, where the SIP reinforcement satisfies the AASHTO strength requirements (AASHTO 2002). It should be noted that the two exterior longitudinal cross rods on the top grating layer underneath the post were removed to allow insertion of the post bar cages: since the forces are transferred into the smooth I-bars by mechanically constraining the core concrete between the cross rods, the contribution thereof were neglected in design. The third objective was to provide a reinforcement layout geometrically compatible with the deck grating. Table 1 summarizes the flexural capacity of the 4 ft (1.2 m) wide post and deck section at the connection (GFRP bars only) and away from the connection (I-bars only). The design goals were met by using concrete with a nominal compressive strength f'_c of

6000 psi (41.4 MPa). An enviromental reduction factor C_E of 0.7 was applied to the guaranteed tensile strength f^*_{fu} of the GFRP reinforcement to determine the design value. The post-deck construction joint was prepared by providing a dry and roughened surface prior to casting the post.

Design of safety barriers and their connections based on empirical or analogy considerations such as for Specimen M1 is common and often effective. In fact, until the late 1980's when crash testing for highway safety appurtenances were not mandatory, systems successfully crash tested could be used even without meeting geometry and static strength criteria. A rigorous procedure was followed for the structural design of Specimen M2 to resist the required 10 kip (44.5 kN) transverse load applied at the mid-height of the 17 in. (432 mm) high rail beam face (AASHTO 2002). Concrete with compressive strength of 4000 psi (27.6 MPa) was assumed, as typically used in steel RC MKCRs. Failure may occur due to concrete crushing or FRP reinforcement rupture in flexure at the weakest connected section, insufficient anchorage of the post or development length of the deck reinforcement, or diagonal tension cracking at the corner. In the last three cases, the design fails to fully utilize the reinforcement, and may yet be retained due to constructability and cost considerations, provided that the strength requirements are met.

The design in Figure 3(b) requires a check against diagonal tension failure at the corner. For readability, all symbols are reported in the List of Symbols, while only key symbols are defined in the text. The transverse load F_p applied to the post produces a compression

force C_p in the post, which is transferred to the deck via formation of a diagonal compression strut of length l_{dc}. In addition, the shear force F_p is transferred to the deck as an axial force $-F_p$ and a bending moment $0.5F_pt_d$, which adds to F_pH_e to produce the resultant moment in the deck M_d that generates the force couple C_d (compression force) and $F_{f,d}$ (tension force along the GFRP reinforcement), as detailed in Figure 5(a) and Figure 5(b). Diagonal cracking may occur prior to flexural failure in the deck as the concrete modulus of rupture f_r is reached along the diagonal strut, thus disabling the main load transfer mechanism.

The accuracy of analytical results based on the theory of elasticity, where a parabolic distribution of the tensile stress along the diagonal crack length l_{dc} is assumed, has been demonstrated with respect to experimental results (Nilsson and Losberg 1976). The original closed-form procedure was herein modified and rendered in an iterative fashion to explicitly account for the effect of the shear force F_p in addition to the bending moment M_d, and is summarized in the flow chart in Figure 6. The tensile force T acting perpendicular to the diagonal strut is computed neglecting any strength contribution of the slab portions adjacent to the connection, and assuming $f_r = 7.5\sqrt{f_c'}$ (psi) [$0.623\sqrt{f_c'}$ (MPa)] (ACI 2005). Figure 5(c) shows the free body diagram of the corner in Specimen M2 with the resultant internal forces. Convergence is achieved for a nominal strength $F_{n,p}$ of 11.9 kip (52.8 kN) at 30% of the nominal flexural capacity of the deck section in Table 1. The design strength is computed as $\phi_{dt}F_{n,p}$ = 10.1 kip (44.9 kN) by assuming a reduction factor for diagonal tension ϕ_{dt} = 0.85, thus meeting the minimum 10 kip (44.5 kN) requirement (AASHTO 2002). A shear key was included at the

construction jont, and pockets were cut from the deck grating to simplify installation of the bar cages.

AASHTO (2002) also requires that the rail beam be designed for a moment due to concentrated load of 10 kip (44.5 kN) at the mid section of the opening of 10 kip × [L_O (ft) / 6] = 6.7 kip-ft (9.0 kN-m) using a 4 ft (1.2 m) opening length L_O. The beam design includes three No. 5 (16 mm) tension bars per side [Figure 3(b)] with effective depth d of 10.2 in. (259 mm), thus providing a nominal and design moment capacity $M_{n,b}$ and $\phi_f M_{n,b}$ of 52.0 kip-ft (70.5 kN-m) and 26.0 kip-ft (35.2 kN-m), respectively. The shear reinforcement consists of No. 4 (13 mm) double-C GFRP stirrups spaced at 4 in. (102 mm) on-center, which provide a design shear strength of 25.1 kip (111.6 kN). The beam design allows to withstand the maximum moment produced by the design load, and to transfer it to the adjacent posts.

Materials

The reinforcement cages of the connection were constructed with pultruded E-glass/vinyl ester GFRP bars. The tensile properties are reported in Table 2, along with those of the I-bars in the deck reinforcement. Normal weight concrete was used, with maximum aggregate size of 3/8 in. (9.5 mm). Six 6 in. (152 mm) by 12 in. (305 mm) cylinders were tested for each casting in accordance with ASTM C 39. Average compressive strength f'_c and standard deviation for Specimen M1 were 7796 psi (53.7 MPa) and 619 psi (4.3 MPa) in the slab, and 5846 psi (40.3 MPa) and 248 psi (1.7 MPa) in the post, respectively. The values for Specimen M2 were 4975 psi (34.3 MPa) and 271 psi (1.9

MPa) in the slab, and 8422 psi (58.1 MPa) and 110 psi (0.8 MPa) in the post, respectively.

Test setup and instrumentation

The test setup is detailed in the schematic in Figure 5(a) and in the photograph in Figure 5(b). The slab was supported on 10 ft (3.0 m) long steel beams and tightened to the laboratory strong floor using two rows of three 1.0 in. (25 mm) steel threaded rods each spaced at 3 ft (0.9 m) on-center. The load was applied at a height of 24 in. (610 mm) from the slab surface using a steel double-C spreader beam, which was engaged by a steel plate and threaded rod assembly that connected via a steel coupler to the hinged fitted-end of a manually operated hydraulic jack.

The load was measured with a 25 kip (111.2 kN) load cell. Direct current voltage transformer (DCVT) and draw-wire sensors were used to measure: horizontal displacements at the top of the post and at the base, to check for slip at the post-deck interface; vertical displacements at the slab edge at the connection and at the tie-downs; and in-plane slab displacements. Inclinometers were mounted at the connection area and on top of the post to measure absolute and differential rotations. Linear potentiometers were used to check vertical and horizontal crack openings at the post-deck interface. Several 0.2 in. (5 mm) and 2.4 in. (60 mm) electrical-resistance strain gauges were used to measure strains in the FRP reinforcement in the connection and in the concrete at the base of the post. Measurements were taken continuously at a frequency of 5 Hz.

EXPERIMENTAL RESULTS AND DISCUSSION

Structural behavior

The horizontal displacement measured at the mid section on top of the post in Specimens M1 and M2 is plotted with respect to the applied load in Figure 7(a) and Figure 7(b), respectively. The dark dashed lines mark the strength requirement for the connections (AASHTO 2002) scaled from 10 kip (44.5 kN) to 9.0 kip (39.8 kN) to account for the height of the applied load line H_e increased from 21.5 in. (546 mm) to 24 in. (610 mm). The grey continuous and dashed lines mark the nominal and design load, respectively, as per analysis according to the procedure in Figure 6 that accounted for the experimental concrete compressive strength.

Linear response of Specimen M1 was recorded until cracking of the deck underneath the post and at the cold joint interface developed between 7.6 kip (33.8 kN) and 10.2 kip (45.4 kN), with a marked decrease in stiffness [Figure 7(a)] accompanied by increasing crack widths. Following, hairline cracks were observed in the slab between the post and the first tie-down line, which did not affect the overall stiffness. At a load of 13.3 kip (59.4 kN) and horizontal displacement of 0.9 in. (22 mm), a net stiffness loss could be observed that was likely triggered by the loss of bond of the smooth I-bars in the top layer of the deck grating, with strain readings in the deck and the post well below that associated with flexural failure. An internal load transfer mechanism developed that allowed the connection carry additional load up to 15.0 kip (66.7 kN) under very large deformations. Diagonal failure at the corner joint was accompanied by a drop in strain in the concrete at the base of the post and in the GFRP tension bars in the deck after

attaining a maximum measurement of –939 με and 756 με, respectively, again well below the analytical levels compatible with flexural failure controlled by concrete crushing. Figure 8 shows the diagonal crack underneath the post as well as the interlaminar shear in the I-bars, which indicates that the deck reinforcement contributed to the resisting mechanism either via bond or constraining action of the surrounding concrete. No slip was measured at the cold joint. The corner crack did not extend into the post that remained attached to the deck, and could be inspected without showing signs of instability. The transverse strength exceeded the required scaled level as well as the theoretical nominal value, which may be partially attributed to the contribution of the deck I-bars in the load-resisting mechanism.

In Specimen M2, deck and post-deck interface cracking developed between 6.2 kip (27.5 kN) and 7.5 kip (33.4 kN) and was accompanied by a marked reduction in stiffness similar to Specimen M1, as seen in Figure 7(b), and increasing crack widths. Following, hairline cracks developed in the slab as shown in Figure 9(a) without affecting the overall stiffness, until failure occurred at a load of 12.3 kip (54.7 kN). The value is in good agreement with the analytical prediction of 12.2 kip (54.1 kN), and meets the AASHTO (2002) requirements. Figure 9(b) shows a closeup of the diagonal fracture surface at the connection extending into the post behind the bent bars, likely driven by the shear key. No slip was measured at the construction joint. The maximum horizontal displacement and rotation at the top of the post were 0.6 in. (16 mm) and 1.1°, respectively. Figure 10(a) shows the location of the strain gauges in a typical section of Specimen M2. The diagonal crack occurred at a concrete strain at the base of the post of –119 με as shown in

Figure 10(b), again far below that attributable to flexural failure of the over-reinforced section. The tensile strain *t1* measured in two bars at a section close to the diagonal strut is also plotted with respect to the load in Figure 10(b). It can be seen that the theoretical limit of 2265 με associated with a net tensile force $F_{f,d} + 0.5F_p$ = 71.3 kip (317.1 kN) from Figure 5(c), thus significantly smaller than the ultimate value of 1.6%, was not exceeded. The post remained attached to the slab and could still carry load up to 6.3 kip (28.1 kN) while undergoing large deformations, in excess of the 6 in. (152 mm) stroke of the actuator.

Both designs did not allow to fully exploit the flexural strength of the FRP RC deck section. The design of Specimen M2 was retained, since: the reinforcement layout was believed to offer constructability advantages; the code requirements could be met while using nominal 4000 psi concrete typically used for bridge decks and railings; transverse strength could be accurately predicted; after failure, the connection did not separate and could still withstand load.

Analytical modeling of connection response

The maximum horizontal displacement at the top of the post with respect to the applied load, $u(F_p)$, can be approximated as the sum of two contributions, namely: that from the rigid body motion due to the rotation θ_d of the overhang subjected to a moment M_d / L_P per unit width; and that from the post cantilever subjected to a transverse load F_p / L_P per unit width applied at a height H_e from the slab surface. The two contributions are illustrated in Figure 11(a) and Figure 11(b), respectively, where a slab strip of width L_P is used for convenience.

Therefore, the displacement function can be expressed on the basis of simple structural analysis in the form

$$u\left(F_p\right) = H \sin\theta_d + u_p \cos\theta_d , \tag{1}$$

where the overhang rotation is computed as

$$\theta_d\left(F_p\right) = F_p\left(H_e + \frac{t_d}{2}\right)\frac{l_{overhang}}{E_c I_d} \tag{2}$$

and the horizontal displacement u_p from cantilever response is

$$u_p\left(F_p\right) = \frac{F_p H_e^3}{3E_c I_p}\left[1 + \frac{3}{2}\left(\frac{H}{H_e} - 1\right)\right]. \tag{3}$$

The nonlinear behavior of the overhang is rendered by replacing the gross moment of inertia with the effective moment of inertia of the connected section as the bending moment M_d exceeds the cracking level M_{cr}. The format of the modified Branson's equation in the current ACI 440 guidelines (ACI 2006)

$$I_d\left(M_d\right) = \left(\frac{M_{cr}}{M_d}\right)^3 \beta_d I_g + \left[1 - \left(\frac{M_{cr}}{M_d}\right)^3\right] I_{cr} \le I_g \tag{4}$$

is adopted, while replacing the reduction coefficient

$$\beta_d = \left(1.5\frac{\rho_f}{\rho_{fb}}\right) \tag{5a}$$

with

$$\beta_d = \left(3.3\frac{I_{cr}}{I_g}\right) \tag{5b}$$

to account for the reduced tension stiffening in FRP RC, and provide a more accurate and conservative estimate (Bischoff 2007). Cracking in the slab at the connection is assumed

to occur concurrently with that at the cold joint between post and slab, as confirmed by the experiments. The gross moment of inertia of the post section is then replaced in Equation 3 with the cracked moment of inertia. A concrete elastic modulus $E_c = 57\sqrt{f_c'}$ (ksi) [$4733\sqrt{f_c'}$ (MPa)] is assumed in the calculations (ACI 2005).

The displacement function in Equation 1 is plotted for Specimens M1 and M2 in Figure 7(a) and Figure 7(b), respectively. Both the strength and stiffness response of Specimen M2 selected for implementation were accurately modeled using the procedure in Figure 6 and Equation 1, respectively. It can be seen that the analytical model that incorporates Equation 5(b) (Bischoff 2007) is in good agreement with the experimental results up to failure, and is clearly more effective than the one that uses Equation 5(a) from the current guidelines (ACI 2006). The connection model can be integrated into the structural analysis of a complete post-and-beam railing system based on Specimen M2, which is addressed in the next section.

IMPLICATIONS IN STRUCTURAL DESIGN

Differently from the AASHTO Standard Specifications (2002), Section 13 (Railings) of the LRFD Bridge Design Specifications (AASHTO 2004) mandates strength criteria at the system level. Whereas the former approach lends itself to analogy- and empirical-based design of post, beam and connection sections, the latter demands more rigorous procedures to evaluate integrated post-and-beam structural systems. Based on the results of full-scale crash tests performed as part of programs conducted under the aegis of the Federal Highway Administration, the American Association of State Highway and Transportation Officials, the National Cooperative Highway Research Program, and

individual states, the dynamic loads imparted by an impacting vehicle under specified crash test conditions (Ross *et al.* 1993) are translated into equivalent factored transverse, longitudinal and vertical static loads. The transverse load F_t is typically the one of concern for RC railing structures. Table 3 summarizes the load demands for the TL-2 crash test level (AASHTO 2004) applicable to the open-post railing of Bridge No. 14802301.

Yield line analysis is typically invoked to evaluate the nominal strength of steel RC railings (Hirsch 1978, AASHTO 2004). Due to the linear elastic behavior of FRP bars up to failure, moment redistribution cannot be accounted for in design, that is, both equilibrium and compatibility conditions must be verified at failure. The methodology herein used to study the structural behavior of the GFRP RC railing in Figure 2 is pursuant to the analysis and design principles set forth in the current ACI 440 guidelines (ACI 2006). First, the post and beam finite elements are defined. Second, the global stiffness matrix is assembled and implemented into the nonlinear finite element analysis (FEA) of the post-and-beam system. Design loads and failure modes are determined and discussed on the basis of the code requirements.

Numerical formulation of post and beam elements

A nonlinear spring is used to idealize the post and its connection to the deck, with a single degree of freedom (DOF) of the node *i* associated with the horizontal displacement u_i at the top of the post, as illustrated in Figure 12(a). The load-displacement function described by Equation 1 is accurately approximated by a trilinear function to reduce the computational demand. It should be noted that the strength reduction factor for diagonal

tension ϕ_{dt} is reduced from 0.85 to 0.75 to reflect use of ACI 440.1R-06 (ACI 2006) in lieu of the 2003 guidelines (ACI 2003).

Figure 12(b) shows the idealization and the numerical formulation of the GFRP RC beam element along the railing opening. A single DOF associated with horizontal displacement is assigned to each end node *i* and *j*, where rigid connections to the adjacent posts are assumed. Torsional effects are neglected, which is a reasonable assumption under small displacements. The nonlinear moment-net displacement function M_b-Δu_{ij} defined via Equation 4 and Equation 5 is again efficiently approximated in a trilinear form. Concrete with compressive strength of 4000 psi (27.6 MPa) is assumed for both elements. An enviromental reduction factor C_E of 0.7 is used to compute the design FRP bar strength.

Nonlinear finite element analysis of railing

Two critical transverse loading scenarios are identified for the open-post railing in Figure 2. *Case A* is sketched in Figure 13(a) and accounts for the equivalent static load F_t applied on a rail beam at the mid-section of the opening. *Case B* is sketched in Figure 13(b) and accounts for the transverse load applied directly on an intermediate post.

The symmetric finite element model (FEM) shown in Figure 13(c) is used to study the structural response of the railing system, where the stiffness k_1 of the post closest to the impact section (that is, at the node $i = 1$) is reduced from k_p in the first load case to $0.5k_p$ in the second load case. The vector of the horizontal displacement of the posts

$$\mathbf{u} = \begin{bmatrix} u_1 & u_2 & u_3 \end{bmatrix}^T \tag{6}$$

is computed for a given transverse force vector

$$\mathbf{F_t} = \begin{bmatrix} \frac{F_t}{2} & 0 & 0 \end{bmatrix}^T \tag{7}$$

by solving the nonlinear system

$$\mathbf{u} = \mathbf{K}\left(\mathbf{u}\right)^{-1} \mathbf{F}_t \,, \tag{8}$$

where the global stiffness matrix of the post-and-beam system in Figure 13(c) is assembled as

$$\mathbf{K}\left(\mathbf{u}\right) = \begin{bmatrix} K_{11}(\mathbf{u}) & K_{12}(\mathbf{u}) & 0 \\ K_{21}(\mathbf{u}) & K_{22}(\mathbf{u}) & K_{23}(\mathbf{u}) \\ 0 & K_{32}(\mathbf{u}) & K_{33}(\mathbf{u}) \end{bmatrix}, \tag{9}$$

with

$$\begin{cases} K_{11}(\mathbf{u}) = \dfrac{2}{L_O} \dfrac{\left|M_b\left(\Delta u_{12}\right)\right|}{\Delta u_{12}} + k_1\left(u_1\right) \\ k_1\left(u_1\right) = \begin{cases} k_p\left(u_1\right) & \text{for impact on rail beam (\textit{Case A})} \\ \dfrac{1}{2} k_p\left(u_1\right) & \text{for impact on post (\textit{Case B})} \end{cases} \end{cases} \tag{10a}$$

$$K_{12}(\mathbf{u}) = K_{21}(\mathbf{u}) = -\frac{2}{L_O} \frac{\left|M_b\left(\Delta u_{12}\right)\right|}{\Delta u_{12}} \tag{10b}$$

$$K_{22}(\mathbf{u}) = \frac{2}{L_O} \left[\frac{\left|M_b\left(\Delta u_{12}\right)\right|}{\Delta u_{12}} + \frac{\left|M_b\left(\Delta u_{23}\right)\right|}{\Delta u_{23}} \right] + k_p\left(u_2\right) \tag{10c}$$

$$K_{23}(\mathbf{u}) = K_{32}(\mathbf{u}) = -\frac{2}{L_O} \frac{\left|M_b\left(\Delta u_{23}\right)\right|}{\Delta u_{23}} \tag{10d}$$

$$K_{33}(\mathbf{u}) = \frac{2}{L_O}\left[\frac{\left|M_b\left(\Delta u_{23}\right)\right|}{\Delta u_{23}} + \frac{\left|M_b\left(\Delta u_{34}\right)\right|}{\Delta u_{34}}\right] + k_p\left(u_3\right). \qquad (10e)$$

Optimal solution strategies may be selected (for instance, Conjugate Gradient, Levenberg-Marquardt, Quasi-Newton) to compute the post displacement vector **u**, from which the internal forces can be retrieved.

The structural adequacy is evaluated on the basis of three criteria: first, the maximum reaction force at a connection cannot exceed the design strength [$k_1(u_1) \leq \phi_{dt}F_{n,p}$]; second, the maximum bending moment at the beam ends cannot exceed the design strength [$M_b(\Delta u_{12}) \leq \phi_f M_{n,b}$], provided that shear does not control design; and third, the exterior post [i = 3 in Figure 13(c)] must be able to resist the shear transmitted by the beam [$V_b(\Delta u_{34}) = 2M_b(\Delta u_{34}) / L_O \leq \phi_{dt}F_{n,p}$].

Table 4 summarizes the maximum post displacement u_1 and the resulting internal forces for load *Case A* and *Case B* at the railing design strength level ϕR_t of 47.3 kip (210.2 kN) and 37.9 kip (168.7 kN), respectively, which are controlled by the beam flexural strength. The FEA results are given for a DOF number N of one, two and three to check convergence of the selected discretization. For N = 1 and N = 2, the stiffness matrix was derived by simply eliminating the last two and one rows and columns, respectively, from **K**(**u**) in Equation 9. It can be seen that assuming three unknown post displacements as in Figure 13(c) allows to achieve a good convergence in the maximum connection displacement (and thus reaction force) and beam moment, while the shear transmitted at the end post rapidly drops well within the design limit. The nonlinear load-maximum

displacement response F_t- u_1 is plotted in Figure 14 for load *Case A* and *Case B.* The design strength ϕR_t always exceeds the TL-2 demand (AASHTO 2004), whose level is associated with very small displacements, as desirable for RC railings for which negligible values are typically measured during crash tests.

The FEA was repeated considering a beam opening length L_O increased from 4 ft (1.2 m) to 6 ft (1.8 m), thus similar to the geometry of the steel RC MKCR, and up to 12 ft (3.6 m), where the component strength requirements in the AASHTO Standard Specifications (2002) are still satisfied. At increased opening lengths, design is controlled by the connection strength instead of the beam moment capacity. The design strengths for load *Case A* and *Case B* are plotted in Figure 15 with respect to the opening length L_O. It is noted that the modifications may result in insufficient design strength with respect to the 27 kip (120.1 kN) TL-2 load demand (AASHTO 2004). In such instances, the design may require modification of either or both the post-deck connection, for example by increasing the post width, and the rail beam, for example adding longitudinal bars.

IMPACT ON DESIGN GUIDELINES

Similarly to the ACI Building Code (ACI 2005), the current ACI guidelines (ACI 2006) do not include specific recommendations for the design of discontinuity regions in RC frames, despite such details are well-known as being affected by a variety of design errors in practice. In light of the increasing use of FRP bars in a number of structural applications where connections may be present, it is believed that a section should be added that addresses design for common reinforcement layouts and load conditions.

Approaches that combine basic structural analysis principles with FRP RC theory should be selected on a case-by-case basis. The case study presented herein has demonstrated the use of a simple method to determine the nominal and design strength of an FRP RC corner joint subjected to combined shear and bending moment. The internal forces were computed by imposing equilibrium conditions at the corner, and the associated bending moment was back-calculated consistently with well established flexural analysis principles for FRP RC. The adoption of similar design algorithms for different details and load cases may enable to design and retain structurally sound solutions where the full flexural strength of the connected sections may not be attained, thereby providing the rational basis to complement legitimate practical and economical considerations.

The experimental results discussed also support the adoption of a more restrictive modification (Bischoff 2007) to the algorithm presently used for the effective moment of inertia to model the post-cracking behavior of FRP RC members, where the former appears to more appropriately account for flexural stiffness changes throughout as well as reduced tension stiffening.

The theoretical results on the lateral strength of rigidly connected post-and-beam systems at increasing beam opening length indicate that the current component-based design approach, although accepted for steel RC, may be inadequate. The implementation of analytical or numerical methods that impose equilibrium and compatibility at the system level becomes necessary to ensure strength and to preliminarly evaluate functionality performances that are related to deflection, such as in the case of bridge railings.

CONCLUSIONS

In the first part of this paper, moving from the results of quasi-static testing of two GFRP RC post-deck subassemblies where deformed bars were used in combination with a smooth deck grating, a rational design for the connection to meet specification mandated criteria at the component level (AASHTO 2002) has been validated and selected for implementation in the open-post railing of an off-system bridge in Missouri. The structural response of the connection until failure was accurately modeled on the basis of simple structural analysis pursuant to well established design principles of FRP RC.

The second part of the paper has demonstrated the application of a methodology for the structural analysis and design an FRP RC open-post railing system where internal forces, deformations and failure modes are rationally determined. The analytical model of the post-deck connection was incorporated into a finite element model defined to study the structural behavior of the post-and-beam system subjected to the equivalent static load up to failure, as prescribed in the current LRFD specifications (AASHTO 2004). The railing design implemented was shown to meet the global strength requirement while undergoing very small deformations, which is typical of crashworthy RC railings.

In terms of potential impact on the current ACI design guidelines (ACI 2006), the research presented herein has introduced the need to rationally address the design of common discontinuity regions in FRP RC frames, as illustrated in the case of a corner joint, and has provided an additional case study that supports the adoption of a more conservative approach to estimate deflections and rotations of cracked members.

Specific to the analysis and design of open-post concrete railings, which are often a preferred choice in bridges, the case studies analyzed numerically show that a simplified nonlinear analysis methodology that satisfies basic equilibrium and compatibility assumptions can be applied to devise more rational and efficient design solutions for either implementation or, when required, for crash testing.

LIST OF SYMBOLS

A_f	=	cross sectional area of FRP tension reinforcement.
C_d, C_p	=	compression force at deck and post connection section.
d	=	distance from extreme compression fiber to centroid of tension reinforcement.
E_f	=	longitudinal modulus of elasticity of FRP.
E_c	=	modulus of elasticity of concrete.
f'_c	=	cylinder compressive strength of concrete.
f^*_{fu}	=	guaranteed tensile strength of FRP bar.
f_r	=	modulus of rupture of concrete.
$F_{f,d}$, $F_{f,p}$	=	tension force in reinforcement at deck and post connection section.
F_l, F_t, F_v	=	longitudinal, transverse and vertical equivalent static load.
$F_{n,p}$	=	nominal strength of post-deck connection.
F_p	=	transverse load applied to post-deck connection.
$\mathbf{F_t}$	=	transverse force vector.
$F_{t,\text{TL-2}}$	=	equivalent transverse static strength requirement for crash Test Level 2 railing.
H	=	height of railing.
H_e	=	height of applied transverse and longitudinal load line with respect to deck surface.
k_1	=	stiffness of post closest to applied equivalent static load in FEM.
k_p	=	stiffness of intermediate post in FEM.
$\mathbf{K}(\mathbf{u})$	=	nonlinear stiffness matrix of railing FEM.

I_b, I_d, I_p = section moment of inertia of rail beam, deck at connection and post.

I_{cr} = moment of inertia of transformed cracked section.

I_g = gross moment of inertia.

l_{dc} = length of diagonal crack.

$l_{overhang}$ = overhang length.

L_l, L_t, L_v = uniform distribution length for longitudinal, transverse and vertical static load.

L_O = length of rail beam opening.

L_P = width of post.

M_b = moment at ends of rail beam element.

M_{cr} = cracking moment.

M_d = deck moment at connection section.

$M_{n,b}$ = nominal moment capacity of FRP RC rail beam section.

N = number of DOF in symmetric railing FEM.

R_t, ϕR_t = nominal and design strength of railing under equivalent transverse static load.

T = tensile force on diagonal crack.

t_d = thickness of bridge deck at connection with post.

u = maximum displacement of post subassembly under transverse load.

u_i = horizontal displacement of post element at node i.

u_p = cantilever displacement component of post subassembly.

$\mathbf{u}$ = horizontal post displacement vector.

V_b = shear at ends of rail beam element.

α = angle of diagonal crack with respect to deck plane.

Δu_{ij} = net horizontal displacement of rail beam element between nodes *i* and *j*.

β_d = reduction coefficient used in computing effective moment of inertia.

ε^*_{fu} = guaranteed rupture strain of FRP bar.

θ_d = maximum rotation of overhang under bending moment.

ϕ_f = strength reduction factor for flexure.

ϕ_{dt} = strength reduction factor for diagonal tension.

ρ_f = FRP reinforcement ratio.

ρ_{fb} = FRP reinforcement ratio produced by balanced strain conditions.

ACKNOWLEDGMENTS

The financial support of the University of Missouri-Rolla University Transportation Center on Advanced Materials and NDT Technologies is acknowledged. The assistance of the industry members of the NSF I/UCRC "Repair of Buildings and Bridges with Composites" (RB^2C), Hughes Brothers, Inc. and Strongwell Corp., in supplying the FRP reinforcement for the railing and the slab, respectively, is acknowledged. Special thanks are extended to the personnel of the UMR Structures Laboratory for valuable help in the test phases, and to the Greene County Highway Department and Great River Engineering of Springfield, Inc., for technical and logistic support throughout the research project.

REFERENCES

ACI Committee 440, "Guide for the design and construction of concrete reinforced with FRP bars," *ACI 440.1R-03*, American Concrete Institute, Farmington Hills, MI, 2003, 42 pp.

ACI Committee 440, "Guide for the design and construction of structural concrete reinforced with FRP bars," *ACI 440.1R-06*, American Concrete Institute, Farmington Hills, MI, 2006, 44 pp.

American Association of State Highway and Transportation Officials (AASHTO), "Load and resistance factor design (LRFD) bridge design specifications," 3rd edition, AASHTO, Washington, D.C., 2004.

American Association of State Highway and Transportation Officials (AASHTO), "Standard specifications for highway bridges," 17th edition, AASHTO, Washington, D.C., 2002.

American Concrete Institute, "Building code requirements for structural concrete," *ACI 318-05*, ACI, Farmington Hills, MI, 2005.

Benmokrane, B., El-Salakawy, E., Desgagné, G., and Lackey, T., "FRP bars for bridges," *Concrete International*, V. 26, No. 8, 2004, pp. 84-90.

Benmokrane, B., El-Salakawy, E., El-Ragaby, A., and Lackey, T., "Designing and testing of concrete bridge decks reinforced with glass FRP bars," *Journal of Bridge Engineering*, V. 11, No. 2, 2006, pp. 217-229.

Bischoff, P. H., "Deflection calculation of FRP reinforced concrete beams based on modifications to the existing Branson equation," *Journal of Composites for Construction*, V. 11, No. 1, 2007, pp. 4-14.

Bradberry, T. E., "Fiber-reinforced-plastic bar reinforced concrete bridge decks," *Proc. 80th Annual Transportation Research Board Meeting*, Jan. 9-13, 2001, Washington, D.C., CD-ROM #01-3247.

Bligh, R. P., Abu-Odeh, A. Y., Hamilton, M. E., and Seckinger, N. R., "Evaluation of roadside safety devices using finite element analysis," *Report FHWA/TX-04/0-1816-1*, Texas Transportation Institute, 2004, 66 pp.

Buth, C. E., Williams, W. F., Bligh, R. P., Menges, W. L., and Haug, R. R., "Performance of the TxDOT T202 (MOD) bridge rail reinforced with fiber reinforced polymer bars," *Report FHWA/TX-03/0-4138-3*, Texas Transportation Institute, 2003, 100 pp.

Canadian Standards Association (CSA), "Canadian highway bridge design code," *CAN/CSA-S6-06*, CSA, Mississauga, Ontario, Canada, 2006, 788 pp

Deitz, D. H., Harik, I. E., Gesund, H., and Zatar, W. A., "Barrier wall impact simulation of reinforced concrete decks with steel and glass fiber reinforced polymer bars," *Journal of Composites for Construction*, V. 8, No. 4, 2004, pp. 369-373.

El-Salakawy, E., Benmokrane, B., Masmoudi, R., Brière, F., and Breaumier, E., "Concrete bridge barriers reinforced with glass fiber-reinforced polymer composite bars," *ACI Structural Journal*, V. 100, No. 6, 2003, pp. 815-824.

Hirsch, T. J., "Analytical evaluation of Texas bridge rails to contain buses and trucks," *Report FHWATX-78-230-2*, Texas Transportation Institute, 1978, 92 pp.

Maheu, J., and Bakht, B., "A new connection between concrete barrier walls and bridge decks," *Proc. Annual Conference of the Canadian Society of Civil Engineering*, June 1-4, 2004, Winnipeg, Manitoba, Canada, pp. 224-229.

Mak, K. K., and Bligh, R. P., "Assessment of NCHRP Report 350 test conditions," *Transportation Research Record*, No. 1797, 2002, pp. 38-43.

Matta, F., and Nanni, A., "Design of concrete railing reinforced with glass fiber reinforced polymer bars," *Proc. 2006 ASCE/SEI Structures Congress*, May 18-20, 2006, St. Louis, MO, CD-ROM, 9 pp.

Matta, F., Nanni, A., Ringelstetter, T. E., and Bank, L. C., "Rapid construction of concrete bridge deck using prefabricated FRP reinforcement," *Proc. Third International Conference on FRP Composites in Civil Engineering (CICE 2006)*, Dec. 13-15, 2006, Miami, FL, USA, pp. 151-154.

Mufti, A., Banthia, N., Benmokrane, B., Boulfiza, M., and Newhook, J., "Durability of GFRP composite rods," *Concrete International*, V. 29, No. 2, 2007, pp. 37-42.

Nanni, A., "Flexural behavior and design of RC members using FRP reinforcement," *Journal of Structural Engineering*, V. 119, No. 11, 1993, pp. 3344-3359.

Nanni, A., "North American design guidelines for concrete reinforcement and strengthening using FRP: principles, applications and unresolved issues," *Construction and Building Materials*, Vol. 17, No. 6-7, 2003, pp. 439-446.

Nanni, A., and Faza, S., "Designing and constructing with FRP bars: an emerging technology," *Concrete International*, V. 24, No. 11, 2002, pp. 53-58.

Nilsson, I. H. E., and Losberg, A., "Reinforced concrete corners and joints subjected to bending moment," *Journal of the Structural Division*, V. 102, No. ST6, 1976, pp. 1229-1254.

Phelan, R. S., Vann, W. P., and Bice, J., “FRP reinforcing bars in bridge decks – Field instrumentation and short-term monitoring,” *Report FHWA/TX-06/9-1520-4*, Texas Tech University, 2003, 51 pp.

Ross, H. E., Sicking, D. L., Zimmer, R. A., and Michie, J. D., “Recommended procedures for the safety performance evaluation of highway features,” *NCHRP Report 350*, National Academy Press, Washington, D.C., 1993.

Trejo, D., Aguiniga, F., Buth, E. C., James, R. W., and Keating, P. B., “Pendulum impact tests on bridge deck sections,” *Report FHWA-01/1520-1*, Texas Transportation Institute, 2001, 31 pp.

TABLES

Table 1 – Reinforcement and flexural capacity of post and deck sections at connection.

Specimen	Connection section	Reinforcement	Nominal moment capacity M_n, kip-ft (kN-m)	Design moment capacity $\phi_f M_n$, kip-ft (kN-m)
M1 [f'_c = 6000 psi (41.4 MPa)]	Post	12 No. 5 (16 mm) ρ_f = 1.1%	161.3 (218.7)	80.7 (109.4)
	Deck (bars only)	10 No. 5 (16 mm), ρ_f = 1.7%	57.8 (78.3)	40.4 (54.8)
	Deck (I-bars only)	11 grating I-bars ρ_f = 1.7%	68.5 (92.8)	43.5 (58.9)
M2 [f'_c = 4000 psi (27.6 MPa)]	Post	10 No. 5 (16 mm) ρ_f = 0.9%	127.5 (172.9)	64.7 (87.7)
	Deck	16 No. 5 (16 mm), ρ_f = 2.2%	83.2 (112.3)	58.3 (79.0)

Table 2 – Properties of GFRP reinforcement.

Reinforcement type	Cross sectional area A_f, in^2 (mm^2)	Modulus of elasticity E_f, msi (GPa)	Tensile strength f_{fu}^*, ksi (MPa)	Ultimate strain ε_{fu}^*, %
No. 5 (16 mm) bar	0.34 (217.5)	5.92 (40.8)	95 (654.6)	1.60
SIP grating I-bar	0.32 (206.4)*	4.50 (31.0)	80 (551.2)	1.78

* Net of pre-drilled holes for longitudinal cross rods.

Table 3 – Factored design forces for crash test level TL-2 railing design (AASHTO 2004).

Transverse force F_t, kip (kN)[a]	27.0 (120.1)
Longitudinal force F_l, kip (kN)[a]	9.0 (40.0)
Vertical force F_v, kip (kN)[b]	4.5 (20.0)
Minimum height H_e for application of F_t and F_l, in. (mm)	20 (508)

[a] uniformly distributed along $L_t = L_l = 4$ ft (1.2 m).

[b] uniformly distributed along $L_v = 18$ ft (5.5 m).

Table 4 – Convergence check for railing FEA for $F_t = \phi R_t$ for load *Case A* and *Case B*[a].

DOF number in post-and-beam FEM	$N = 1$	$N = 2$	$N = 3$
Maximum transverse post displacement u_1, in. (mm)	0.19 (4.8) 0.19 (4.7)	0.21 (5.4)	0.21 (5.4)
Maximum transverse force resisted by post $k_1(u_1)$ kip (kN)	8.9 (39.5) 8.8 (39.2)	9.3 (41.5)	9.3 (41.5)
Maximum bending moment in railing beam $M_b(\Delta u_{12})$, kip-ft (kN-m)	29.5 (40.0) 29.1 (39.5)	28.6 (38.8)[b]	28.6 (38.8)[b]
Shear force transmitted by railing beam to end post $V_b(\Delta u_{N,N+1})$, kip (kN)	14.7 (65.6) 14.6 (64.8)	8.1 (35.9)	6.8 (30.2)

[a] Values on top for *Case A* and bottom for *Case B* when different ($N = 1$).

[b] Design moment capacity of beam $\phi_f M_{n,b}$ = 28.6 kip-ft (38.8 kN-m) controls.

FIGURES

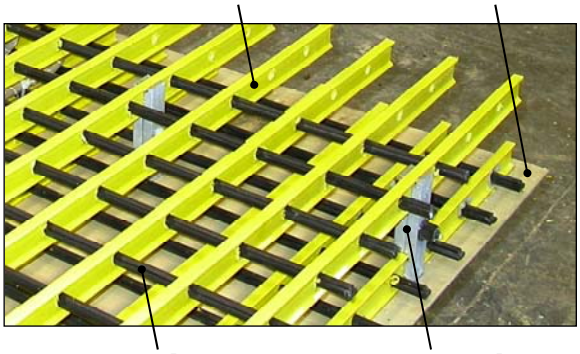

Figure 1 – Prefabricated GFRP stay-in-place deck reinforcement.

(a)

(b)

Figure 2 – Rehabilitation of Bridge No. 14802301: (a) GFRP reinforcement cages prior to casting of railing; and (b) open post railing in service.

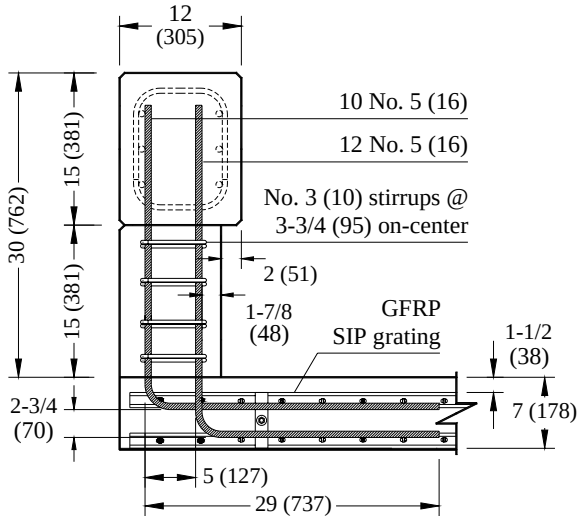

(a)

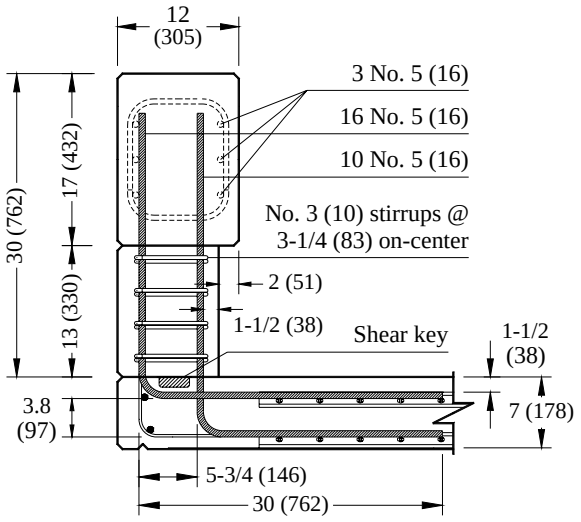

(b)

Figure 3 – Reinforcement layout of post-deck connection subassemblies: (a) Specimen M1; and (b) Specimen M2. Dimensions in in. (mm).

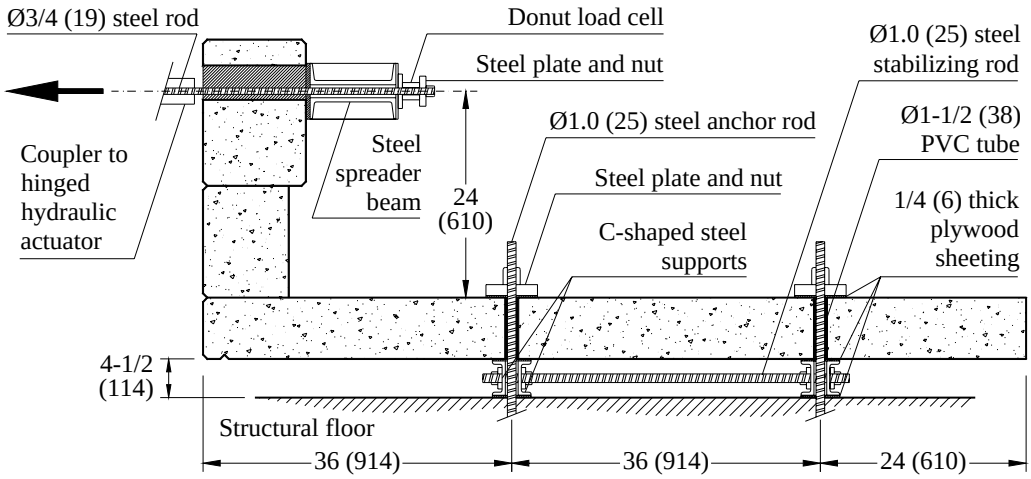

(a)

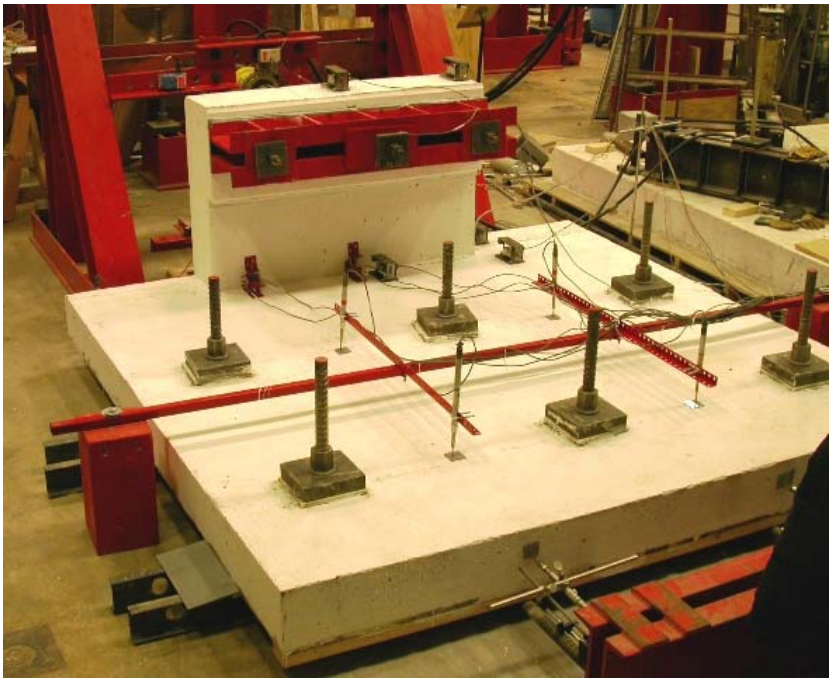

(b)

Figure 4 – Test setup: (a) schematic; and (b) photograph. Dimensions in in. (mm).

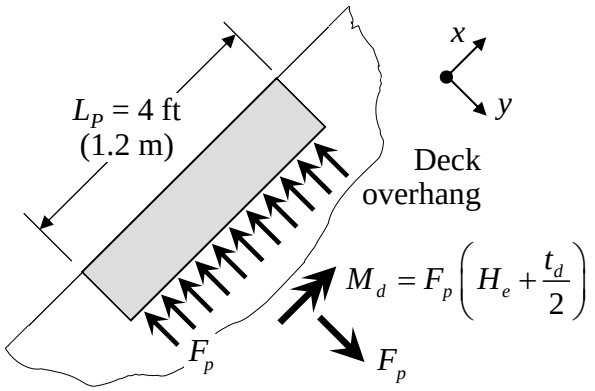

(a)

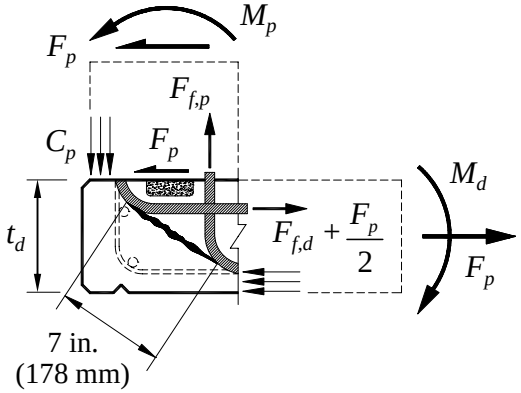

(b)

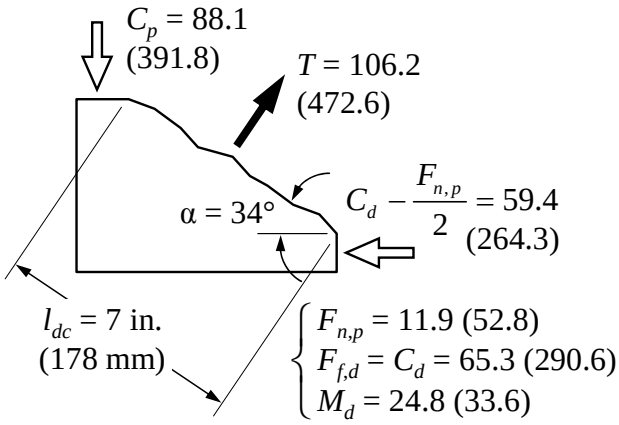

(c)

Figure 5 – Design of Specimen M2: (a) applied force and reactions in deck; (b) internal forces at connection; and (c) free body diagram of corner joint. Forces and moment in kip (kN) and kip-ft (kN-m).

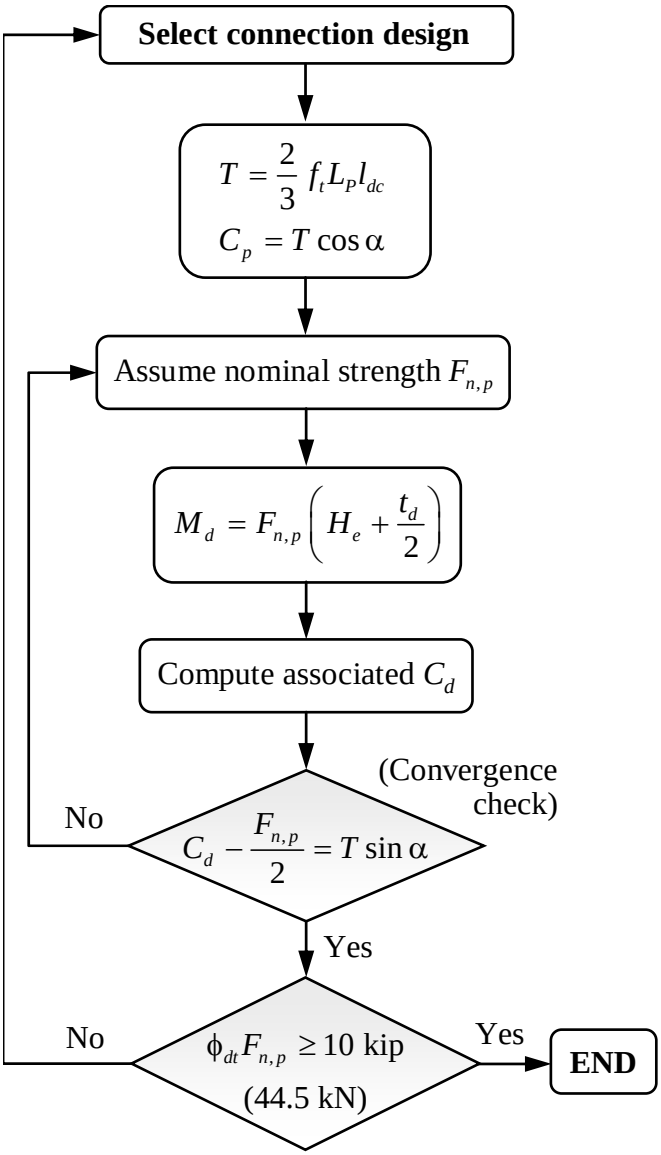

Figure 6 – Flow chart for post-deck connection design controlled by diagonal tension failure at corner.

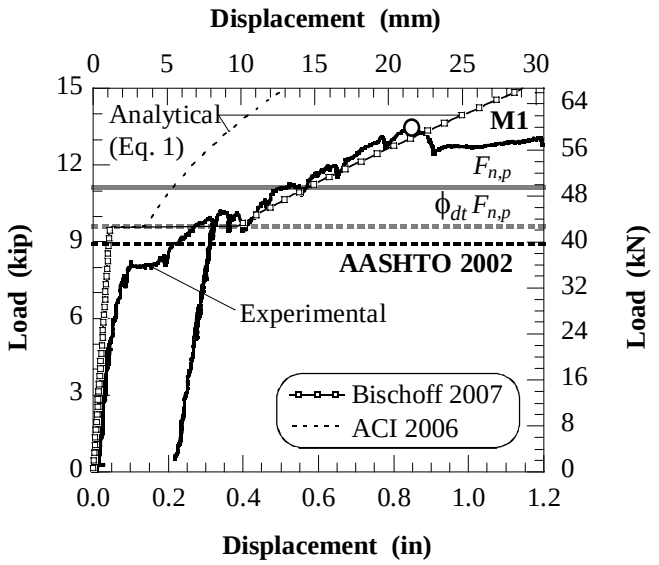

(a)

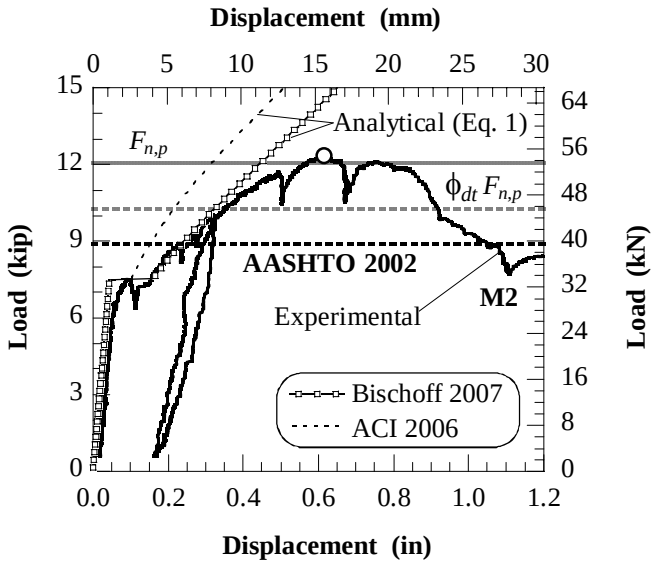

(b)

Figure 7 – Load-displacement response: (a) Specimen M1; and (b) Specimen M2. Blank circles indicate experimental strength of connections.

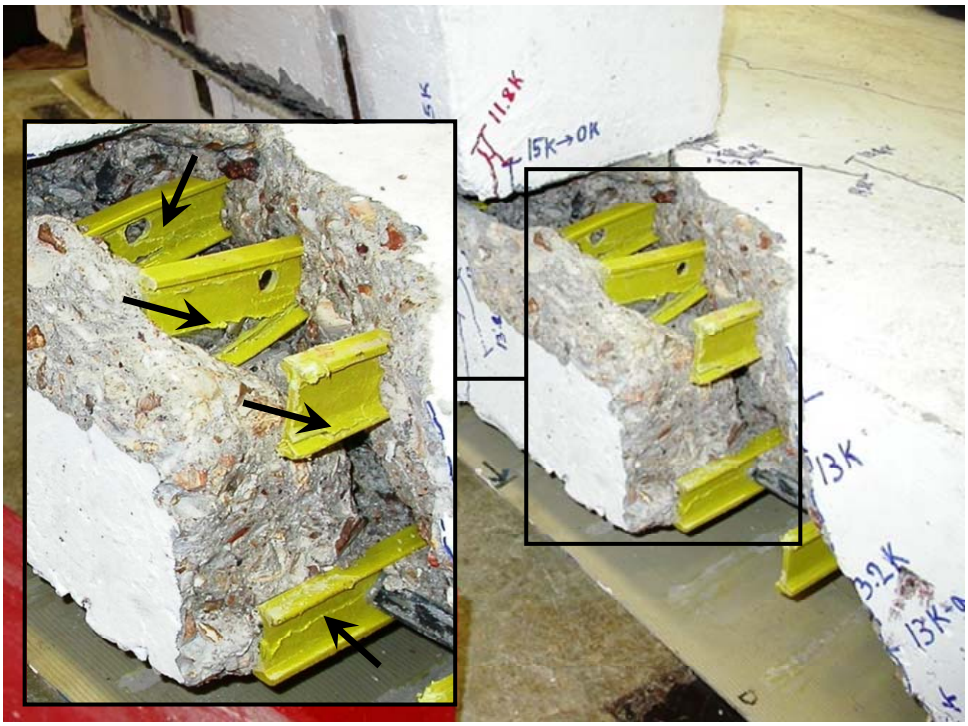

Figure 8 – Close-up of diagonal fracture surface at corner in Specimen M1. Arrows indicate interlaminar shear failure of I-bars at top layer of deck grating.

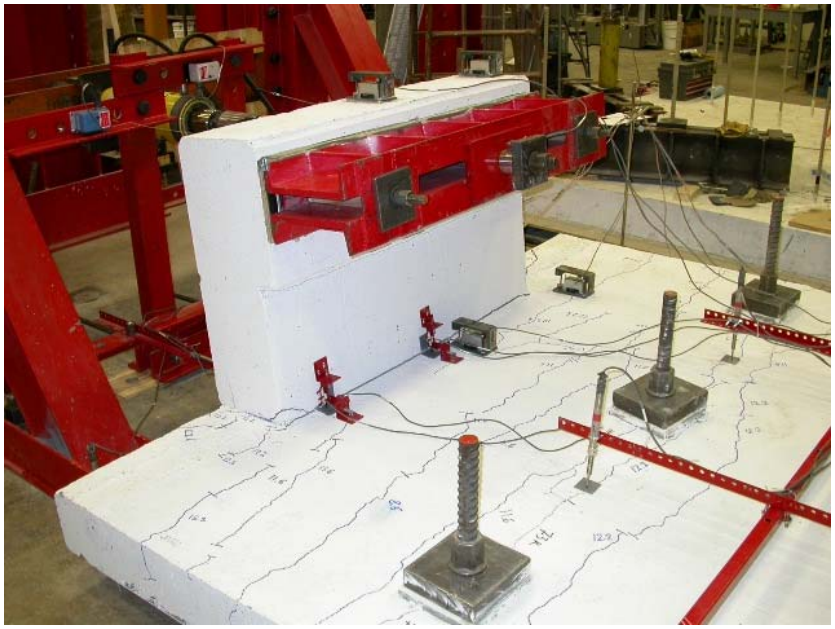

(a)

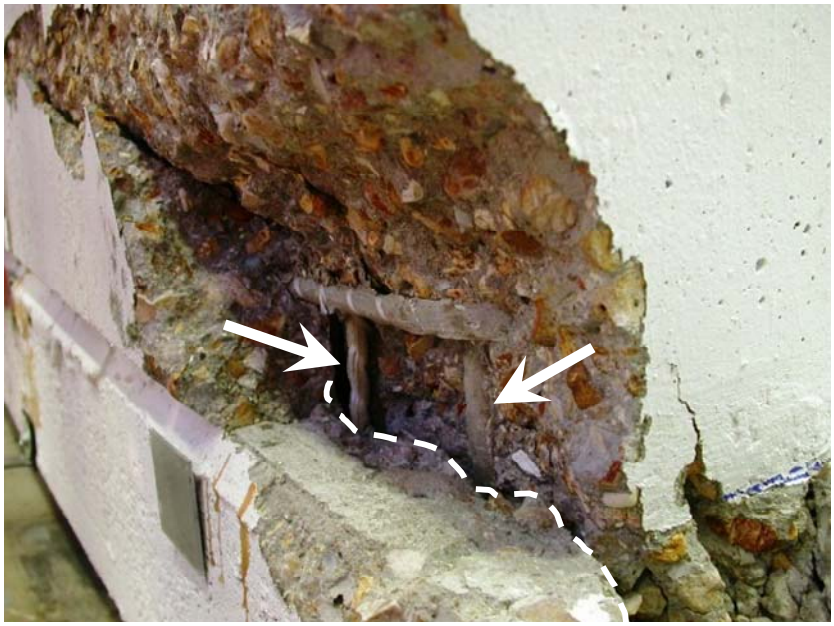

(b)

Figure 9 – Failure of Specimen M2: (a) photograph; and (b) close-up of diagonal fracture surface at corner joint. Blank arrows and dashed line indicate back of bent bars within post and fracture surface, respectively.

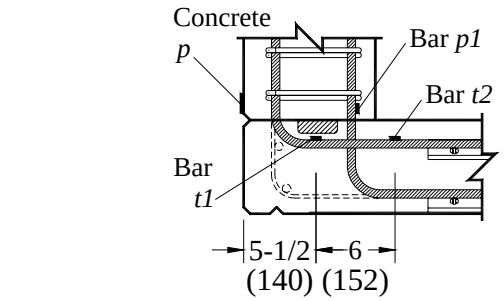

(a)

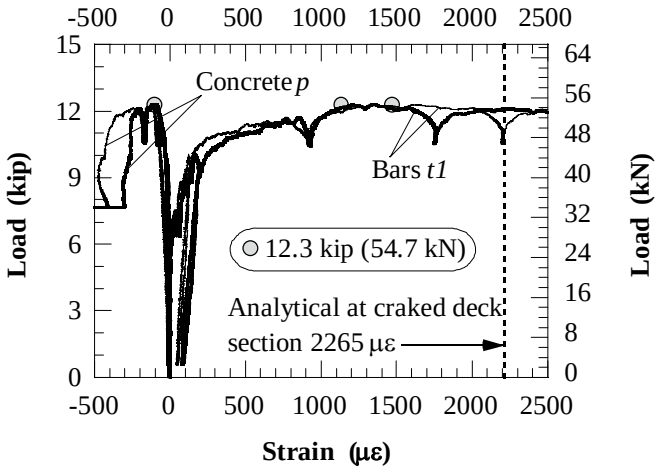

(b)

Figure 10 – Load-strain response of Specimen M2: (a) location of sensors at typical section; and (b) concrete *p* and bar *t1* strains at two sections. Gray circles indicate strain at failure.

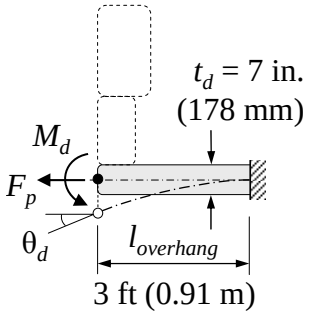

(a)

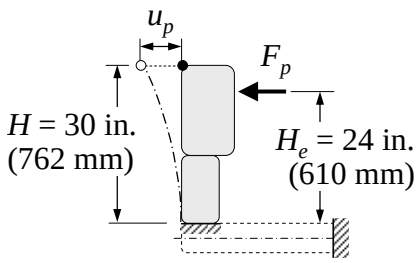

(b)

Figure 11 – Analytical modeling of horizontal post displacement: (a) rotation of overhang under applied moment M_d; and (b) post cantilever under applied force F_p.

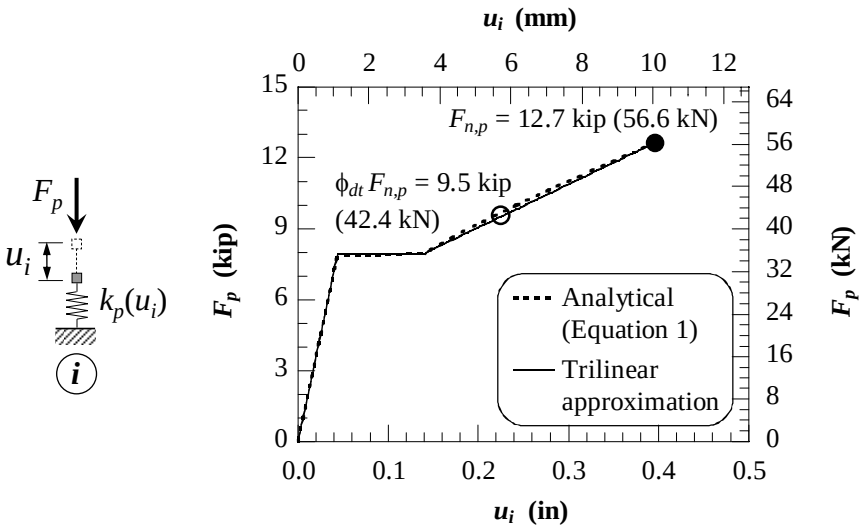

(a)

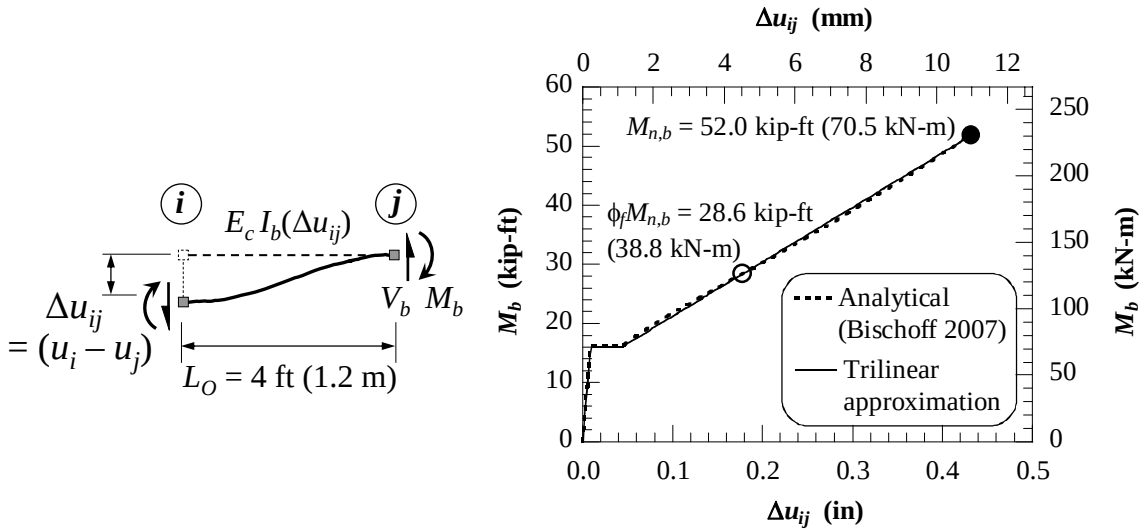

(b)

Figure 12 – Finite element formulation: (a) spring element for post; and (b) beam element along opening. Filled and unfilled circles indicate nominal and design strength, respectively.

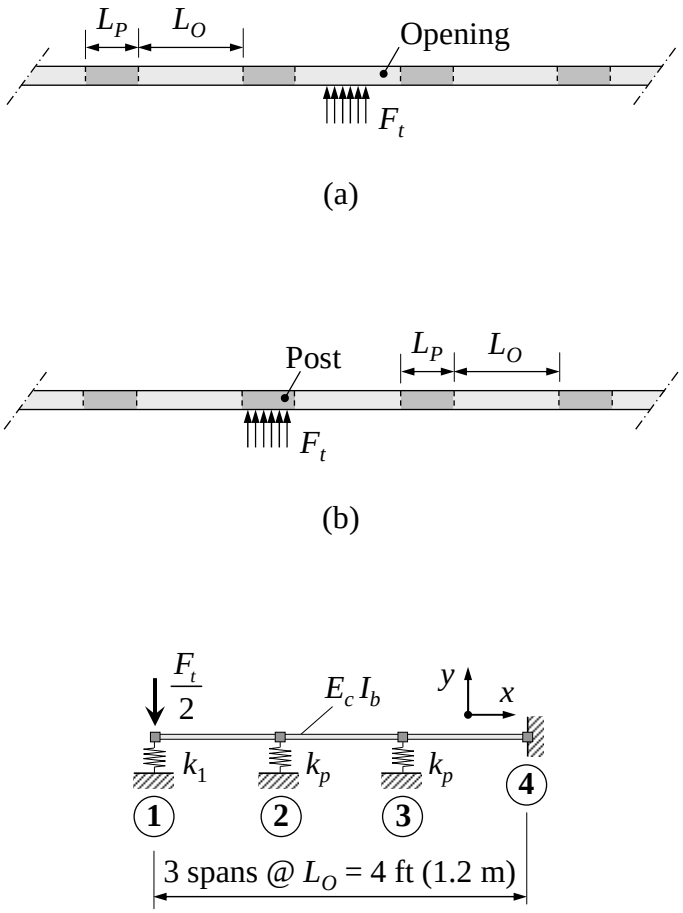

Figure 13 – Structural analysis of railing: (a) load applied to rail beam at opening (*Case A*); (b) load applied to post (*Case B*); and (c) three-DOF FEM of symmetric post-and-beam system.

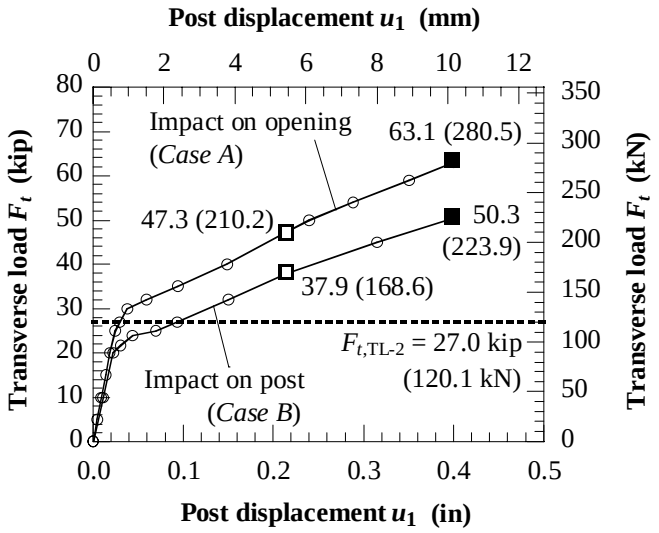

Figure 14 – Numerical load-displacement response of Bridge No. 1482301 railing. Filled and unfilled squares indicate nominal and design strength, respectively.

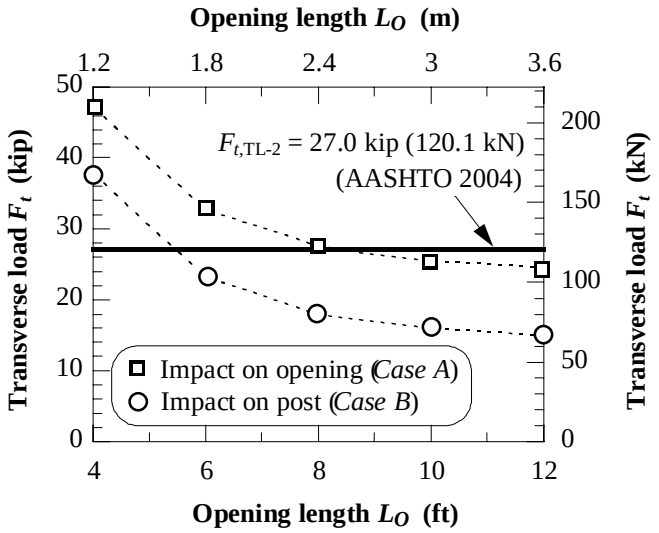

Figure 15 – Design strength of railing at varying opening length L_O.

PAPER 2

EXTERNALLY POST-TENSIONED CARBON FRP BAR SYSTEM FOR DEFLECTION CONTROL

Fabio Matta[a,*], Antonio Nanni[b],

Ahmad Abdelrazaq[c], Doug Gremel[d], and Ryan Koch[d]

[a] Center for Infrastructure Engineering Studies, University of Missouri-Rolla

[b] Dept. of Civil, Architectural and Environmental Engineering, University of Miami

[c] Engineering & Construction Group, Samsung Corporation

[d] Hughes Brothers, Inc.

ABSTRACT

Externally post-tensioned steel tendons have long been an attractive option for increasing the design loads or correcting strength and serviceability problems in bridge and building structures. Recently, alternative solutions have been developed and implemented that use straight post-tensioned carbon fiber reinforced polymer (CFRP) tendons, ideally enlisting their high strength to failure, small relaxation, corrosion resistance, and light weight. In this paper, a novel CFRP system for external post-tensioning is presented. The solution

---

* Graduate Research Assistant. Corresponding author – 220 Engineering Research Laboratory, 1870 Miner Circle, 65409-0710 Rolla, MO, USA. Tel +1 (573) 341-6661, Fax -6215, E-mail: *mattaf@umr.edu*.

consists of unbonded CFRP bars connected to dead- and live-end steel anchors by means of couplers that allow the bar to develop the full tensile strength. Intermediate deviators can be extended vertically to impart additional post-tensioning (PT) force and achieve a profiled bar configuration. The required uplift forces for deflection control of a flexural member are provided by modifying the number, position and extended length of the deviators, similarly to commercially available systems that use steel wire strands. The structural efficiency of such approach in controlling deflection is analyzed and discussed for single-span one-way members on the basis of a parametric study that considers the influence of member geometry, flexural stiffness, boundary conditions, and PT system layout.

Keywords: Bars; Carbon; Deflection; Fiber reinforced polymers; External post-tensioning; Serviceability; Tendons.

INTRODUCTION

The use of externally post-tensioned (EPT) steel tendons has been a recurrent choice in the structural rehabilitation of timber, concrete and steel bridges over the past 50 years (Klaiber *et al.* 1987, Naaman and Breen 1990, Li *et al.* 1995, Daly and Witarnawan 1997). The method is well suited for the strengthening and repair of flexural members, especially when performance under service conditions needs to be improved, for example relieving tensile overstress with respect to service loads in both positive and negative moment regions (Klaiber *et al.* 1998), decreasing the magnitude of fatigue stress (Li *et al.* 1995), and controlling deflection by recovering excessive short-term deformations and reducing the effect of sustained loads on long-term deformations. In concrete structures, superimposing compressive forces in tension areas enables the reduction of the width of existing cracks, thereby mitigating the effects of corrosion of the internal reinforcement, and possibly decreasing the amplitude of vibrations induced by live loads. These issues are faced rather frequently by bridge engineers. Considerable potential also exists to enhance the shear and torsional strength by means of EPT reinforcement (Emmons 1993, Lees *et al.* 2002), with concrete box girders being the ideal test bed for such applications (Klaiber *et al.* 1987).

The cost-effectiveness of external post-tensioning is enhanced by the ability to perform field installation with minimal or no service disruption. In addition, the design of straight threaded rod or profiled wire strand strategies can be tailored depending on specific needs and cost-benefit considerations (Klaiber *et al.* 1987, Li *et al.* 1995, Ahmadi-Kashani 2005). In the latter case, prefabricated saddles or deviators are arranged to provide the

desired uplift forces at intermediate locations between the end anchors, thereby combining the optimal use of high-strength steel with more efficient force systems, while adding negligible dead load. The post-tensioning (PT) forces are typically imparted using hydraulic jacks at the live ends.

The technology has been successfully implemented in the building arena, as the need for structural upgrade has arisen due to aging, deterioration from exposure to aggressive environments (e.g., in the case of parking garages and structures in proximity of salt water), or due to changes in use demanding higher design loads, more stringent serviceability requirements, or correction of design and construction errors (Krauser 2006, Nanni *et al.* 2006).

Recently, alternative solutions have been developed and validated that use EPT carbon fiber reinforced polymer (CFRP) reinforcement in both new construction (Grace and Abdel-Sayed 1998a, 1998b, 1999) and rehabilitation (Berset 2002, Schnerch 2005, Choi *et al.* 2006, El-Hacha and Elbadry 2006, Shang *et al.* 2006). CFRP materials are ideally suited for both pre- and post-tensioned elements, in the form of bars, plates, and strands, due to their high tensile strength (typically in excess of 1800 MPa), small relaxation (typically below 3% of the initially applied stress), and corrosion resistance (ACI 2004). In new construction, the use of EPT CFRP elements may provide improved constructability and durability performance compared to that of internally grouted tendons, which is often of concern (Mutsuyoshi 2001). Magnetic transparency and nonconductivity are also peculiarities that may be valuable in specific applications when

fibers other than carbon are used (ACI 2004). The reduced weight of CFRP tendons of about 1.5 gr/cm^3 represents an additional benefit, especially when installed on structural members with relatively long spans.

The challenge in the use of CFRP tendons is in the development of anchor systems that allow the exploitation of the full material strength in tension. In fact, transverse mechanical properties of CFRP are resin dominated and are typically two orders of magnitude smaller than those in the direction of the fibers. To date, few external post-tensioning systems have been developed for structural rehabilitation. Limited field applications are reported that consist of straight near-surface bonded or unbonded CFRP plates with relatively sophisticated anchorage systems mounted either on the slab or girder soffit or sides, using hydraulic jacks to apply the PT forces (Basler *et al.* 2004, Ändra and Maier 2005, Zoghi 2006). Unbonded EPT CFRP bars were previously used in an early demonstration project on a three-span continuous steel I-girder bridge with load ratings that may have required posting (Phares *et al.* 2006). The system comprised CFRP bars with diameter of 9.5 mm, running parallel to the top side of the bottom flange of the I-girder upgraded, which were connected to end anchors made of steel stiffened angles by means of steel-tube anchors and couplers. Portable hydraulic jacks were used to post-tension the rods.

The objective of this paper is twofold. First, a novel and complete EPT CFRP system is presented. It consists of unbonded CFRP bars connected to dead- and live-end steel anchors, devised to apply the PT force without the need of hydraulic jacks. In addition to

the bending moment produced by eccentric PT force, vertical (uplift) forces at intermediate sections between the end anchors can be imposed by engaging extendable deviators, thereby achieving a profiled configuration similar to commercially available systems with high-strength steel wire strands (Daly and Witarnawan 1997, Klaiber *et al.* 1998). Second, the structural analysis implications of member geometry, flexural stiffness, boundary conditions, and EPT system layout for straight and profiled bar configurations in the typical case of a single-span one-way member are analyzed and discussed to provide guidance on the relevant criteria for the selection and design of EPT solutions for deflection control. The effect of post-tensioning on stress relief in the structural member is not covered herein.

PRACTICAL SIGNIFICANCE

Cost-effective alternatives to increase shear and flexural strength using non-prestressed, externally bonded (EB) FRP sheets or strips have been developed, validated, and are rapidly becoming mainstream (Nanni 2006). However, EB FRP systems are not as effective in controlling deflection (Tan and Saha 2006) and addressing serviceability issues in general, which represents an important niche ideally covered by EPT CFRP options. In addition to deflection control, post-tensioning allows a more efficient use of the CFRP material, thus minimizing the amount needed.

Typical tradeoffs are the additional cost for the anchor systems as well as specialized equipment, along with installation procedures that may involve time-consuming operations, sometimes to be performed by specially trained personnel. Another concern

is the vulnerability of CFRP tendons to intentional vandalism or post-installation work. There is still considerable margin to advance the constructability characteristics, structural efficiency, and safety of EPT solutions for rehabilitation using CFRP elements. The availability of a simple analytical tool for the selection and preliminary design of candidate rehabilitation strategies using efficient and geometrically compatible EPT configurations is also of practical relevance.

EXTERNALLY POST-TENSIONED CFRP SYSTEM

Description

The base configuration of this EPT system is illustrated in Figure 1. It consists of a set of two pultruded CFRP bar assemblies, each with a dead- and a live-end forged stainless steel anchor and an intermediate deviator. Each bar, with nominal diameter d_b = 12.7 mm (other diameters can be used), is equipped at either end with stainless steel swage couplers, which were engineered to allow the bars to develop the CFRP ultimate strength. At the dead end, the bar assembly terminates with a steel thread adapter and a threaded steel rod with a clevis end-fitting that connects to the steel T-shaped anchor by means of a HEX steel bolt, thereby allowing free end rotation. The arrangement of the live end features a AS2545 hybrid turnbuckle that is mounted between a threaded steel rod from the HEX thread adapter connected to the bar assembly, and a threaded rod with a clevis end-fitting that connects to the forged T-anchor similar to the dead end, as shown in Figure 1(b). The anchor fixtures can be secured to concrete surfaces using adhesive bonded high-strength steel threaded rods, where the structural adhesive should be selected among those suitable for overhead applications under circumstances as in Figure

1(c), which depicts a trial installation onto the soffit of a reinforced concrete slab. Mechanical connections with high-strength steel bolts can be used on metallic structural members. The PT force can be applied by operating each turnbuckle at the live end with a wrench, while using another wrench to block rotation of the rod assembly at the HEX thread adapter. A long-arm wrench may be convenient to facilitate the operation when feasible. The present configuration replicates that typical of straight near-surface CFRP tendons (Phares 2003, Basler *et al.* 2004, Ändra and Maier 2005, Zoghi 2006), and provides a comparable structural performance for the same amount of reinforcement material used.

Each deviator, to be mounted between the end anchors, consists of two high-strength steel threaded bolts reacting on a base plate and running through the bent plate in contact with the CFRP bars. The contact plate is displaced by operating the spreader heads of the bolts using a wrench or a socket wrench. Bent ultra-high molecular weight polyethylene (UHMW) covers provide a low-friction yet abrasion- and corrosion-resistant contact surface with the CFRP bar. The radius of curvature of the bend, R = 1900 mm for a bar diameter d_b = 12.7 mm, is designed to limit the maximum strain induced by local bending upon full engagement of the deviator to 20% of the ultimate tensile strain. By extending the contact plate, additional PT force is applied with the progressive engagement of the CFRP bar, thus introducing a resultant axial force in the threaded bolts that directly pushes upwards. The deviator can be installed on the soffit of a structural member to be rehabilitated, as in the example in Figure 1(c) where sets of two bars are used, or when feasible, bolted on the sides by using a modified fixture, as in the case of stems of T-

beams. By appropriately selecting the PT force applied from the live ends, and the number, position and extended length of the deviators, the uplift force can be designed to achieve the serviceability or strength improvement sought. When designing a CFRP EPT system with a profiled bar configuration to be installed onto soffits (e.g., slabs and bridge decks) or on the outer face of steel or concrete girder elements to maximize eccentricity, vertical clearance becomes a major factor. In buildings where false ceilings are used to accommodate air conditioning ducts and other utility lines and equipment, the possibility to extend deviators up to 150-200 mm without interfering with the usable living space enhances the potential to design effective solutions.

The introduction of an extendable deviator to combine eccentric axial PT forces in the CFRP bars and vertical reaction forces at specific locations provides a more efficient mechanism to increase flexural (and also shear) strength, to relieve tensile stresses, to reduce second order effects, and to recover vertical deflection, compared to systems where the tendon is straight. This may become critical when designing active systems aimed primarily at controlling short- and long-term deflections. The relative ease and rapidity of installation of the end anchors and of application of the PT forces (Gremel *et al.* 2006) decidedly enhance the cost-effectiveness of the solution proposed, which does not require complex and time-consuming operations such as adhesive bonding of post-tensioned elements, and use of hydraulic jacks and other special equipment, which may be impractical in some instances. The high CFRP tensile strength enables to design maintaining a considerable reserve capacity in the EPT bar, with enhanced flexibility to adjust the PT force by operating at both the live end and the intermediate deviator.

Laboratory validation of CFRP bar assembly

Uniaxial tensile tests were performed on five CFRP bar assemblies to assess the ability to reach the maximum bar strength without experiencing failure at the coupler attachments. The specimens consisted of 1220 mm long CFRP bars connected at either end with a swage coupler and a coupler adapter. Available bars with cross-sectional area A_b = 126.6 mm^2 were used to provide an upper-bound contact area with the coupler for a nominal diameter d_b = 12.7 mm, which has typically nominal A_b = 108.3 mm^2, thus simulating the most demanding boundary conditions for gripping. Two high-strength steel threaded rods were used to connect each specimen to the crosshead of an electromechanical testing machine with capacity of 534 kN. The tensile deformation was checked using an axial extensometer with gauge length of 152 mm up to a load of 50% of the nominal tensile strength, when the sensor was removed to prevent its damage. The ultimate deformation was measured from the machine cross-head displacement.

Table 1 reports the test results for each sample, including the measured ultimate load and the computed longitudinal elastic modulus (E_f), tensile strength (f_{fu}) and ultimate strain (ε_{fu}), and the observed failure modes. Failure always occurred in the CFRP bar at an average load of 239.7 kN, with failure modes being rupture of the carbon fibers (brooming) and cleavage, as depicted in Figure 2(a) and Figure 2(b), respectively.

STRUCTURAL IMPLICATIONS OF EPT SYSTEM CONFIGURATION

Post-tensioning forces introduced via an EPT system affect the short-term and, to a different extent depending on the time of installation and the loads to be carried, the long-

term deflections. A profiled bar (king-post) configuration is intuitively more effective in recovering vertical deflections by actively counteracting the self-weight and the superimposed permanent and live loads. In this section, the structural implications of relevant parameters that define geometry, flexural stiffness, and degree of end constraint or continuity of a single-span, one-way member to be upgraded are analyzed and discussed, along with the EPT system layout for basic straight and profiled tendon schemes. For clarity, all symbols introduced are reported in the List of Symbols, while only key symbols are defined in the text.

Structural efficiency and effect of boundary conditions

The typical case of a single-span, one-way structural member with uniform cross section, such as a bridge girder, a floor beam, or a slab strip, is illustrated in Figure 3. External post-tensioning is applied using straight and profiled tendons in symmetric arrangements, with a single midspan deviator for the latter. For the same amount of reinforcement and total PT force applied, T, the maximum (midspan) short-term deflection recovery using a straight and profiled bar scheme, respectively, is given by

$$\delta_S = \delta_{S,1} \tag{1}$$

and

$$\delta_P = \sum_{i=1}^{3} \delta_{P,i} \tag{2}$$

where the expressions for the single contributions to midspan uplift, $\delta_{S,1}$ and $\delta_{P,i}$, from the force and moment components introduced by post-tensioning and illustrated in Figure 4 are summarized in Table 2. Since second-order effects due to axial force components, $T\cos\alpha$, are neglected (but obviously should be considered in the analysis of stress relief),

the equations are valid irrespective of the translational stiffness at the simple support, k_Δ. The rotational stiffness, k_φ, characterizes the degree of end constraint or continuity along with k_Δ and is assumed the same at both ends. Linear behavior is considered by assuming constant flexural stiffness, *EI*, which is normally acceptable in preliminary analysis aimed at selecting candidate EPT schemes. This assumption is actually realistic in the case of steel and aluminum structural members, whereas in cracked reinforced and prestressed concrete members, a progressive increase in stiffness up to the value associated with the moment of inertia of the uncracked section is determined during application of the PT forces, as the cracks along the span length are closed.

A comparative measure of the structural efficiency of a profiled scheme with respect to its straight bar counterpart (i.e., being the sole difference the presence of an intermediate deviator extended by a length *D* and thus increasing the maximum eccentricity of the PT force from *e* to *e* + *D*) is given by the efficiency ratio of deflection recovery:

$$R_E = \frac{\delta_P}{\delta_S} \tag{3}$$

where δ_P and δ_S are the midspan uplift with profiled and straight bar scheme, respectively. For any k_φ, Equation 3 can be rendered in a nondimensional format as follows:

$$R_E\left(\eta,\kappa,\lambda,\mu\right) = \cos\alpha\left(\lambda\right) + 2\kappa\sin\alpha\left(\lambda\right)\frac{\left(1-2\mu\right)\left[1+4\mu+8\eta\left(1+\mu\right)\right]}{24\left(\mu+2\mu\eta+\eta\right)} \tag{4a}$$

where

$$\eta = \frac{EI}{k_\varphi L} \tag{4b}$$

$$\kappa = \frac{L}{2e} \tag{4c}$$

$$\lambda = \frac{D}{L_b} = \frac{D}{L - 2a} \tag{4d}$$

$$\mu = \frac{a}{L},\ 0 \le \mu \le \frac{1}{2} \tag{4e}$$

are nondimensional parameters that incorporate the relevant mechanical and geometric variables related to: 1) dimensions of the structural member (L); 2) flexural stiffness (EI); 3) degree of end constraints (k_φ); and 4) layout of the EPT schemes (L_b, e, D), where the angle of inclination of the longitudinal bar axis with respect to the straight position is $\alpha(\lambda) = \arctan(2\lambda)$. For relatively small distances d between the CFRP bar ends and the soffit of the one-way member having longitudinal axis at a depth $h / 2$, the parameter $\kappa = L / (h + 2d)$ reduces to a representative measure of the span-to-depth ratio, L / h.

The contributions to midspan uplift of each PT force and moment components in Figure 4 are also provided in nondimensional format in Table 2. For the limit cases of simple supports ($k_\varphi = 0$) and fixed ends ($k_\varphi = \infty$), Equation 4 reduces to the following two equations, respectively:

$$R_E(\kappa, \lambda, \mu) = \cos\alpha(\lambda) + 2\kappa \sin\alpha(\lambda) \frac{1 - \mu(3 - 4\mu^2)}{3(1 - 4\mu^2)} \tag{5a}$$

and

$$R_E(\kappa, \lambda, \mu) = \cos\alpha(\lambda) + 2\kappa \sin\alpha(\lambda) \frac{1 - 4\mu^2(3 - 4\mu)}{24\mu(1 - 2\mu)} \tag{5b}$$

respectively.

Beam with simple supports

In Figure 5, the efficiency ratio R_E for the simply supported case defined in Equation 5a is plotted as a function of D / L_b and for different values of a / L. The two cases presented, $\kappa = 15$ in Figure 5(a) and $\kappa = 40$ in Figure 5(b), are representative of upper and lower bounds of practical relevance where span-to-depth ratios in that range are typically encountered, such as in single-span RC slab highway bridges, non-prestressed concrete girders or steel I-girders, and thin prestressed concrete slabs in buildings, respectively. The diagrams show that the efficiency ratio increases almost linearly with the extended length of the deviator, with the anchors being kept at the same location (i.e., at constant μ for the same span length). The ratio also increases as the end anchors are positioned closer to the member supports, specifically at decreasing values of a (and $\mu = a / L$), to avoid areas subjected to relatively high tensile stresses, where stress concentrations may become of concern for either post-installed anchors in concrete or fastened connections to metallic elements.

Beam with rotational end constraints

The benefit of a profiled EPT scheme is capitalized as the degree of rotational constraint at the ends becomes significant, such as in case of continuous spans or bays with intermediate supports or integral connections with structural walls. In fact, the maximum eccentricity, $e + D$, can be provided at selected sections away from the ends, thereby resulting in more effective PT moment diagrams and uplift while correctly positioning the end anchors close to the supports. When straight tendons are used, as in Figure 3(a), with an applied PT moment $M_{PT} = (T\cos\alpha)e$, a relatively high reaction moment M_R with

absolute value

$$\left|M_R\right| = \left|M_{PT}\right| \frac{L - 2a}{2\left(\frac{EI}{k_\varphi} + \frac{L}{2}\right)},\ 0 \le a \le \frac{L}{2} \tag{6}$$

may be produced at increasing values of rotational end stiffness k_φ and as the end anchors are located closer to the member supports. The concept is illustrated in the three sketches in Figure 6(a). The first sketch represents the most favorable condition when the PT moment is applied at a given distance a from simply supported ends (M_R = 0). The second sketch shows how the effective portion of PT moment is decreased when the member ends are fixed, and positioning the end anchors at a greater distance from the ends as in the third sketch may be necessary to attain the uplift sought. In Figure 6(b), the ratio

$$\left|\frac{M_R}{M_{PT}}\right| = \frac{1 - 2\mu}{1 + 2\eta} \tag{7}$$

is plotted for as a function of a / L and for four different degrees of end constraint, including the limit cases of simple supports and fixed ends. Higher $|M_R / M_{PT}|$ ratios, with upper limits obviously reached in the case of fixed ends, translate into a less efficient distribution of the post-tensioning bending moments, with a detrimental effect on the uplift capacity. This effect is illustrated in Figure 7, where the midspan uplift at a given span-to-depth ratio normalized with respect to the upper limit for end anchors installed at simple supports (a = 0 and k_φ = 0)

$$\frac{\delta_S}{\delta_{S\,(a=0,k_\varphi=0)}} = \frac{\delta_S}{M_{PT}L^2/8EI} = 1 - 4\mu^2 - \left(\frac{1 - 2\mu}{1 + 2\eta}\right) \tag{8}$$

is plotted as a function of a / L. Four curves are shown where the two limiting ones

correspond to: a) dashed line $k_\varphi = 0$, where the maximum (unit) value is reached by imparting the PT moment M_{PT} at the simple support sections; and (b) solid line $k_\varphi = \infty$, where the maximum uplift is produced when the PT moment M_{PT} is applied at a distance $a = 0.25L$; obviously, no uplift is produced when M_{PT} is applied at the fixed end sections ($|M_R / M_{PT}| = 1$).

The efficiency ratio R_E for the case of single-span one-way members with fixed ends, defined in Equation 5b, is plotted in Figure 8 as a function of D / L_b and for different values of a / L. Again, an almost linear increase at constant a / L can be observed, although with improved benefit compared to the simply supported case. Therefore, the use of profiled EPT bars compliant with clearance limitations may enable to attain deflection recovery levels otherwise impractical, while positioning the end anchors close enough to the supports.

Post-tensioning forces applied via deviators and selection of bar diameter and number

In the EPT system presented, the design PT force in each CFRP bar, T / n_b, is applied in two separate steps, first at the live ends (T_e) and following by engaging the extendable deviator (T_d). For a given bar number and diameter, n_b and d_b, the combination of T_e and T_d depends on the extended length of the deviator, D, and the bar length, L_b, and therefore on their ratio λ as defined in Equation 4d, which may often be the controlling factor due to clearance limitations. In the base configuration in Figure 3, moving from the selected T and λ, T_e can be back-calculated via the following algorithm:

$$T_e = \frac{T}{n_b} - T_d(\lambda) \tag{9a}$$

$$T_d(\lambda) = \left(\sqrt{4\lambda^2 + 1} - 1\right) E_f A_b, \ \lambda \le \lambda_{\max} \tag{9b}$$

where $T_d(\lambda)$ is directly computed by imposing deformation compatibility and is plotted in Figure 9 for each bar diameter. The parameter λ cannot exceed the limit defined by rearranging Equation 9b as

$$\lambda_{\max} = \frac{1}{2}\sqrt{\left[1 + \left(\varepsilon_{d,\max}\right)\right]^2 - 1} \tag{10a}$$

$$\varepsilon_{d,\max} = 0.55\varepsilon_{fu} - \left(\varepsilon_e + \varepsilon_{curv}\right) \tag{10b}$$

where $\varepsilon_{d,\max}$ is the allowable uniform tensile strain in the CFRP bar introduced by engaging the deviator and is determined as the difference between the allowable strain upon application of the total PT force, $0.55\varepsilon_{fu}$ (ACI 2004), and the maximum tensile strain from: a) the PT force applied from the live end, limited to $\varepsilon_e \le 0.25\varepsilon_{fu}$ to allow performing the post-tensioning in a straightforward manner and without concerns of twisting the bars, as observed in tests aimed at assessing the ease of installation and application of the PT forces; and b) the local bending at the deviator plate having contact surface with radius of curvature R, which introduces a local maximum tensile strain ε_{curv}. Due to the relatively high values of R relevant to design, ε_{curv} can be accurately computed as $d_b / 2R$ for any practical purposes and is plotted in Figure 10 as a ratio to the ultimate CFRP strain, ε_{fu}, for d_b = 6.3 mm, 9.5 mm or 12.7 mm.

Equation 9 and Equation 10 provide the rationale to iteratively select the bar number and diameter, n_b and d_b, depending on the EPT system configuration and total PT force, as

well as refining the design, as detailed in the flowchart in Figure 11. When the extension needed for the deviator is excessive either due to clearance limitations (i.e., $D > D_{max}$) or because $\lambda > \lambda_{max}$ (i.e., the PT force sought introduced by engaging the deviator, T_d, cannot be reached since $\varepsilon_{b,max} > 0.55\varepsilon_{fu}$, where $\varepsilon_{b,max}$ is the maximum tensile strain in the CFRP bar introduced by post-tensioning), the use of alternative configurations with additional bars and/or larger diameter and/or multiple deviators may be considered.

Design of adhesive anchors in concrete

The design of anchors fastened to steel members is addressed in the AISC Specifications (AISC 2001). In the case of concrete members, despite the extensive use of post-installed adhesive anchors in practice, the design provisions in ACI 318-05 (ACI 2005) only cover post-installed and cast-in-place mechanical anchors. Design guidelines for adhesive anchors are usually provided by the manufacturers, including failure criteria for combined shear and tension loads, V and N, and allowable loads, V_{all} and T_{all}, for different embedment lengths and anchor diameters. Typically, the failure criterion adopted for combined design shear and tension forces is that of the AC58 product evaluation standard accepted by ICC-ES (2005), which mimics that for mechanical anchors in ACI 318-05 (ACI 2005):

$$\left(\frac{V}{V_{all}}\right)^{\frac{5}{3}} + \left(\frac{N}{N_{all}}\right)^{\frac{5}{3}} \leq 1, \tag{11}$$

where V_{all} and T_{all} are obtained by applying a factor of safety of four to the average ultimate strength in shear and tension obtained experimentally for a given anchor diameter and embedment length (ICC-ES 2005).

The bonded anchors should be designed to allow the design strength of the CFRP bar to be attained. The load components acting on each tee-shaped end anchor are sketched in Figure 12(a), while Figure 12(b) shows the allowable design domain [V / V_{all}, N / N_{all}] for each bonded threaded rod subjected to maximum shear and tension. The forces acting on the critical (exterior) anchors are $V = 0.5\,(0.55F_u \cos\alpha)$ and $N = 0.5\,(0.55F_u \sin\alpha) + N_d$, where N_d is the tension force contribution produced by the force couple $0.5\,(0.55F_u \sin\alpha)$ d, d being the minimum distance between the center of the tee-anchor eye and the contact surface between tee-anchor base plate and concrete.

SUMMARY

A novel EPT system for deflection control of flexural members has been presented. The system consists of an unbonded CFRP bar used as a tendon and an anchor that allows the development of the bar strength. The PT force can be applied by pulling the bar at one end and by pushing down an extendable deviator. The combination of tendon length and location of anchors along the flexural member in addition to the dual mode to generate force in the bar (pulling and pushing) allow for the optimization of an EPT system. Geometry and degree of end constraint of the flexural member are also critical for the design.

The structural implications of relevant geometric and mechanical parameters for the design and analysis of EPT systems aimed at controlling deflection of single-span, one-way members have been analyzed. The improved structural efficiency of a profiled bar configuration with respect to its straight bar counterpart becomes more significant as: a)

the degree of rotational constraint or continuity at the supports increases, which is representative of real case scenarios; and b) the end anchors are positioned closer to the member supports, which is typically required to minimize the effect of tensile stresses on either mechanical anchors in metallic members or post-installed mechanical and adhesive anchors in concrete. When evaluating the use of profiled EPT bars for deflection control, clearance limitations and cost-benefit considerations become important factors that may in some circumstances offset efficiency as defined from a purely structural standpoint.

LIST OF SYMBOLS

a = distance of end anchors from supports.

A_b = cross sectional area of CFRP bar.

d = minimum distance between center of tee-anchor eye (end of bar) and contact surface between anchor base plate and rehabilitated member.

d_b = diameter of EPT CFRP bar.

D = extended length of deviator.

D_{max} = maximum extended length of deviator due to clearance limitations.

e = eccentricity of end anchors with respect to longitudinal axis of one-way member.

E_f = longitudinal modulus of elasticity of CFRP.

EI = flexural stiffness of uniform cross section.

f_{fu} = tensile strength of CFRP.

F_u = axial load capacity of CFRP bar.

h = depth of uniform cross section.

I = moment of inertia of uniform cross section.

k_Δ = translational stiffness at simple support.

k_φ = rotational stiffness at simple support.

L = length of one-way member span.

L_b = length of EPT bar.

M_{PT} = applied PT moment at end anchor sections.

M_R = reaction moment at one-way member ends produced by applied PT moment.

n_b = number of EPT bars.

N = tension force on adhesive bonded anchor.

N_{all} = allowable tension force on adhesive bonded anchor.

N_d = tension force produced by force couple $0.5(F_u \sin\alpha)d$ on adhesive bonded anchor.

R = radius of curvature of deviator plate in contact with EPT bar.

R_E = efficiency ratio for deflection recovery of profiled to straight bar counterpart.

T = total PT force applied to n_b EPT bars.

T_d = post-tensioning force applied in each bar by engaging deviator.

T_e = post-tensioning force applied in each bar from live end.

V = shear force on adhesive bonded anchor.

V_{all} = allowable shear force on adhesive bonded anchor.

α = angle of inclination of longitudinal axis of profiled EPT bar with respect to straight configuration.

$\delta_{P,i}$ = contribution to maximum uplift for profiled bar configuration from *i*-th force and moment components introduced by post-tensioning.

$\delta_{S,1}$ = maximum uplift for straight bar configuration.

$(\delta_S)_{norm}$ = maximum uplift for straight bar configuration normalized with respect to limit case of simply supported member with end anchors at supports (a = 0, k_φ = 0).

$\varepsilon_{b,\max}$ = maximum tensile strain in CFRP introduced by post-tensioning.

ε_{curv} = maximum tensile strain in EPT bar due to local bending at the deviator plate.

ε_d = uniform tensile strain in CFRP bar produced by T_d.

$\varepsilon_{d,\max}$ = allowable uniform tensile strain in CFRP bar produced by T_d.

ε_e = uniform tensile strain in CFRP bar produced by T_e.

ε_{fu} = ultimate tensile strain of CFRP.

η = $EI / k_\varphi L$.

κ = $L / 2e = L / (h + 2d)$.

λ = $D / L_b = D / (L - 2a)$.

$\lambda_{\max}$ = upper bound value for λ.

μ = a / L.

σ_m = net stress on member surface at end anchor sections.

σ_{lim} = limiting value of net stress on member surface at end anchor sections.

ACKNOWLEDGMENTS

The financial support of the NSF Industry-University Cooperative Research Center "Repair of Buildings and Bridges with Composites" (RB^2C) at the University of Miami, and the technical support of the Center's member Hughes Brothers, Inc., are gratefully acknowledged.

REFERENCES

ACI Committee 318, "Building code requirements for structural concrete," *ACI 318-05*, American Concrete Institute, Farmington Hills, MI, 2005.

ACI Committee 440, "Prestressing concrete structures with FRP tendons," *ACI 440.4R-04*, American Concrete Institute, Farmington Hills, MI, 2004.

Ahmadi-Kashani K., "Strengthening box-girder bridges using external post-tensioning," *Proc. 5th International Conference on Bridge Management (BM 5)*, Guildford, UK, 11-13 April 2005, pp. 97-104.

American Institute of Steel Construction (AISC), "Manual of steel construction – Load and resistance factor design," 3rd edition, AISC, Chicago, IL, 2001.

Andrä, H.-P., and Maier, M., "Instandsetzung von brücken mit einer neuen generation von spanngliedern auf basis von CFK-bändern (Rehabilitation of bridges by a new generation of tendons based on CFRP)," *Bauingenieur*, V. 80, 2005, pp. 7-16.

Berset, T., "Development of a post-tensioning system using unbonded CFRP tendons," *Proc. 4th PhD Symposium in Civil Engineering*, Munich, 19-21 Sept. 2002. 6 pp.

Basler, M., Clénin, R., and Desroches, M., "Bridge strengthening with prestressed CFRP plate systems," *Proc. 4th International Conference on Advanced Composite Materials in Bridges and Structures (ACMBS IV)*, Calgary, Alberta, Canada, 20-23 July 2004. 8 pp.

Choi, K.-S., You, Y.-C., Park, Y.-H., Park, J.-S., and Kim, K.-H., "Behavior of RC beams strengthened with externally post-tensioning CFRP strips," *Fiber reinforced composite reinforcement for concrete structures – FRPRCS-7 (ACI SP-230)*, American Concrete Institute, Farmington Hills, MI, 2006, pp. 515-527.

Daly, A. F., and Witarnawan, W., "Strengthening of bridges using external post-tensioning," *Paper PA3307/97*, Transportation Research Laboratory, Berkshire, UK, 1997. 17 pp.

El-Hacha, R., and Elbadry, M., "Strengthening concrete beams with externally prestressed carbon fiber composite cables: experimental investigation," *PTI Journal*, V. 4, No. 2, 2006, pp. 53-70.

Emmons, P. H, "Concrete repair and maintenance illustrated," RS Means, Kingston, MA, 1993, 295 pp.

Grace N. F., and Abdel-Sayed, G., "Behavior of CFRP externally draped tendons in prestressed concrete bridges," *PCI Journal*, V. 43, No. 5, 1998a, pp. 88-101.

Grace N. F., and Abdel-Sayed, G., "Ductility of prestressed bridges using CFRP strands," *Concrete International*, V. 20, No. 6, 1998b, pp. 25-30.

Grace N. F., and Abdel-Sayed, G., "Continuous CFRP prestressed concrete bridges," *Concrete International* V. 21, No. 10, 1999, pp. 42-47.

Gremel, D., Koch, R., Nanni, A., and Matta, F., "Externally post-tensioned CFRP system for deflection control of reinforced concrete slabs – Volume II: installation guide," *Report CAE 06-02*. Department of Civil, Architectural and Environmental Engineering, University of Miami, Miami, FL, 2006, 27 pp.

ICC Evaluation Service, Inc., "Acceptance criteria for adhesive anchors in concrete and masonry elements," *AC58*. ICC-ES, Whittier, CA, 2005.

Klaiber, F. W., Dunker, K. F., Wipf, T. J., and Sanders, W. W. Jr, "Methods of strengthening existing highway bridges," *NCHRP Report 293*, Transportation Research Board, Washington, D.C., 1987.

Klaiber, F. W., Wipf T. J., and Fanous, F. S., "Strengthening of two continuous-span steel stringer bridges," *Construction and Building Materials*, V. 12, No. 2-3, 1998, pp. 151-159.

Krauser, L., "Repairs, modifications, and strengthening with post-tensioning," *PTI Journal*, V. 4, No. 1, 2006, pp. 24-40.

Lees, J. M., Winistörfer, A. U., and Meier, U., "External prestressed carbon fiber-reinforced polymer straps for shear enhancement of concrete," *Journal of Composites for Construction* V. 6, No. 4, 2002, pp. 249-256.

Li, W., Albrecht, P., and Saadatmanesh, H., "Strengthening of composite steel-concrete bridges," *Journal of Structural Engineering*, V. 121, No. 12, 1995, pp. 1842-1849.

Mutsuyoshi, H., "Present situation of durability of post-tensioned PC bridges in Japan," *Durability of post-tensioning tendons – fib Bulletin 15*. Fédération Internationale du Béton, Lausanne, Switzerland, 2001, pp. 75-88.

Naaman, A. E., and Breen J. E., editors, "External prestressing in bridges," *ACI SP-120*, American Concrete Institute, Farmington Hills, MI, 1990, 458 pp.

Nanni, A., "Innovation in structural engineering: strengthening with composites and in-situ load testing," *Proc. 2nd fib Congress*, Naples, Italy, 5-8 June 2006. 12 pp.

Nanni, A., Matta, F., and Galati, N., "Externally post-tensioned CFRP system for deflection control of reinforced concrete slabs – Volume I: design and analysis. *Report CAE 06-01*. Miami, FL: Department of Civil, Architectural and Environmental Engineering, University of Miami, 2006. 92 p.

Phares, B. M., Wipf, T. J., Klaiber, F. W., Abu-Hawash, A., and Lee Y.-S., "Strengthening of steel girder bridges using FRP," *Proc. 2003 Mid-Continent Transportation Research Symposium*, Ames, IA, 21-22 August 2003. 12 pp.

Schnerch, D. A., "Strengthening of steel structures with high-modulus carbon fiber reinforced polymer (CFRP) materials," Ph.D. dissertation, Department of Civil, Construction, and Environmental Engineering, North Carolina State University, 2005. 265 pp.

Shang, S., Jin, Y., Peng, H., Wang, M., and Leng, Q., "Reinforcement technology by prestressed carbon fiber reinforced plastics (CFRP)," *Proc. 3rd International Conference on Composites in Civil Engineering (CICE 2006)*, Miami, FL, 13-15 December 2006, pp. 479-482.

Tan, K. H., and Saha, M. K., "Long-term deflections of reinforced concrete beams externally bonded with FRP system," *Journal of Composites for Construction*, V. 10, No. 6, 2006, pp. 474-482.

Zoghi, M., "Post-strengthening prestressed concrete bridges via post-tensioned CFRP-laminates," *SAMPE Journal*, V. 42, No. 2, 2006, pp. 24-30.

TABLES

Table 1 – Results of uniaxial tensile tests on Ø12.7 mm CFRP bar assemblies.

Sample ID	Failure load, F_u (kN)	Tensile strength, $f_{fu} = F_u / A_b$ (MPa)	Longitudinal elastic modulus, E_f (GPa)	Ultimate strain, $\varepsilon_{fu} = f_{fu} / E_f$ (με)	Failure mode
1	228.8	1806.6	135.8	13301	Brooming
2	261.8	2067.1	137.9	14991	Mixed brooming/ cleavage
3	223.0	1760.9	131.7	13372	Brooming
4	235.1	1856.7	137.2	13532	Brooming
5	249.6	1970.6	137.9	14290	Cleavage
Mean	239.7	1892.4	136.1	13897	-
Standard deviation	15.8	125.1	2.6	727	-

Table 2 – Dimensional and nondimensional expressions for midspan uplift produced by PT forces and couples in Figure 4 (second-order effects due to axial compression force neglected).

Boundary conditions	$\delta_{S,1}$ ($\alpha = 0$), $\delta_{P,1}$	$\delta_{P,2}$	$\delta_{P,3}$
Any	$(T\cos\alpha)e\left[\dfrac{L^2-4a^2}{8EI}-\dfrac{L^2(L-2a)}{16EI\left(\dfrac{EI}{k_\varphi}+\dfrac{L}{2}\right)}\right]$ $\dfrac{\cos\alpha}{16\kappa}\left[1-4\mu^2+\left(\dfrac{2\mu-1}{2\eta+1}\right)\right]$	$2(T\sin\alpha)\left[\dfrac{L^3}{48EI}-\dfrac{L^4}{128EI\left(\dfrac{EI}{k_\varphi}+\dfrac{L}{2}\right)}\right]$ $\dfrac{\sin\alpha}{96}\left(\dfrac{8\eta+1}{2\eta+1}\right)$	$-(T\sin\alpha)\left[\dfrac{a(3L^2-4a^2)}{24EI}-\dfrac{aL^2(L-a)}{16EI\left(\dfrac{EI}{k_\varphi}+\dfrac{L}{2}\right)}\right]$ $-\sin\alpha\left\{\dfrac{\mu\left[\begin{matrix}(3-4\mu^2)(2\eta+1)\\-3(1-\mu)\end{matrix}\right]}{24(2\eta+1)}\right\}$
$k_\varphi = 0$ ($\eta = \infty$)	$(T\cos\alpha)e\dfrac{L^2-4a^2}{8EI}$ $\dfrac{\cos\alpha}{16\kappa}(1-4\mu^2)$	$2(T\sin\alpha)\dfrac{L^3}{48EI}$ $\sin\alpha\left(\dfrac{1}{24}\right)$	$-(T\sin\alpha)\dfrac{a(3L^2-4a^2)}{24EI}$ $-\sin\alpha\left[\dfrac{\mu(3-4\mu^2)}{24}\right]$
$k_\varphi = \infty$ ($\eta = 0$)	$(T\cos\alpha)e\dfrac{a(L-2a)}{4EI}$ $\dfrac{\cos\alpha}{8\kappa}\left[\mu(1-2\mu)\right]$	$2(T\sin\alpha)\dfrac{L^3}{192EI}$ $\sin\alpha\left(\dfrac{1}{96}\right)$	$-(T\sin\alpha)\dfrac{a^2(3L-4a)}{24EI}$ $-\sin\alpha\left[\dfrac{\mu^2(3-4\mu)}{24}\right]$

FIGURES

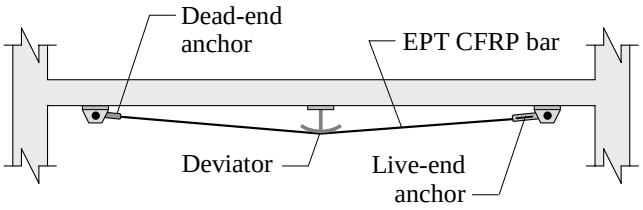

(a)

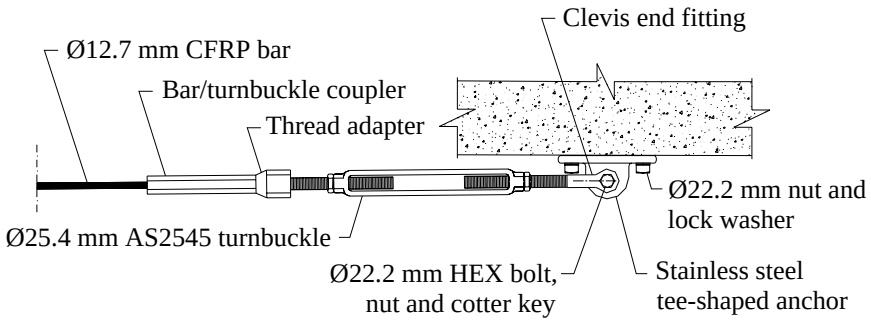

(b)

(c)

Figure 1 – Externally post-tensioned CFRP system: (a) schematic of base configuration; (b) live-end anchor for Ø12.7 mm bar; and (c) trial installation onto slab soffit.

(a)

(b)

Figure 2 – Tensile testing of Ø12.7 mm CFRP bar assembly: (a) failure resulting in brooming; and (b) cleavage.

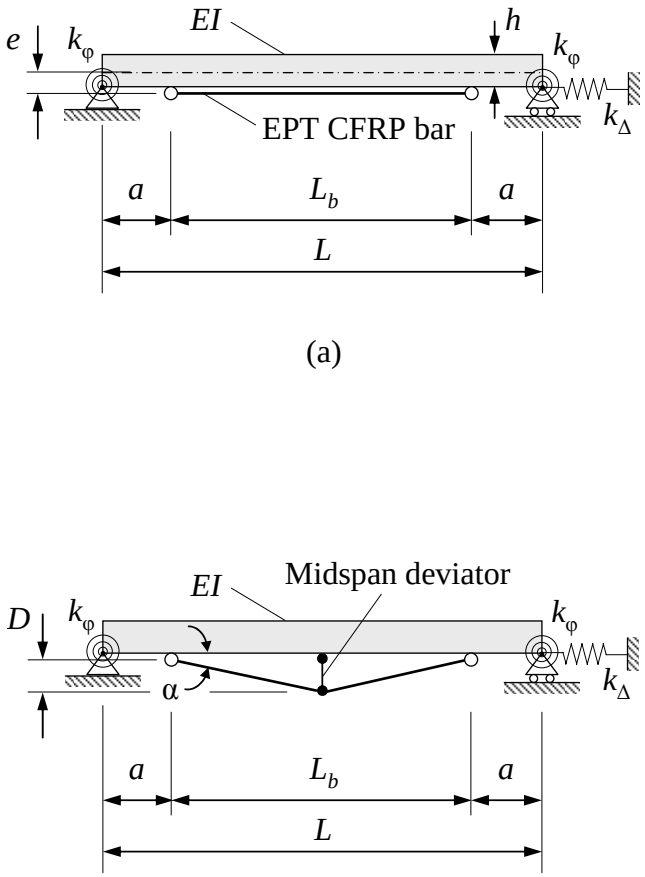

Figure 3 – Schematic of single-span member with EPT system: (a) straight bar scheme with PT force applied at live end; and (b) profiled bar scheme with extendable midspan deviator.

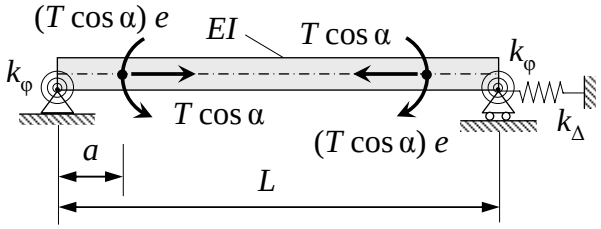

(a)

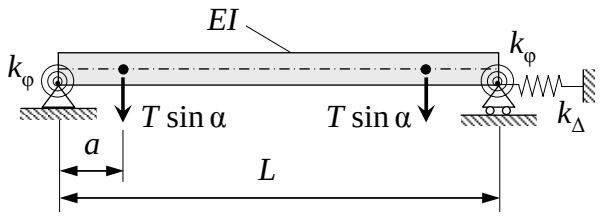

(b)

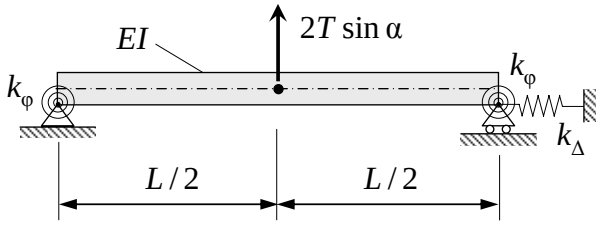

(c)

Figure 4 – Schematic of PT force and bending moment components producing maximum uplift: (a) $\delta_{S,1}$ ($\alpha = 0$) and $\delta_{P,1}$; (b) $\delta_{P,2}$; and (c) $\delta_{P,3}$.

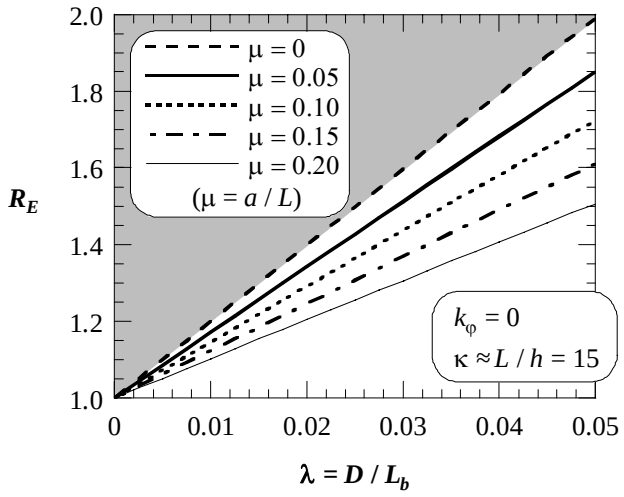

(a)

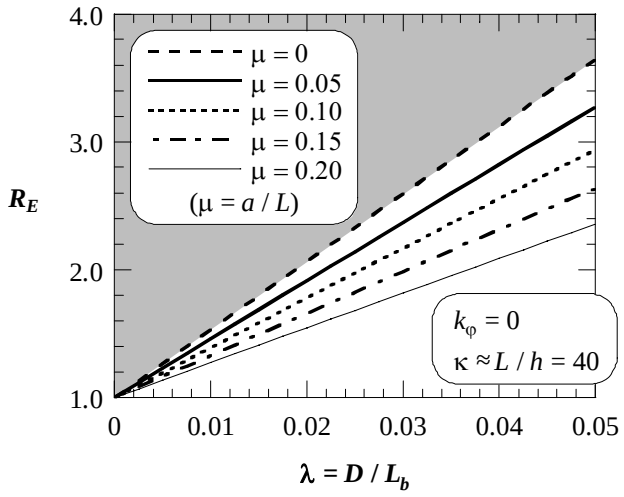

(b)

Figure 5 – Efficiency ratio for deflection recovery with respect to D / L_b and a / L for simply supported end condition ($k_\varphi = 0$): (a) $\kappa \approx L / h = 15$; and (b) $\kappa \approx L / h = 40$.

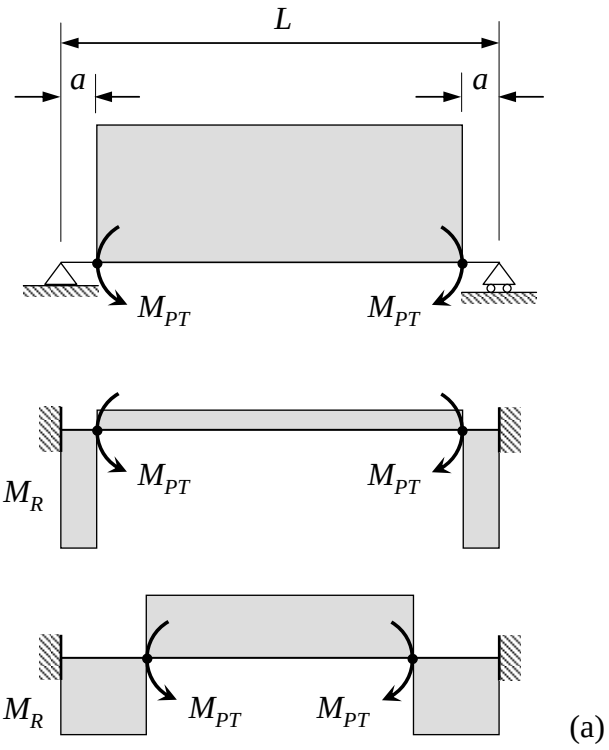

(a)

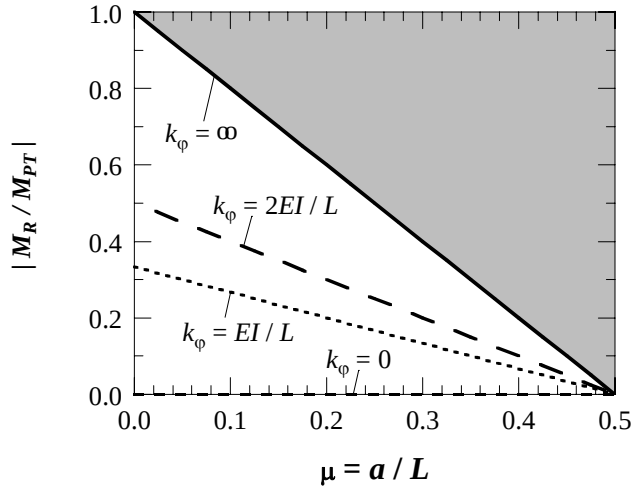

(b)

Figure 6 – Effect of boundary conditions and distance of anchors from supports on effective PT moment along L: (a) schematic; and (b) ratio of reaction moment to applied PT moment as function of a / L at different values of rotational stiffness k_φ.

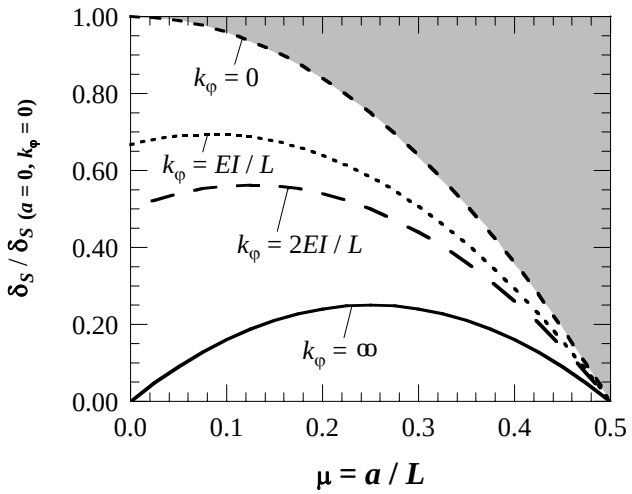

Figure 7 – Normalized midspan uplift produced by same PT force as function of a / L at different values of rotational stiffness k_φ. Values normalized with respect to limit case of anchors located at ends of simply supported member (a = 0 and k_φ = 0).

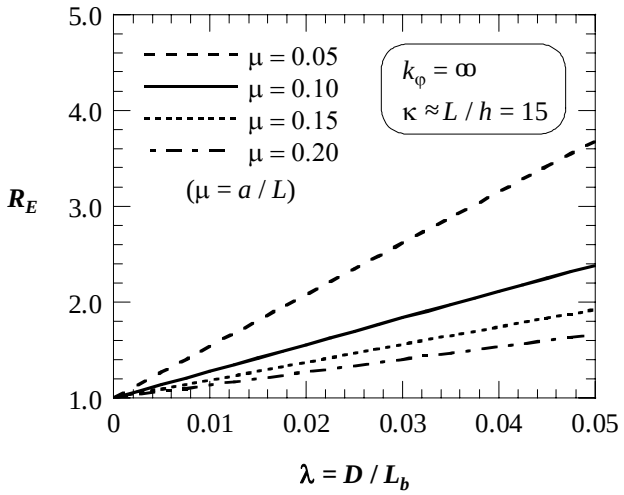

(a)

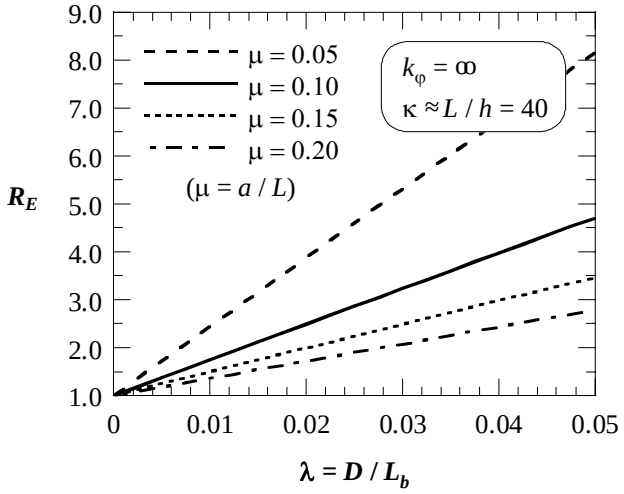

(b)

Figure 8 – Efficiency ratio for deflection recovery with respect to D / L_b and a / L for fixed end condition ($k_\varphi = \infty$): (a) $\kappa \approx L / h = 15$; and (b) $\kappa \approx L / h = 40$.

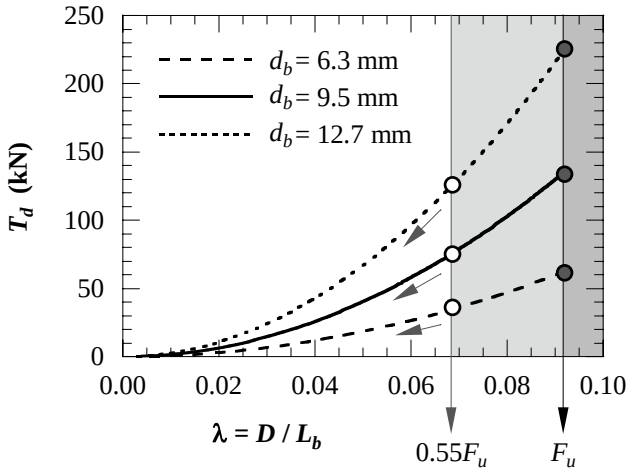

Figure 9 – Plot of PT force applied by engaging deviator as function of D / L_b for different bar diameters. Filled and blank circles indicate ultimate and allowable axial force, respectively. Arrows indicate reduction in usable capacity due to applied T_e and curvature of contact plate.

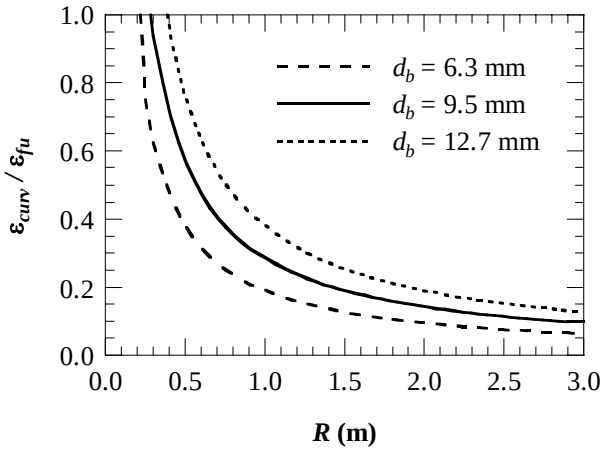

Figure 10 – Ratio $\varepsilon_{curv} / \varepsilon_{fu}$ as function of radius of curvature of deviator plate in contact with CFRP bar.

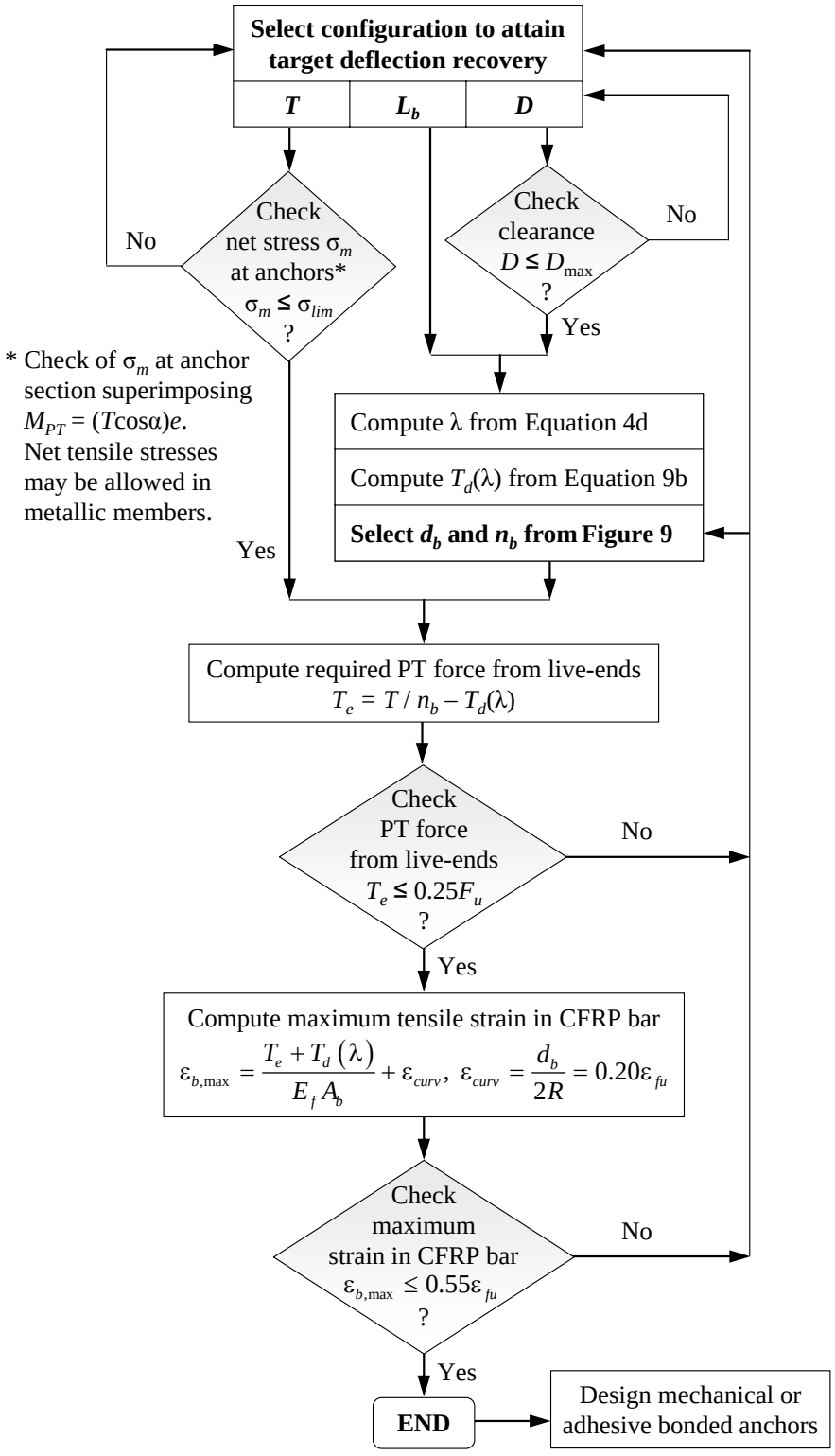

Figure 11 – Design flowchart for EPT system.

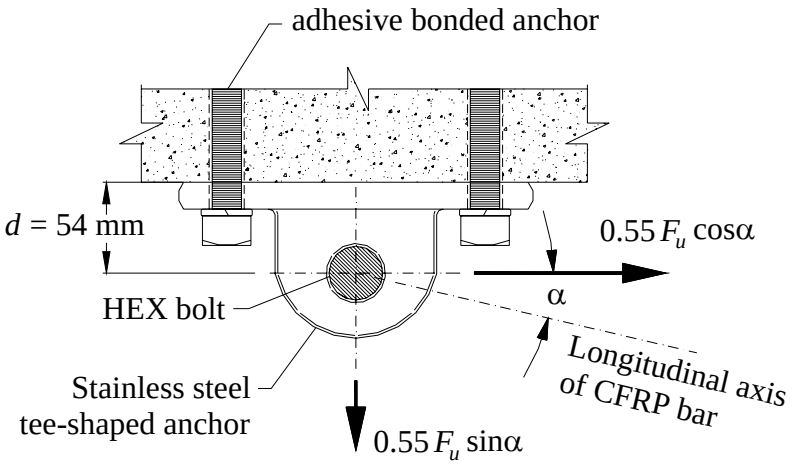

(a)

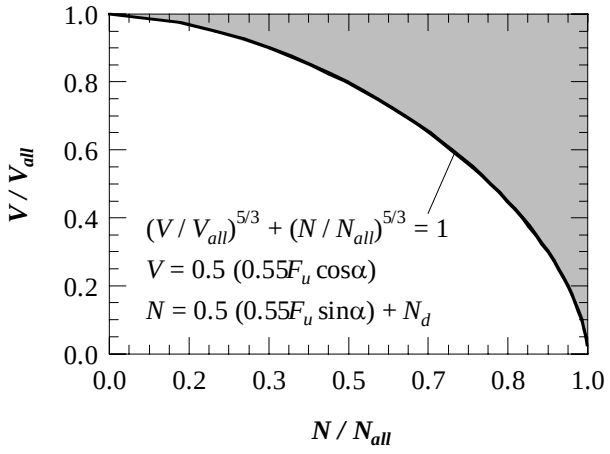

(b)

Figure 12 – Design of post-installed adhesive anchors in concrete: (a) force components on tee-anchor; and (b) design failure envelope for combined tension and shear.

PAPER 3

MEASUREMENT OF DISTRIBUTED STRAIN IN STEEL BRIDGE: VALIDATION THROUGH DIAGNOSTIC LOAD TEST

Fabio Matta[a,*], Filippo Bastianini[a], Nestore Galati[a], Paolo Casadei[b], and Antonio Nanni[c]

[a] Center for Infrastructure Engineering Studies, University of Missouri-Rolla

[b] Tec.Inn. S.r.l. – Innovative Technologies

[c] Dept. of Civil, Architectural and Environmental Engineering, University of Miami

ABSTRACT

Fiber optic sensing technologies are emerging as valid alternatives for the health monitoring of civil structures. Distributed sensors based on Brillouin scattering add the unique capability of measuring strain and temperature profiles along optical fibers. Measurement is performed by establishing the correlation between fiber strain and temperature, and the frequency shift of the Brillouin backscattered light induced by a monochromatic light pulse. The technology holds potential for use on large structures and integrated transportation infrastructure. Its effectiveness has been assessed through

---

* Graduate Research Assistant. Corresponding author – 220 Engineering Research Laboratory, 1870 Miner Circle, 65409-0710 Rolla, MO, USA. Tel +1 (573) 341-6661, Fax -6215, E-mail: *mattaf@umr.edu*.

scaled laboratory experiments, whereas field validation is limited to very few demonstration projects conducted to date. This paper presents a pilot application of Brillouin Optical Time Domain Reflectometry (BOTDR) to measure strain profiles along the high performance steel (HPS) girders of a multi-span slab-on-girder bridge subjected to diagnostic load testing. One of the exterior continuous girders required heat-straightening after falling during construction due to wind. The significance of applying a distributed measurement technique lies in the potential to assess the global girder response, which would be impractical and uneconomical using discrete measurement techniques. A 1.16 km long sensing circuit was installed onto the web of four girders for a length of up to 80 m on two continuous spans. The circuit comprises bare optical fiber sensors, and a novel adhesively bonded fiberglass tape with embedded sensing fibers for strain measurement and thermal compensation. The strain profiles were first converted into deflection profiles and validated against discrete deflection measurements performed with a state-of-the-art, high-precision total station system. Structural assessment based on comparison of the strain profiles with the results of three-dimensional finite element analysis of the bridge superstructure, and with specification mandated criteria, indicated that the response of the girder under investigation was within the design limits, and did not pose serviceability concerns.

Keywords: Bridge tests; Fiber optics; Monitoring; Sensors; Structural assessment.

INTRODUCTION

Recent advances in fiber optic sensor (FOS) technologies have fostered the development of innovative solutions for the health monitoring of civil engineering structures (Uttamchandani 1994, Casas and Cruz 2003, Li *et al.* 2004). Compelling advantages of FOSs over conventional electrical sensors such as resistance strain gauges are the easy embeddability, due to their light-weight, high degree of miniaturization, and corrosion and chemical resistance; the multiplexability that allows to series-connect multiple FOSs; the immunity to electromagnetic fields, due to the sensors dielectric nature; and the suitability for remote monitoring.

Brillouin Optical Time Domain Reflectometry (BOTDR) FOSs based on Brillouin scattering (Brillouin 1922) add the unique ability to measure the long-range (of the order of tens of km) distributed strain and temperature along standard telecom-grade optical fibers, otherwise attainable in a quasi-distributed fashion only with several sensors applied at discrete locations. In addition, access to only one end of a sensing fiber is required, thereby enabling measurements even in case of damage or interruption of the sensing circuit at a random point. The technology holds significant potential for the health monitoring of large structures, including bridges, buildings, dams, nuclear reactors, pipelines, stadiums, tunnels (Komatsu *et al.* 2002), and, in perspective, integrated transportation systems (Fujihashi *et al.* 2003).

Advancing the validation of BOTDR techniques is critical to address the development of monitoring systems with improved accuracy and spatial resolution tailored for civil

applications. However, very few demonstrative field applications have substantiated the promising outcomes of a number of large-scale laboratory experiments (Naruse *et al.* 2000, Yasue *et al.* 2000, Bastianini *et al.* 2003, Murayama *et al.* 2003, Wu *et al.* 2006).

Thévenaz *et al.* (1998) used a sensing system based on stimulated Brillouin scattering to monitor the temperature of concrete during the curing process of a 15×20×3 m^3 casting in a dam in Luzzone (Switzerland), and to observe the temperature fluctuations of deep waters in relation with seasonal conditions in the Lake of Geneva. Ohno *et al.* (2002) measured the vertical strain of two cast-in-place concrete foundation piles with diameter of 1.2 m and length of 11.0 m and 7.6 m, respectively, which were tested to evaluate the contribution of frictional forces to the bearing capacity. FOSs were installed into grooves cut along the steel rebars and filled with epoxy resin. Shi *et al.* (2003) report on the six-month monitoring of a 750 m portion of the concrete box structure of the Gulou Tunnel in Nanjing (P.R. of China), whose deformations were verified to lie within the safety limits. Kihara *et al.* (2002) measured strains in the Nyodo River (Japan) levee to assess effectiveness in detecting early stages of collapse due to water penetration. Bastianini *et al.* (2005a) used a BOTDR system to measure the deformations of externally bonded "smart" fiber reinforced polymer (FRP) sheets with embedded FOSs, which were used for the seismic retrofit of masonry vaults and walls of the historical Elmi-Pandolfi building (1600) in Foligno, Italy, during an in-situ load test. In another field project on two small concrete bridges subjected to load test, Bastianini *et al.* (2005c) used bonded "smart" FRP tapes to assess effectiveness with respect to stand-alone FOS cables.

This paper presents a pilot application of BOTDR for the distributed strain measurement in the high performance steel (HPS) I-girders of a multi-span highway bridge in Missouri, USA, which was subjected to a diagnostic load test. The research objectives were to:

- assess the structural response of an exterior girder that had required heat-straightening after falling during construction from a height of about 15 m, due to the effect of high wind. The implementation of a distributed measurement technique becomes relevant to attempt studying the global girder response, when discrete measurement techniques present objective practical and economical limitations;
- evaluate the performance of a commercially available BOTDR system in conjunction with a novel fiberglass tape with embedded FOSs for strain and temperature measurement, when implemented on a large bridge structure subjected to controlled loads, and with the FOSs being installed in the field and in non-artificial conditions compared to that of the laboratory.

First, the measured strain profiles are rendered as deflection curves and validated against benchmark vertical displacements measured at discrete locations using a state-of-the-art high-precision Automated Total Station (ATS) system. Then, the validated strain measurements are discussed and compared to the theoretical strains from three-dimensional finite element analysis, and from one-dimensional beam analysis that accounts for the girder load distribution factor mandated by the specifications used in design (MoDOT 2002).

BOTDR SENSING PRINCIPLES

Spontaneous Brillouin scattering arises from the interaction between optical and acoustic waves propagating in the same physical medium. When the medium is illuminated with a monochromatic light source, a partial energy transfer occurs between the colliding photons and phonons, the latter being generated by either pressure or temperature fluctuations. The resulting change in density of the medium, and therefore in its refractive index and mechanical properties (elastic modulus and Poisson's ratio), determines a Doppler-shift in the frequency of the backscattered photons (Brillouin, 1922), which is given by

$$\nu_B = 2nV_a / \lambda , \qquad ...(1)$$

where n = refractive index, V_a = velocity of acoustic wave, and λ = wavelength of incident light. Recently developed techniques have enabled to scan the Brillouin scattered light spectrum in single-mode optical fibers with high resolution by using a coherent receiver. The Brillouin frequency shift was found to increase linearly with strain (Horiguchi *et al.* 1989) and temperature (Kurashima *et al.* 1990), i.e.,

$$\nu_B(\varepsilon) \approx \nu_B(0)\left[1 + C_s\varepsilon\right], \qquad ...(2)$$

$$\nu_B(t) \approx \nu_B(t_0)\left[1 + C_t(t - t_0)\right], \qquad ...(3)$$

where t_0 = reference temperature, and C_s and C_t = proportional coefficients of strain and temperature, respectively, which are characteristic of the optical fiber.

The basic concept is illustrated in Figure 1. At any point along the fiber, the Brillouin spectrum detected is accurately approximated by a Lorentzian function with resonance frequency of ν_B, and a Gauss function, from which either the strain or temperature can be

derived by applying the specific $\nu_B(\varepsilon)$ and $\nu_B(t)$ correlation functions of the FOS. The measurement position along the FOS is computed from the light velocity in the fiber core and the time elapsed between launching the pulsed light and detecting the backscattered light. The spatial resolution is determined as

$$\Delta z = \frac{c\tau}{2n}, \qquad ...(4)$$

where c = light velocity in a vacuum, and τ = pulse width of incident light, which typically translates into values up to 2 m, depending on the selected pulse width. When operating on a large structure, comparable resolutions may be attained only by means of a very high number of discrete sensors, which may not be practical nor cost-effective.

BRIDGE DESCRIPTION

Bridge No. A6358 carries US Route 54 over the Osage River in Osage Beach, Missouri, USA. The superstructure, built in 2004, has five continuous symmetric spans with no skew, as shown in Figure 2(a), with a total bridge length of 263.4 m. The cross section is shown in Figure 2(b) and comprises five identical welded plate I-girders equally spaced at 2.6 m on-center, and a 216 mm thick reinforced concrete (RC) deck with New Jersey continuous concrete barriers. The out-to-out deck and clear roadway widths are 12.4 m and 11.6 m, respectively. Bolted splices at the contraflexure areas connect the girder sections designed to resist the maximum positive and negative moments. The girders were fabricated using ASTM A709 Grade HPS 345W steel (yield strength $F_y \geq 345$ MPa) except at the intermediate supports, where the hybrid sections include top and bottom flanges made of ASTM A709 Grade HPS 485W steel ($F_y \geq 485$ MPa). Bridge design is composite in the positive moment regions, and non-composite in the sections resisting

maximum negative moments over the interior supports. Fixed and sliding bearings were built on the bents at Piers 2-3 in Figure 2(a), and on the other supports, respectively.

DIAGNOSTIC LOAD TEST

Load passes and procedure

The load test was conducted using six ten-wheel, three-axle dump trucks prior to opening the bridge to traffic. The vehicles were fully loaded at a gross weight load between 192.8 kN and 268.1 kN, with approximate distribution of 3/8 in the front axle and 5/8 in the rear axles, in the configuration illustrated in Figure 3(a). The four load passes detailed in Figure 3(b) and Figure 3(c) were designed to produce maximum strains in the exterior girders using two symmetric lanes of two and three trucks each on Span 1 (Girders 1 and 5, Passes A and B), and a single train of six trucks on Span 2 (Girder 5, Pass C) and Span 1 (Girder 1, Pass D). Focus on the exterior girders was aimed at assessing the response of Girder 1 along Span 1, which was heat-straightened after falling during construction due to high wind, as documented in Figure 4. The wheel loading locations were marked on the deck to set a distance of 2.74 m between the front axle of each truck and the rear axle of the preceding one. A 15-minute interval was allowed at each load pass before performing any measurements.

BOTDR setup

Tight-buffered FOSs (9/125 μm single-mode optical fibers with 900 μm diameter and tight PA buffer coating) were used for strain measurement. Loose-buffered FOSs (9/125 μm silica single-mode optical fibers with 900 μm diameter, and either loose dry-coupled

PVA or wet-coupled PE buffer coating) were used for thermal compensation and installed parallel to the mechanical strain sensors. The sensing circuit included bare optical cables, and a tape made of woven E-glass fiber strands that carried two strain- and two temperature-sensing FOSs, designated with the letters S and T, respectively, in Figure 5. The tape was used due to the ease of handling and to reduce the risk of damaging the optical fibers during installation under non-ideal field conditions.

The empirical correlation functions between mechanical and temperature induced strain and the Brillouin frequancy shift were established by testing each FOS under predetermined mechanical strain and temperature using a specially made fixture and an environmental chamber, respectively. The FOSs were adhesively bonded onto the web of Girders 1, 2, 4 and 5 with a two-part epoxy resin, upon pretreatment of the steel surface by manual surface roughening followed by solvent wiping. The girders were instrumented at different depths with either bare optical cables or tape running continuously through the gaps at the transverse stiffeners, as detailed in Figure 6(a) and Figure 6(b). The sensors were installed along Span 1 and Span 2 starting at about 6 m from Abutment 1, and up to the third bolted joint at a distance of 87.2 m from Abutment 1. A cart designed to move along the entire bridge by rolling over the bottom flanges of two adjacent girders was used for the installation work (Matta *et al.* 2005).

The FOSs were series-connected with a fusion splicer to form a 1159 m long circuit. The optical attenuation was contained within 6 dB in the first 1026 m of the circuit, excluding the end portion with the tape along Girder 4 at Location I, where a steep power decay

from 5.8 dB/km to over 37.6 dB/km was detected. A BOTDR AQ8603 optical fiber strain/loss analyzer, manufactured by Yokogawa Electric Corporation, was used to measure the strain along the FOSs from one end of the sensing circuit. A minimum accuracy of ±40 με is specified by the manufacturer for measurements using FOS circuits with steep geometric discontinuities. The spatial resolution is 1 m at a pulse width τ = 10 ns (2 m at τ = 20 ns) within a 2 dB (6 dB) optical loss, and repeatability < 0.04% (0.02%). The strain analyzer was connected to a laptop PC via standard ethernet interface, and a proprietary software was used to process the strain and temperature data in real-time (Bastianini *et al.* 2005b). The setup, which is shown in Figure 6(c), accounted for a measurement accuracy of ±40 με on a length resolution of 2 m, with the strain analyzer set for 20 ns laser pulses with wavelength of 1.55 μm. The accuracy was expected to considerably improve away from the geometric discontinuities along the optical circuit (for example at the bolted joints, where the FOSs were bonded onto the adjoining web plates in the gap between the bottom flange and the web splice plates), and the near-zero strain areas (such as at the contraflexure regions). Selected sections were instrumented with bonded and unbonded strain gauges to measure mechanical- and temperature-induced deformations, respectively.

ATS setup

To provide a reliable benchmark for the validation of the BOTDR results, girder deflections were measured at discrete points using a high-precision ATS system. The total station combines the features of an electronic distance measurement unit with an electronic theodolite (Wolf 2002) and is extensively used in practice. The instrument

sends a laser ray to a set reflecting prisms (targets) mounted on the structure and to fixed reference prisms, thus enabling the built-in computer to determine the movements of the target points based on triangulation. The system is based on the Leica TCA2003 total station, which allows to automatically measure vertical displacements of preselected targets with an accuracy of 0.5 sec on angular measurement, and 1 mm + 1 ppm on distance measurements in average atmospheric conditions, with a working range up to 150 m. A total of 22 prisms, denoted as P1 to P22 in Figure 7(a), were mounted onto the bottom flange of the girders along Spans 1 and 2. Four reference targets were used. Figure 7(b) and Figure 7(c) show photographs of a prism and of the test setup, respectively. The total station was secured on a custom-built leveling steel plate mounted on top of a concrete pile to minimize systematic errors. Four readings were taken for each target, two direct and two inverse, to further reduce measurement errors.

VALIDATION OF DISTRIBUTED STRAIN MEASUREMENT

The strain profiles measured along the girders through the FOSs closer to the bottom flanges [Location I in Figure 6(a)] were converted into vertical deflection profiles to allow validation via direct comparison with the benchmark ATS measurements. The curvature profiles were computed by dividing the strains, herein denoted as $\varepsilon_{BOTDR}(x)$ where x indicates the distance of the reference section from Abutment 1 in Figure 3(a), by the vertical distance $h_S(x)$ between the measurement point and the neutral axis at the correspondent section. Due to the relatively high effective span-to-girder spacing ratio in excess of 12, steel-concrete composite girders with effective flange width replicate of the girder spacing of 2.64 m were assumed to determine $h_S(x)$ as 1788 mm and 1658 mm

along Span 1 and Span 2, respectively, under service loads (Amadio and Fragiacomo 2002, Ahn *et al.* 2004). In order to provide continuous and yet accurate curvature functions, the profiles were approximated through least squares fitting of *N*th-order polynomial functions as

$$y''(x) = \frac{\varepsilon_{BOTDR}(x)}{h_S(x)} \approx a_0 + a_1 x + a_2 x^2 + ... + a_N x^N , \qquad ...(5)$$

where N was selected to ensure a coefficient of determination R^2 greater than 0.95. The computation of the vertical deflection function $y(x)$ at a given load condition reduces to the solution of the boundary value problem

$$\begin{cases} y''(x) = \sum_{i=0}^{N} a_i x^i \\ y(0) = y(44.8\text{ m}) = 0 \qquad \text{for Span 1} \\ y(44.8\text{ m}) = y(101.2\text{ m}) = 0 \quad \text{for Span 2} \end{cases} \qquad ...(6)$$

where the ordinary differential equation is the Euler-Bernoulli beam equation for the selected composite girder and load test pass, and the boundary conditions impose zero vertical displacement at the supports.

The experimental and approximated curvature functions for Girder 1 at Passes A, B and D are plotted in Figure 8. The derived vertical deflection profiles are shown in Figure 9(a) together with the discrete ATS measurements. It can be seen that the deflections computed from the measured distributed strains are good agreement with those from the ATS system. Improved results are obtained as the coefficient of determination increases in Figure 8, where the regression sum of squares approaches the total sum of squares from Passes A to B to D (R^2 from 0.95 to 0.99), meaning that agreement between

BOTDR and ATS improves as the load levels are increased and result in smoother strain profiles. This is also noted in Figure 9(b) in the case of Girder 5 at Pass C, where the curvature was approximated with a function having R^2 of 0.99 and translated into a deflection profile that matches the ATS measurements along Span 2.

On the basis of the comparative results presented, the strain measurements were validated and could be used for structural assessment, which is addressed in the next section, and to discuss the performance of the BOTDR setup. In addition, it is clear from Figure 9 that the maximum deflections of Girder 1 and Girder 5 under a six-truck lane load in Pass D and Pass C, respectively, remained well below the optional limit of 1/800 times the span length set forth in the American Association of State Highway and Transportation Officials (AASHTO) LRFD Bridge Design Specifications (AASHTO 2004).

STRUCTURAL ASSESSMENT

The diagnostic load test was designed primarily to assess the structural response of Girder 1 along Span 1 under service loads. In particular, the effective implementation of a distributed strain measurement technique was intended to describe the deformation in a continuous fashion along the entire structural member, and possibly overcome the limitations of discrete measurement that provide data only at selected sections. Two criteria were used for assessment. First, the maximum tensile strain must not exceed that associated with the design load distribution factor (LDF), which yields conservative estimates of the ratio between the maximum girder bending moment at a given load condition, and the maximum moment assuming the entire truck load applied to a single

composite girder. A value of S / 3.36 = 0.788 was used, where S is the 2.64 m girder spacing, according to the semi-empirical specifications used to design the bridge (MoDOT 2002). The second criterion required the strain profiles to be in qualitative agreement with those from three-dimensional finite element analysis (FEA) on a bridge model constructed to yield rational upper-bound strains.

The finite element model (FEM) was developed using a commercially available software (Strand7 2005) and is illustrated in Figure 10. Two-node shear-flexible Timoshenko beam elements (BEAM2) and eight-node quadrilateral shell elements (QUAD8) were used to model the steel girders and the RC deck, respectively. The deck and girder elements are eccentrically connected by means of rigid links in the sections where shear studs were designed, accounting for an average deck haunch of 50 mm, thereby imposing the compatibility of composite behavior. This numerical approach was chosen to produce accurate results while minimizing the computational effort (Chung and Sotelino 2006). Pinned links connect the girder elements and the eccentric deck elements to model the non-composite sections within the bolted joints over the intermediate supports, where shear connectors were not present. The support boundary conditions were approximated by imposing either simple support (Abutments 1 and 2, and Piers 1 and 4) or hinge (Piers 2 and 3) constraints at the corresponding beam centroid nodes. Lateral girder displacements were not constrained. The mesh of the deck shell elements is characterized by a maximum in-plane aspect ratio of 2:1, and was designed to accurately apply the transverse and longitudinal wheel loads replicating the test conditions. For conveniency, 0.37 m^2 square tire contact areas are used. The elastic moduli used for steel,

E_s, and concrete, E_c, are 195 GPa and 25 GPa, respectively. The latter was determined as $E_c = 4733\sqrt{f_c'}$ (MPa), where f'_c is the specified concrete cylinder compressive strength of 28 MPa (ACI 2005). The stiffening effects of secondary structural members such as the cross-frames and the concrete barriers were neglected.

The experimental and theoretical strain profiles along Girder 1, Span 1 at Location I [Figure 6(a)] are shown in Figure 11(a), Figure 11(b) and Figure 11(c) for Passes A, B and D, respectively. The strain profiles measured with the FOSs in the FRP tape and located at 22 mm from the bottom flange surface are fairly regular and closely reproduce those from the FEA, and no anomalies were thus observed. Good agreement is also noted with the measurements of strain gauges mounted on the upper face of the bottom flange at 20.0 m from Abutment 1, where the maximum strain at Pass D was expected.

The measured distributed strain peaked at Pass D at 413 με, which is 20% smaller than the value of 518 με associated with the design LDF for the exterior girder (MoDOT 2002), and over four times smaller than the theoretical yield strain of the ASTM A709 Grade HPS 345W steel. It was concluded that Girder 1 met both the assessment criteria defined and did not present any serviceability concern.

PERFORMANCE OF BOTDR SYSTEM

Valid BOTDR measurements from the FOSs embedded in the FRP tapes were performed in the positive moment regions along the span directly subjected to truck loads, as shown in Figure 11 for Girder 1. In particular, more regular profiles were obtained at increasing

strain levels, such as at Pass D in Figure 11(c), when a simple second-order least square fitting polynomial function allowed to attain a coefficient of determination of 0.99. This suggests that measurements may be affected by some initial fiber misalignment, whose effects are mitigated as the optical fibers are stretched, and may be overcome by pre-straining the FOSs using special fixtures (Komatsu *et al.* 2002). Such effect could not be exploited along the spans adjacent to that directly loaded, where the bending moment is steadily negative, and where a reduced measurement accuracy at the bottom flanges may result from relatively small compressive strains and localized distortion of the FOSs, as in the case of Girder 5, Span 2 at Pass A in Figure 12(a).

Another plausible source of reduced accuracy is the combination of relatively small strains with their transition from tensile to compressive in the contraflexure regions. This can be clearly seen in Figure 12(a) for Girder 5, Span 1 at Location I at Pass A, where the strain discontinuity peaks at the theoretical contraflexure section. Localized strain nonlinearities may also cause the BOTDR measurement accuracy to approach the ±40 με limit suggested by the manufacturer of the strain analyzer, such as in the case of local strain relief at the cross-frame connection sections, or in case of strain drop at the bolted joints, where the FOSs ran directly across the butt joint between adjoined girder portions. The latter effect may be recognized through the steep strain discontinuity in Girder 5, Span 1 at Location I at Pass C in Figure 12(b), and was likely enhanced by the local transition from composite to non-composite behavior anticipated in the FEA profile, as well as by distortion of the FOSs under compression. Conversely, a smooth strain profile was obtained along Span 2, which was directly loaded with a six-truck lane.

The tensile strain profile measured with the bare FOS cables at Location III [close to the top flange, as shown illustrated Figure 6(a)] along Girder 5, Span 1 at Pass C is shown in Figure 12(c). The readings between the bolted joint and Pier 1 follow the pattern of those from the FEA, thus corroborating the assumption of non-composite behavior for relatively high service loads. This is also indicated by the tendency of the maximum negative strains measured at Location I (close to the bottom flange) over the intermediate support at Pier 1 to approach or exceed the FEA peaks in both the exterior girders, as shown in Figure 11 and Figure 12 for Girder 1 and Girder 5, respectively.

The readings from Girder 4 at Location I were confirmed to be not relevant, due to the low accuracy determined by the optical power loss that was detected along the terminal portion of the FOS circuit, between 1026 m and 1159 m. The results from the bare FOS cables along Girder 2 at Location II (at a vertical distance of 711 mm from the upper face of the bottom flange) were also not meaningful, since approximately zero strain was measured. This may be attributed to: low strain levels from the benchmark strain gauge readings at 23.0 m from Abutment 1, which are one order of magnitude smaller than those from the strain gauges mounted on the bottom flange of Girder 1 at 20.0 m from Abutment 1, as shown in Figure 13(a); and presence of several vertical circuit portions at about 7.3 m intervals, usually partially unbonded and with relatively sharp bends at the cross-frame sections, where the fibers were drawn through the gaps between the gusset plates and bottom flanges, as depicted in Figure 13(b), which may have resulted in undesired perturbations in the signals detected.

CONCLUSIONS

A pilot application of a BOTDR-based optical fiber sensor system to measure distributed strains along the steel I-girders of a highway bridge has been presented herein. The structure was subjected to a diagnostic load test, where a primary goal was to assess an exterior girder that had been repaired after falling during erection of the superstructure. The relevance of distributed strain measurement lies in its unique potential for investigating the structural response along the girder length in a quasi-continuous fashion, thereby overcoming typical practical and economical limitations of discrete sensing techniques. A 1.16 km optical circuit was installed onto the girders that included sensing fibers for strain measurement and thermal compensation. A high-precision total station system for deflection measurement was used to provide a solid benchmark.

The experimental strain profiles were converted into vertical deflection profiles and were in good agreement with the total station measurements, thereby validating the BOTDR system implemented despite the non-ideal logistic and operational field conditions encountered during installation of the sensing circuit. The BOTDR measurements were then enlisted for structural assessment purposes. The tensile strain profiles matched with those from three-dimensional finite element analysis of the bridge superstructure, and the maximum tensile strain measured remained well below the design limit, thus prompting no serviceability concerns.

The global girder response was effectively described by the BOTDR measurements. The accuracy largely outperformed the ±40 με limit suggested for the strain/loss analyzer,

which contemplates worst-case scenarios that involve either step-like discontinuities (such as at the bolted joint sections) or very small strain levels that exceed the measurement sensitivity (such as at the contraflexure zones), especially under negative strains when local distortion of the optical fibers may occur, and when several bends are imposed on the sensors to reach the desired locations during installation. The measurement quality appeared to improve at increasing strain levels, which may suggest the use of pre-straining fixtures when feasible, while the characterization of the optical attenuation in the Brillouin backscattered light spectrum enabled the systematic identification of a portion of the sensing circuit where the measurement accuracy decayed.

The project demonstrated the practical potential of BOTDR distributed strain measurement for the structural health monitoring and assessment of large-scale structures. Further research is needed to improve and refine the technology, develop dedicated solutions for the structural health monitoring of constructed facilities, and advance their field validation.

ACKNOWLEDGMENTS

The financial support from the Missouri Department of Transportation and the University of Missouri-Rolla University Transportation Center on Advanced Materials and NDT Technologies is gratefully acknowledged. Special thanks are due to Leica Geosystems, Inc., Isaberg Rapid, Pirelli Cavi e Sistemi S.p.A., SEAL S.p.A., Yokogawa Corp. of America, Rolla Technical Institute-Machine Technology and Precision Manufacturing, and Strongwell Corp., industry member of the NSF Industry-University Cooperative Research Center "Repair of Buildings and Bridges with Composites" (RB^2C), for providing precious technical and logistic assistance, materials, and equipment.

REFERENCES

Ahn, I. S., Chiewanichakorn, M., Chen, S. S., and Aref, A. J., "Effective flange width provisions for composite steel bridges," *Engineering Structures*, V. 26, No. 12, 2004, pp. 1843-1851.

Amadio, C., and Fragiacomo, M., "Effective width evaluation for steel-concrete composite beams," *Journal of Constructional Steel Research*, V. 58, No. 3, 2002, pp. 373-388.

American Association of State Highway and Transportation Officials (AASHTO), "Load and resistance factor design (LRFD) bridge design specifications," 3rd edition, AASHTO, Washington, D.C., 2004.

American Concrete Institute, "Building code requirements for structural concrete," *ACI 318-05*, ACI, Farmington Hills, MI, 2005.

Bastianini, F., Cargnelutti, M., Di Tommaso, A., and Toffanin, M., "Distributed Brillouin fiber optic strain monitoring applications in advanced composite materials," *Proc. SPIE*, V. 5057, 2003, pp. 478-485.

Bastianini, F., Corradi, M., Borri, A., and Di Tommaso, A., "Retrofit and monitoring of an historical building using "smart" CFRP with embedded fibre optic Brillouin sensors," *Construction and Building Materials*, V. 19, No. 7, 2005a, pp. 525-535.

Bastianini, F., Matta, F., Galati, N., and Nanni, A., "A Brillouin smart FRP material and a strain data post processing software for structural health monitoring through laboratory testing and field application on a highway bridge," *Proc. SPIE*, V. 5765, 2005b, pp. 600-611.

Bastianini, F., Rizzo, A., Deza, U., Galati, N., and Nanni, A., "Discontinuous Brillouin strain monitoring of small concrete bridges: comparison between near-to-surface and "smart" FRP fiber installation techniques," *Proc. SPIE*, V. 5765, 2005c, pp. 612-623.

Brillouin, L., "Diffusion de la lumière et des rayons X par un corps transparent homogéne - Influence de l'agitation thermique," *Annales de Physique*, V. 17, 1922, pp. 88-122.

Casas, J. R., and Cruz, P. J. S., "Fiber optic sensors for bridge monitoring," *Journal of Bridge Engineering*, V. 8, No. 6, 2003, pp. 362-373.

Chung, W., and Sotelino, E. D., "Three-dimensional finite element modeling of composite girder bridges," *Engineering Structures*, V. 28, No. 1, 2006, pp. 63-71.

Fujihashi, K., Uehara, H., Okutsu, M., and Komatsu, K., "Development of a road disaster monitoring system using optical fiber sensing technology," *NTT Technical Review*, V. 1, No. 9, 2003, pp. 48-52.

Horiguchi, T., Kurashima, T., and Tateda, M., "Tensile strain dependence of Brillouin frequency shift in silica optical fibers," *IEEE Photonics Technology Letters*, V. 1, No. 5, 1989, pp. 107-108.

Kihara, M., Hiramatsu, K., Shima, M., and Ikeda, S., "Distributed optical fiber strain sensor for detecting river embankment collapse," *IEICE Transactions*, V. E85-C, No. 4, 2002, pp. 952-960.

Komatsu, K., Fujihashi, K., and Okutsu, M., "Application of optical sensing technology to the civil engineering field with optical fiber strain measurement device (BOTDR)," *Proc. SPIE*, V. 4920, 2002, pp. 352-361.

Kurashima, T., Horiguchi, T., and Tateda, M., "Thermal effects of Brillouin gain spectra in single-mode fibers," *IEEE Photonics Technology Letters*, V. 2, No. 10, 1990, pp. 718-720.

Li, H.-N., Li, D.-S., and Song, G.-B., "Recent applications of fiber optic sensors to health monitoring in civil engineering," *Engineering Structures*, V. 26, No. 11, 2004, pp. 1647-1657.

Matta, F., Vath, M., Galati, N., and Nanni, A., "Modular frame concept cart for inspection of slab-on-girder bridge superstructure," *Proc. 5th International Conference on Bridge Management*, April 11-13, 2005, Guildford, Surrey, UK, Thomas Telford, pp. 187-194.

Missouri Department of Transportation (MoDOT), "Bridge design manual," MoDOT, Jefferson City, MO, 2002.

Murayama, H., Kageyama, K., Naruse, H., Shimada, A., and Uzawa, K., "Application of fiber-optic distributed sensors to health monitoring for full-scale composite structures," *Journal of Intelligent Material Systems and Structures*, V. 14, No. 1, 2003, pp. 3-13.

Naruse, H., Uchiyama, Y., Kurashima, T., and Unno, S., "River levee change detection using distributed fiber optic strain sensor," *IEICE Transactions*, V. E83-C, No. 3, 2000, pp. 462-467.

Ohno, H., Naruse, H., Kurashima, T., Nobiki, A., Uchiyama, Y., and Kusakabe, Y., "Application of Brillouin scattering-based distributed optical fiber strain sensor to actual concrete piles," *IEICE Transactions*, V. E85-C, No. 4, 2002, pp. 945-951.

Shi, B., Xu, H., Chen, B., Zhang, D., Ding, Y., Cui, H., and Gao, J., "Feasibility study on the application of fiber-optic distributed sensors for strain measurement in the Taiwan Strait Tunnel project," *Marine Georesources and Geotechnology*, V. 21, No. 3-4, 2003, pp. 333-343.

Strand7 Pty Ltd., "Using Strand7 – Introduction to the Strand7 finite element analysis system," Strand7 Pty Ltd., Sydney, Australia, 2005, 292 pp.

Thévenaz, L., Niklès, M., Fellay, A., Facchini, M., and Robert, P., "Truly distributed strain and temperature sensing using embedded optical fibers," *Proc. SPIE,* V. 3330, 1998, pp. 301-314.

Uttamchandani, D., "Fibre-optic sensors and smart structures: developments and prospects," *Electronics & Communication Engineering Journal*, V. 6, No. 5, 1994, pp. 237-246.

Wolf, P. R., "Surveying and mapping: history, current status, and future projections," *Journal of Surveying Engineering*, V. 128, No. 3, 2002, pp. 79-107.

Wu, Z., Xu, B., Hayashi, K., and Machida, A., "Distributed optic fiber sensing for a full-scale PC girder strengthened with prestressed PBO sheets," *Engineering Structures*, V. 28, No. 7, 2006, pp. 1049-1059.

Yasue, N., Naruse, H., Masuda, J., Kino, H., Nakamura, T., and Yamaura, T., "Concrete pipe strain measurement using optical fiber sensor," *IEICE Transactions*, V. E83-C, No. 3, 2000, pp. 468-474.

FIGURES

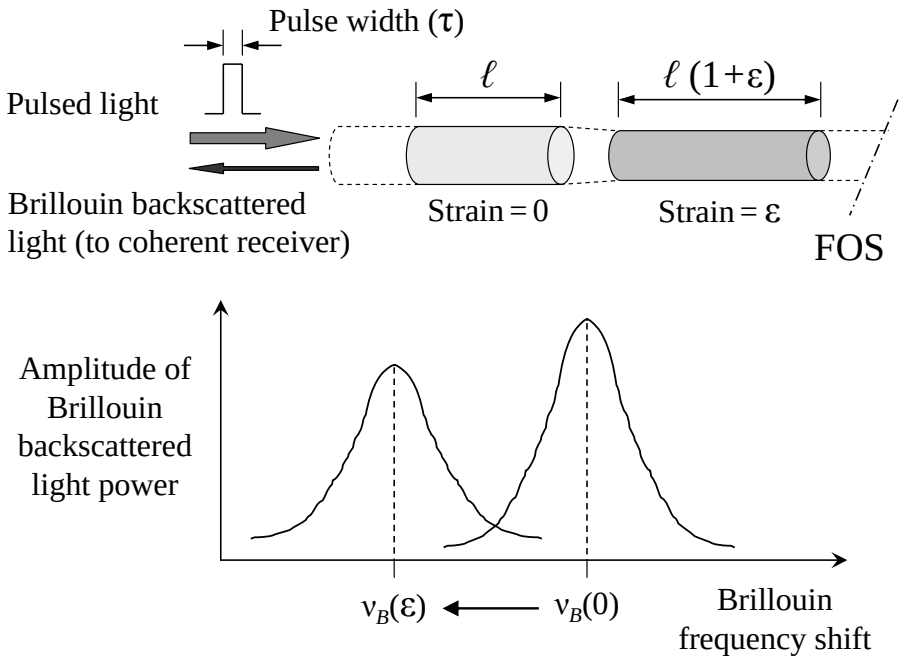

Figure 1 – Schematic of Brillouin frequency shift in FOS subjected to mechanical- or temperature-induced deformation.

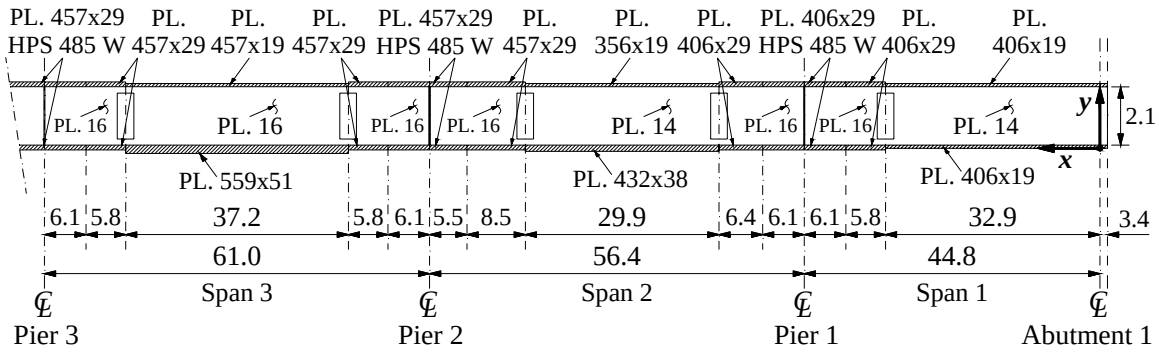

(a)

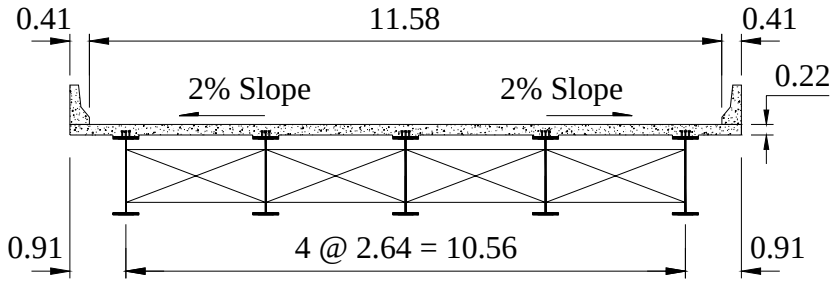

(b)

Figure 2 – Bridge No. A6358: (a) elevation of steel girder; and (b) cross section of superstructure. ASTM A709 Grade HPS 345W used unless specified. Lengths in m, steel plate dimensions in mm.

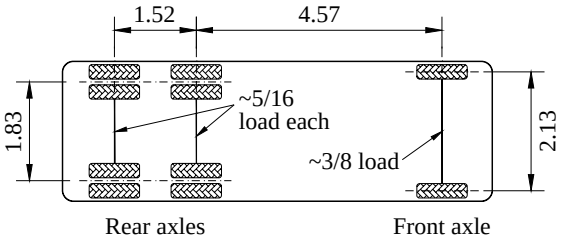

(a)

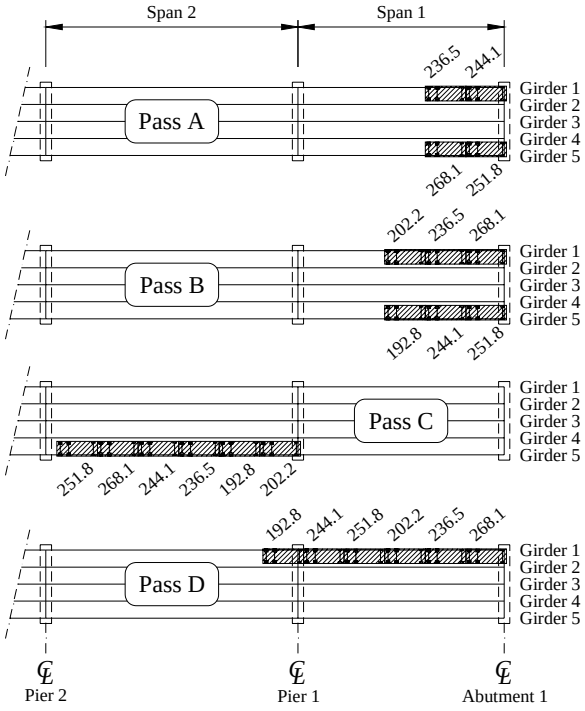

(b)

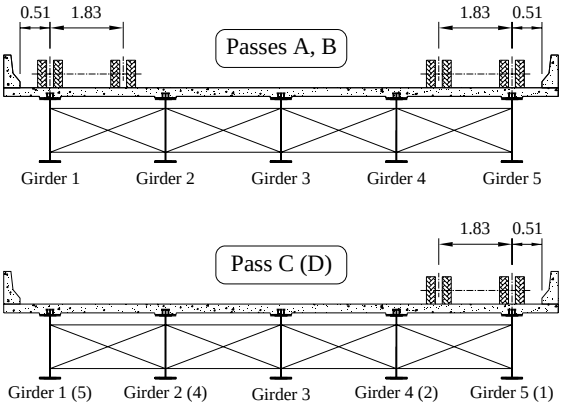

(c)

Figure 3 – Diagnostic load test: (a) dump truck configuration; (b) longitudinal and (c) transverse schematic of load test passes with truck loads. Dimensions in m, loads in kN.

Figure 4 – Photograph of exterior girder fallen during erection due to high wind (courtesy of Missouri Department of Transportation).

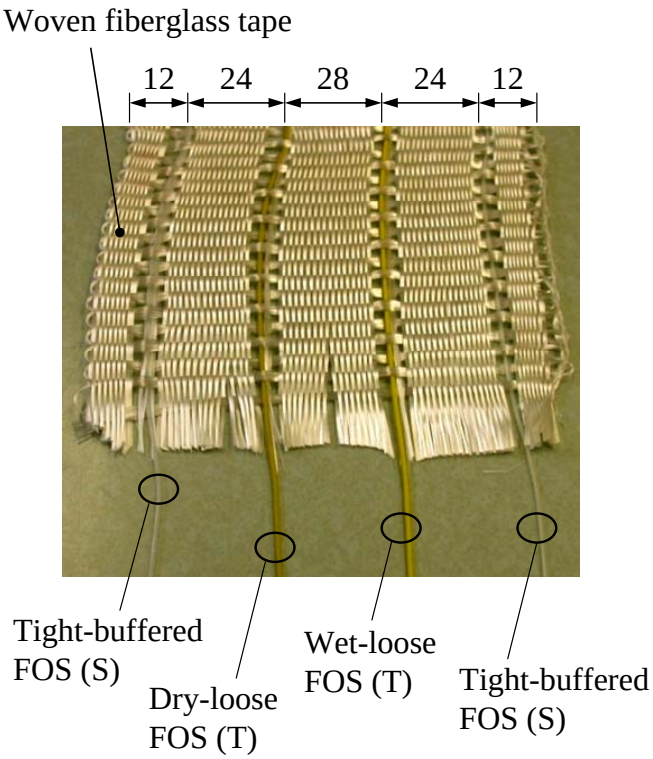

Figure 5 – Fiberglass tape with embedded FOSs for strain (S) and temperature (T) measurement. Dimensions in mm.

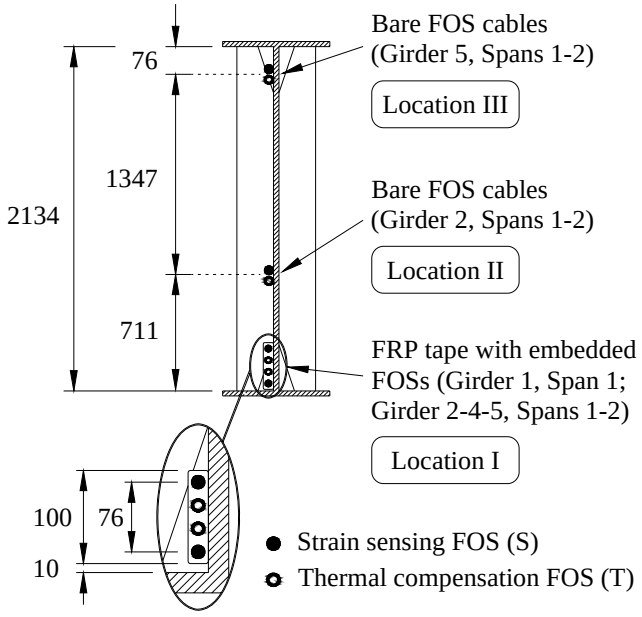

(a)

(b)

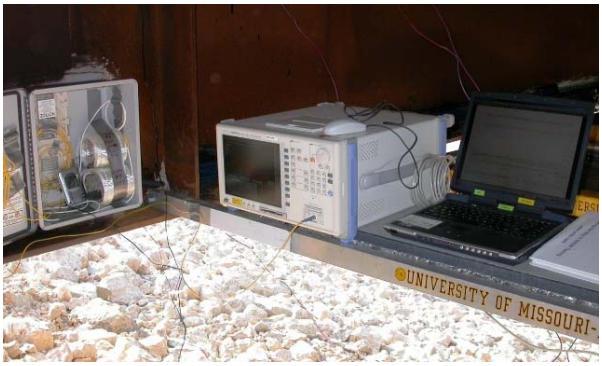

(c)

Figure 6 – BOTDR setup: (a) schematic of FOS locations; (b) photograph of sensors installed along Girder 5 (tape at Location I, and bare FO cables at Location III); and (c) data acquisition and processing station.

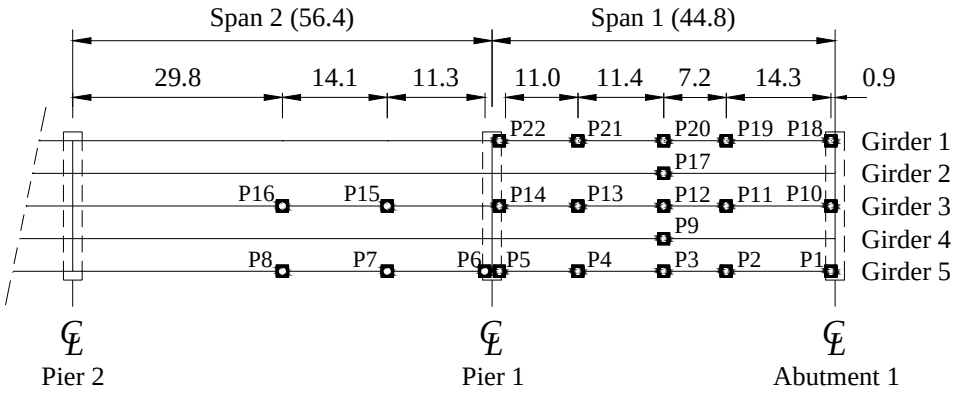

(a)

(b)

(c)

Figure 7 – ATS setup: (a) schematic of location of targets; (b) reflecting prism; and (c) photograph of setup with total station. Dimensions in m.

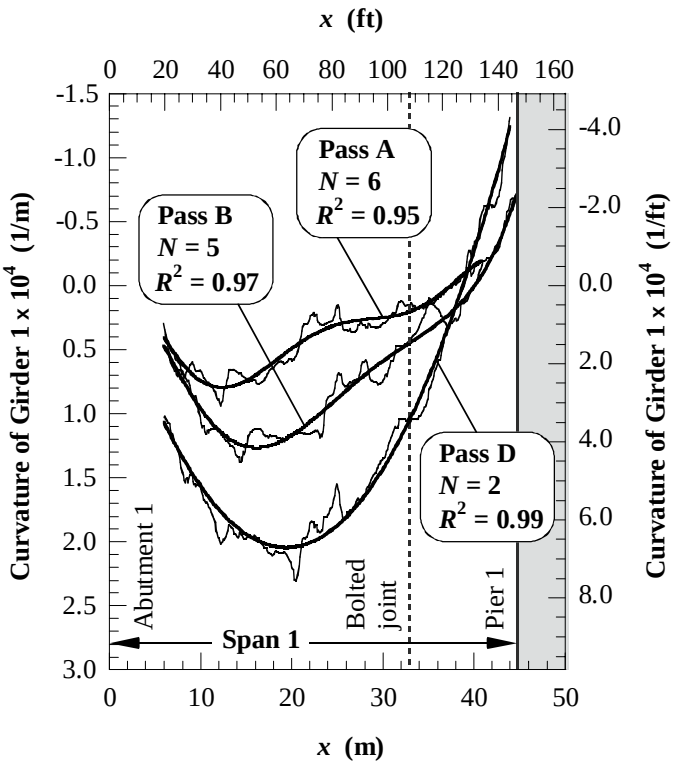

Figure 8 – Least squares polynomial fitting of BOTDR curvature profiles along Girder 1, Span 1 at Location I at Passes A, B and D.

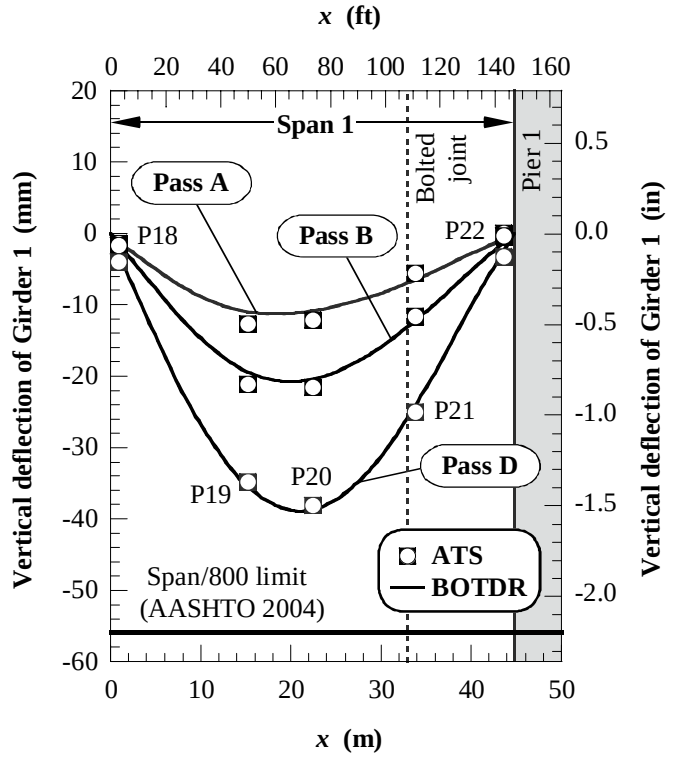

(a)

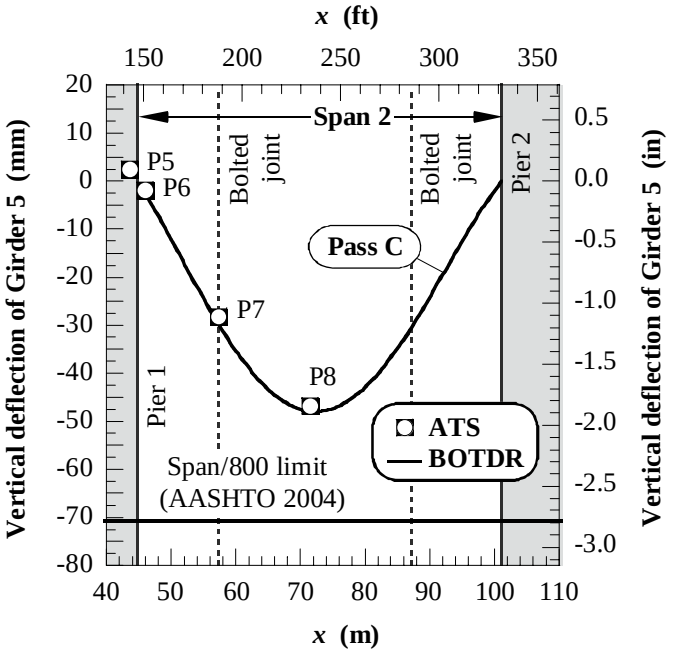

(b)

Figure 9 – Deflection profiles derived from BOTDR measurements and discrete ATS measurements: (a) Girder 1, Span 1 at Passes A, B and D; and (b) Girder 5, Span 2 at Pass C.

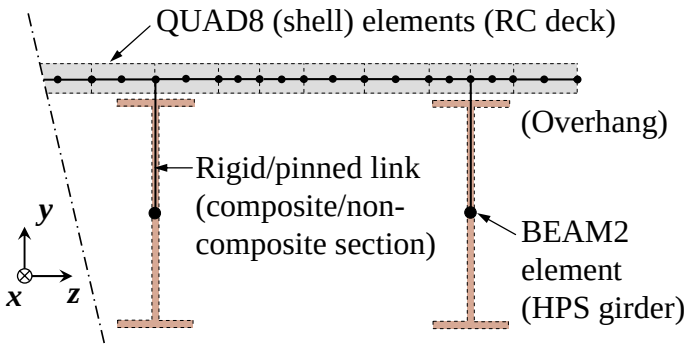

Figure 10 – Schematic of finite element model of bridge superstructure.

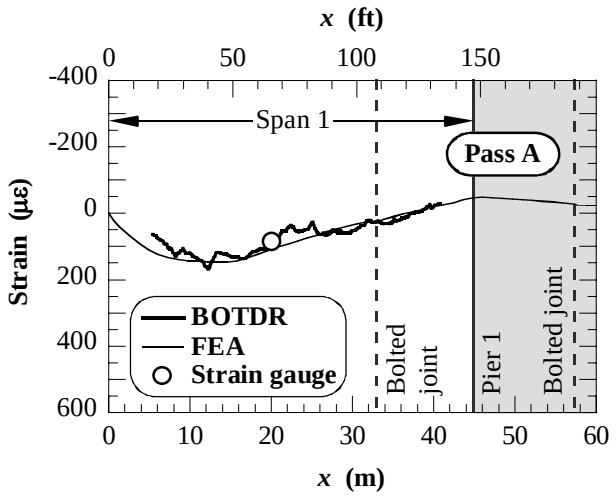

(a)

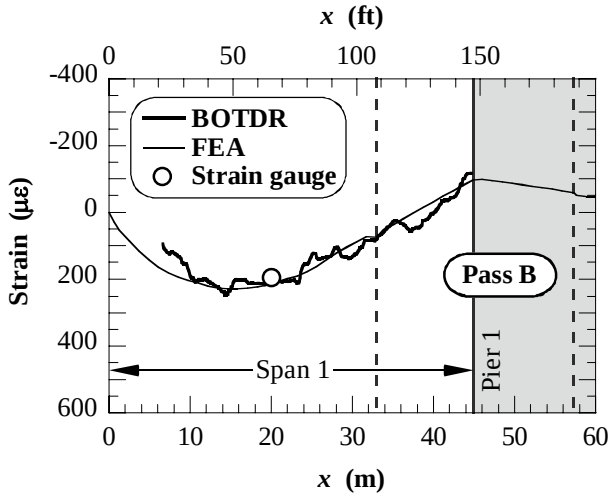

(b)

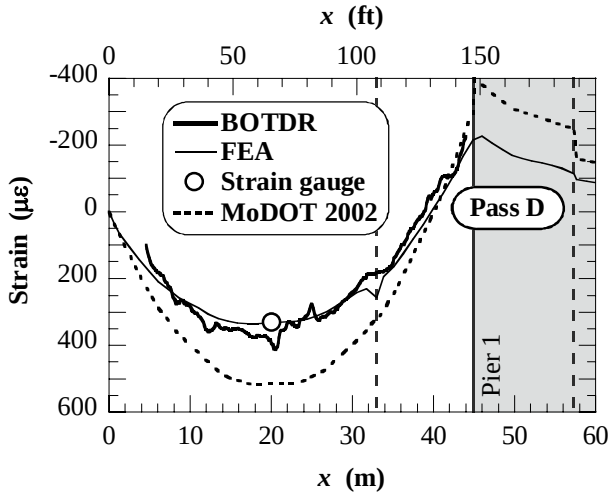

(c)

Figure 11 – Experimental and theoretical strain profiles at Location I along Girder 1, Span 1: (a) Pass A; (b) Pass B; and (c) Pass D.

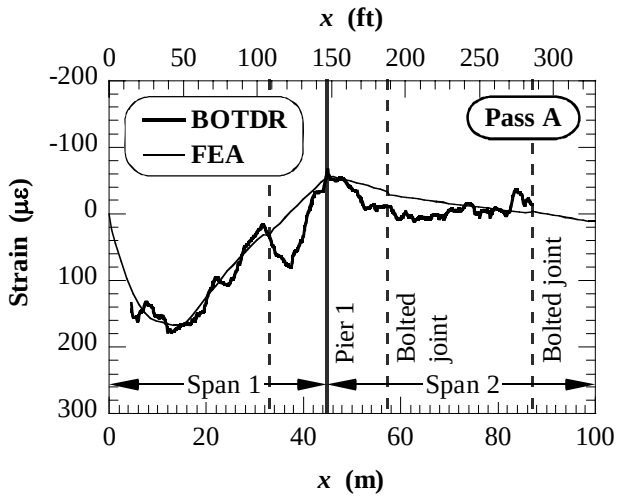

(a)

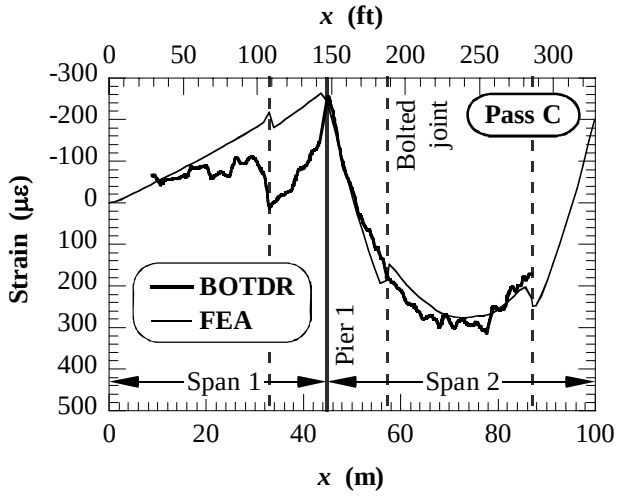

(b)

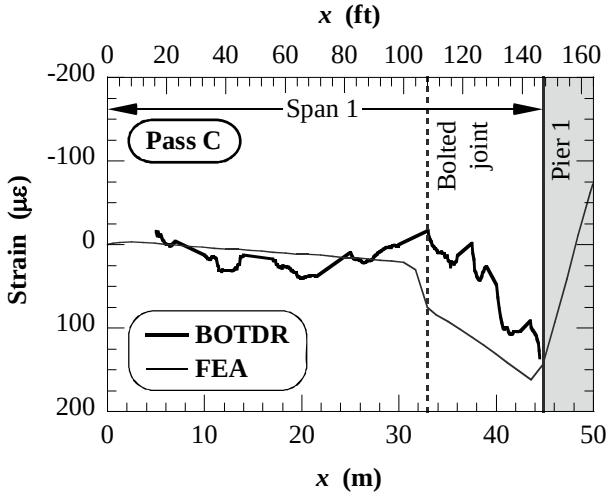

(c)

Figure 12 – Experimental and FEA strain profiles along Girder 5: (a) at Location I at Pass A; (b) at Location I at Pass C; and (c) at Location III at Pass C.

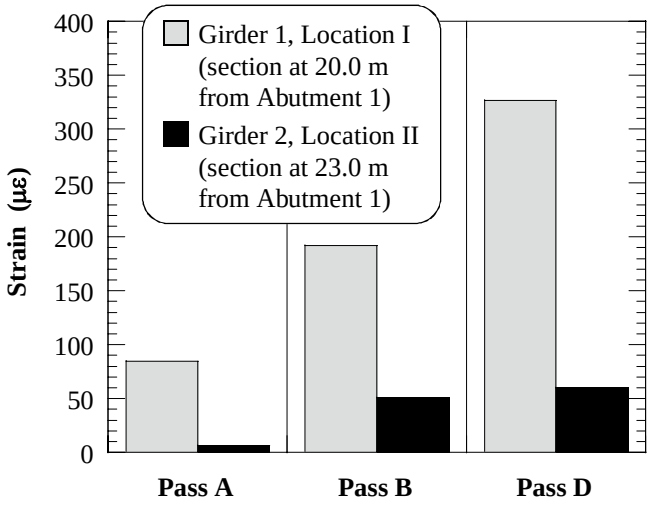

(a)

(b)

Figure 13 – Strain gauge measurements on Girder 2 at Location II: (a) comparison with Girder 1 at Passes A, B and D; and (b) photograph of FOS arrangement.

SECTION

2. CONCLUSIONS AND RECOMMENDATIONS

This section condenses the overall conclusions and recommendations that are drawn from the work presented in this dissertation, and summarizes further research needs.

2.1. BRIDGE CONSTRUCTION

The innovative concept and technology introduced consist of prefabricated pultruded glass FRP reinforcement for concrete deck and railing systems. The latter has been presented in PAPER 1 of this dissertation, which focuses on the design and validation of a post-deck connection that was implemented in the open-post reinforced concrete railing of an off-system bridge.

The practical impact is twofold:

- first, the use of internal FRP reinforcement eliminates the risk of corrosion that afflicts steel bars;
- second, the light-weight of FRP reinforcement, typically of the order of one fourth of that of steel, enables to pre-engineer and prefabricate in a quality-controlled environment large reinforcing cages for deck and railing elements, which can be installed with easier, faster, and safer procedures.

The research has demonstrated that:

- the design of FRP RC post-deck connections can be rationally addressed

and validated also when the full moment capacity of the weaker connected section is not attained, which may be acceptable due to constructability and economical considerations;

- on the basis of theoretical results, the design of FRP RC open-post railings that combine post-deck connection and rail beam components that meet the strength criteria of the AASHTO Standard Specifications (AASHTO 2002) may not provide the required strength as imparted on railing system. Structural crashworthiness should be investigated by analyzing the overall post-and-beam system, and without neglecting equilibrium of forces and compatibility of deformations.

The following recommendations are offered:

- a section should be added to the current ACI 440 design guidelines (ACI 2006) to provide guidance on the design of discontinuity regions in FRP RC frames with common reinforcement layouts and load conditions. Design algorithms may be selected on a case-by-case basis that combine general structural analysis principles with FRP RC mechanics principles, thereby providing the rational basis to complement legitimate practical and economical considerations made by designers and contractors;
- the design and the performance of FRP railing systems should be further investigated analytically, numerically, and experimentally. The goal is to develop methodologies pursuant to design principles of FRP RC, and to the philosophy of Section 13 (Railings) of the AASHTO LRFD Bridge Design Specifications (AASHTO 2004), which mandate strength criteria

at the system level. Yield line analysis, which is typically invoked to evaluate the nominal strength of steel RC railings (Hirsch 1978, AASHTO 2004), is not applicable. The overarching objective is clearly the development of LRFD design specifications for RC deck systems with internal FRP reinforcement, where suitable approaches must be included to enable the design of structurally safe railings, or of test specimens in instances where crash testing is mandatory.

2.2. BRIDGE REHABILITATION

The innovative technology introduced consists of a CFRP bar system for external post-tensioning. The system was designed to be used in profiled tendon configurations with intermediate extendable deviators, and has been presented in PAPER 2 of this dissertation.

The practical impacts are:

- the option of using corrosion-resistant and high-strength CFRP tendons in recovering short-term deflections and controlling long-term deflections;
- the feasibility of implementing externally post-tensioned (EPT) solutions that do not require any specialized equipment nor time-consuming installation operations, which are typical of any EPT applications.

The research has provided:

- experimental evidence of the ability of the anchor system to allow the CFRP tendons to attain the full tensile strength;
- guidance on the relevant criteria for the selection and design of EPT

solutions for deflection control. In particular, the structural analysis implications of member geometry, flexural stiffness, boundary conditions, and EPT system layout, for straight and "king-post" profiled bar configurations, have been analyzed and discussed in the common case of single-span one-way members;

- a design methodology for "king-post" EPT CFRP solutions for deflection control that use the system presented, pursuant to the design guidelines proposed by ACI Committee 440 (ACI 2004).

The following recommendations are offered:

- experimental research should be conducted on RC and metallic members or specimens to advance the validation process of the EPT CFRP system presented. Possible failure modes need to be investigated. In particular, the effectiveness of alternative anchorages of tendon assemblies into the rehabilitated members should be evaluated from the structural and constructability standpoints, irrespectively of the material used for the tendons (for example, CFRP or high-strength steel).
- further research should address unresolved issues that are common to external FRP systems. In primis, fire resistance and vulnerability of CFRP tendons to intentional vandalism and post-installation work.

2.3. BRIDGE STRUCTURAL HEALTH MONITORING

The innovative technology demonstrated uses common telecom-grade fiber optic sensors to measure continuous strain profiles, and is based on spontaneous Brillouin

scattering (Brillouin 1922). A distributed strain measurement setup was validated in the field and then used to assess the structural response of a steel girder in a slab-on-girder highway bridge. The girder fell during construction and was heat-straightened prior to being repositioned. The project has been presented in PAPER 3 of this dissertation.

The practical impacts sought in the development and field validation of this technology are:

- the feasibility of accurately monitoring the global response of structural members in the form of continuous strain profiles, as produced by either physical or thermal loads. Such capability would overcome the inherent limitations of discrete measurement techniques, and prove valuable in a number of applications. In bridge engineering, the detection and monitoring of fatigue cracks along steel girders and tension members is perhaps the most interesting;
- the availability of sensor systems that are simple to install and that effectively protect the optical fibers during handling, installation operations, and while in service. In the project presented, available fiberglass tapes with embedded sensors were used.

The research has provided:

- experimental evidence to validate the technology in the field;
- a pilot demonstration of successful structural assessment of a bridge girder based on distributed strain measurement;
- identifications of factors that may affect the measurement accuracy, such as: misalignment of the fiber optic sensors, which may suggest the use of

pre-straining fixtures; relatively small strain levels, especially at contraflexure regions; and layout of the sensors along the sensing circuit, such as in the case of alternation of vertical and horizontal portions with sharp bends, which may become an issue in the case of structures with significant geometric discontinuities.

Further research is needed to improve and refine the technology, to develop dedicated solutions for the structural health monitoring of constructed facilities, and to advance the field validation process.

APPENDIX A.

MATERIAL AND CONSTRUCTION SPECIFICATIONS FOR GLASS FIBER REINFORCED POLYMER BARS FOR BRIDGE NO. 14802301, GREENE COUNTY, MO

A.1 MATERIALS AND MANUFACTURING

A.1.1. Description

GFRP Reinforcing Bars shall consist of furnishing and placing fiber reinforced polymer bars as shown on the plans and required by the contract. All GFRP Reinforcing Bars will be supplied by Greene County, MO.

A.1.2. Classification of constituent materials

A.1.2.1. Fibers

Any commercial grade E-glass is permitted. The fiber may be in the form unidirectional rovings or tows of any size or weight, or can be in the form of stitched, woven, braided or non-woven fabrics, or mats of any size or weight. Fiber sizings and coupling agents shall be appropriate for the resin system used. The manufacturer of the fiber itself and the manufacturer of any fabrics or mats must be reported.

A.1.2.2. Resins

Any commercial grade vinylester thermosetting polymer resin is permitted. A vinylester resin is defined as a thermosetting reaction product of an epoxy resin with an unsaturated acid, usually methacrylic acid, which is then diluted with a reactive monomer, usually styrene (ASTM C904). The base polymer in the resin system may not contain any

polyester. Blending of vinylester resins is permitted. The manufacturer of the polymer resin must be reported. Styrene may be added to the polymer resin during processing. The amount of styrene, as a weight percentage of the polymer resin, added during processing shall be reported. Added styrene shall be less than 10% by weight of resin (pph resin).

A.1.2.3. Fillers

Commercial grade inorganic fillers such as kaolin clay, calcium carbonate, and alumina trihydrate are permitted and shall not exceed 20% by weight of the polymer resin constituent. The type and manufacturer of the inorganic filler must be reported. Commercial grade additives and process-aids, such as, release agents, low-profile shrink additives, initiators, promoters, hardeners, catalysts, pigments, fire-retardants, and ultra-violet inhibitors are permitted as appropriate for the processing method. Shrink additives shall be less than 10% by weight of the polymer resin. Commercial grade inorganic or organic non-woven surfacing mats or veils are permitted.

A.1.3. Manufacturing process

FRP materials must be produced using the pultrusion manufacturing process or by a process approved by the Engineer-of-Record (Engineer). All FRP material parts provided to the job site must be produced using the same pultrusion die and in the same production lot.

Manufacturer shall report upon request the maximum internal pultrusion die temperature measured by thermocouple. Manufacturer shall report the date of production and the lot size.

A.1.3.1. Straight bars

Straight bars are cut to a specified length from longer stock lengths in a fabricator's shop or at the manufacturing plantT.

A.1.3.2. Bent bars

Bending FRP rebars made of thermoset resin should be carried out before the resin is fully cured. After the bars have cured, bending or alteration is not possible due to the inflexibility or rigid nature of a cured FRP bar. Because thermoset polymers are highly cross-linked, heating the bar is not allowed as it would lead to a decomposition of the resin, thus a loss of strength in the FRP.

The strength of bent bars varies greatly for the same type of fiber, depending on the bending technique and type of resin used. The strength of the bent portion should be determined based on tests performed in accordance with recommended methods cited in the literature. Bars in which the resin has not yet fully cured can be bent, but only according to the manufacturer's specifications and with a gradual transition, avoiding sharp angles that damage the fibers.

A.1.4. Fiber architecture

Three classes of fiber architecture are permitted. The division into the three classes depends on the total fiber volume fraction (expressed as a percent of the total material volume) and the total volume of continuous longitudinal fiber (expressed as a percent of the total fiber volume) along the longitudinal axis of the laminate (also called the 0 degree axis). Laminates cut from a three-dimensional part must have the same longitudinal axis.

A.1.4.1. Class 1 FRP material

The material must have a total fiber volume fraction of 55% or greater and must have a total longitudinal fiber volume (relative to the total fiber volume) of 95% or greater.

A.1.4.2. Class 2 FRP material

The material must have a total fiber volume fraction of 40% or greater and must have a total longitudinal fiber volume (relative to the total fiber volume) of 75% or greater.

A.1.4.3. Class 3 FRP material

The material must have a total fiber volume fraction of 40% or greater and must have a total longitudinal fiber volume (relative to the total fiber volume) of 40% or greater.

Non-woven continuous filament mats (CFM) of the primary reinforcement type are included in the total fiber volume fraction count. Only continuous fibers in the longitudinal direction are included in the total longitudinal fiber volume.

A.1.5. Classification

The material is classified on the laminate level according to its fiber type, resin type and fiber architecture. Laminates having at least three-dimensional transversely isotropic symmetry or two-dimensional (in-plane) orthotropic symmetry are permitted. For in-plane orthotropy laminates must be balanced and symmetric. The classification is applied to every distinct laminate thickness and fiber architecture within the FRP part. The classification nomenclature is as follows: fiber type, polymer resin type, class (e.g., GV2 designates a glass/vinylester class 2 FRP material). Manufacturer shall report items detailed above in a tabular form as shown in Table 1 for the FRP materials produced.

A.1.6. Physical and mechanical properties

A.1.6.1. Full-section testing

The manufacturer shall provide full-section longitudinal strength and stiffness properties for all sizes of GFRP bars specified in the plans. Full-section tests shall be conducted on as-produced lengths of GFRP rebar and require specialized end anchorages and gripping devices. A

minimum of three full-section tests is required for each size bar. Longitudinal tensile strength and stiffness of GFRP bars tested in full-section shall meet or exceed values shown in Table 2.

Table 1 – Reporting requirements for constituent materials of GFRP bars.

Item	Type	Manufacturer	Special requirements
Fiber	E-glass roving type	E-glass roving manufacturer	NA
	E-glass fabric type(s)	E-glass fabric manufacturer	NA
	E-glass mat type	E-glass mat manufacturer	NA
Veil	Surface veil type	Surface veil manufacturer	NA
Resin	Vinylester type(s)	Vinylester manufacturer	NA
	Styrene type	Styrene manufacturer	pph (< 10 pph resin)
Filler	Filler type	Filler manufacturer	pph (< 20 pph resin)
Additives	Shrink additive type	Shrink additive manufacturer	pph (< 10 pph resin)
Process	Pultusion die temperature	NA	NA
	Date of production	NA	NA
	Lot size	NA	NA

Table 2 – Limiting full-section properties for GFRP bars.

Bar Size	Nominal diameter	Strength	Stiffness
#3	0.375 in (9.53 mm)	110 ksi (760 MPa)	5.92 msi (40.8 GPa)
#4	0.500 in (12.7 mm)	100 ksi (690 MPa)	5.92 msi (40.8 GPa)
#5	0.625 in (15.9 mm)	95 ksi (655 MPa)	5.92 msi (40.8 GPa)
#6	0.750 in (19.1 mm)	90 ksi (620 MPa)	5.92 msi (40.8 GPa)
#7	0.875 in (22.2 mm)	85 ksi (586 MPa)	5.92 msi (40.8 GPa)
#8	1.000 in (25.4 mm)	80 ksi (550 MPa)	5.92 msi (40.8 GPa)
#10	1.25 in (31.8 mm)	75 ksi (517 MPa)	5.92 msi (40.8 GPa)

A.1.6.2. Coating for bond to concrete

FRP Rebars shall have a proprietary coating applied to their entire outside surface to ensure bond to the concrete. FRP rebars shall have a bond strength of not less than 1450 psi (10 MPa) when measured in a direct pull-out test.

A.1.6.3. Sealing of cut-ends

Manufacturer shall seal all cut-ends of the pultruded FRP rebars with an epoxy or vinylester resin prior to shipment.

A.1.7. Quality assurance

A.1.7.1. GFRP reinforcing bars

Quality control should be carried out by lot testing of GFRP bars. The manufacturer should supply adequate lot or production run traceability. Tests conducted by the manufacturer or a third-party independent testing agency can be used.

All tests should be performed using the recommended test methods cited in the literature. Material characterization tests that include the items detailed in Table A.1 and in Table 2 should be performed at least once before and after any change in manufacturing process, procedure, or materials.

The manufacturer should furnish upon request a certificate of conformance for any given lot of GFRP bars with a description of the test protocol. An authorized company representative shall sign, date and certify all test reports. Two copies of the certified test reports shall be provided at the time of material delivery. Reports and certifications shall be provided by the manufacturer to the Engineer for approval.

A.1.7.2. Referenced ASTM methods

Standards of the American Society of Testing and Materials referred to in this paper are listed below. All standards appear in the current annual edition of ASTM standards published by the American Society of Testing and Materials, West Conshohocken, PA.

C904 - Standard Terminology Relating to Chemical-Resistant Nonmetallic Materials.

D570 - Standard Test Method for Water Absorption of Plastics.

D618 - Standard Practice for Conditioning Plastics for Testing.

D638 - Standard Test Method for Tensile Properties of Plastics.

D695 - Standard Test Method for Compressive Properties of Rigid Plastics.

D696 - Standard Test method for Coefficient of Linear Thermal Expansion of Plastics between -30° and 30° with a Vitreous Silica Dilatometer.

D2344 - Standard Test Method for Short-Beam Strength of Polymer Matrix Composite Materials and Their Laminates.

D2583 - Standard Test Method for Indentation Hardness of Rigid Plastics by Means of a Barcol Impressor.

D2584 - Standard Test Method for Ignition Loss of Cured Reinforced Resins.

D3039 - Standard Test Method for Tensile Properties of Polymer Matrix Composite Materials.

D3171 - Standard Test Method for Constituent Content of Composite Materials.

D3410 - Standard Test Method for Compressive Properties of Polymer Matrix Composite Materials with Unsupported Gage Section by Shear Loading.

D3418 - Standard Test Method for Transition Temperatures of Polymers By Differential Scanning Calorimetry.

D3916 - Standard Test Method for Tensile Properties of Pultruded Glass-Fiber-Reinforced Plastic Rod.

D3917 - Standard Specification for Dimensional Tolerance of Thermosetting Glass-Reinforced Plastic Pultruded Shapes.

D4475 - Standard Test Method for Apparent Horizontal Shear Strength of Pultruded Reinforced Plastic Rods By The Short-Beam Method.

D5083 - Standard Test Method for Tensile Properties of Reinforced Thermosetting Plastics Using Straight-Sided Specimens.

E1356 - Standard Test Method for Assignment of the Glass Transition Temperatures by Differential Scanning Calorimetry or Differential Thermal Analysis.

A.2. CONSTRUCTION METHODS

A.2.1. Field handling and storage

Delivered FRP reinforcement to the job site must be unloaded using fabric slings anchored to avoid excessive deformation. During storage all FRP materials must be kept clean and protected from excessive exposure to moisture.

A.2.2. Cutting of FRP materials

Cutting of any FRP materials must be done with the use of a toothless chop disk or diamond coated circular blade. All field cuts of the bar materials must be sealed with Concresive 1090 or similar sealant approved by the Engineer.

A.2.3. Securing of FRP reinforcement system

The FRP deck reinforcement system must be properly secured to ensure stabilization and prevention of wind uplift prior to concrete placement.

A.2.4. Ties

Only non-metallic ties, either plastic cable ties or coated wire can be used to tie down grid panel or reinforcement bars.

A.2.5. Reinforcing bar placement

The FRP reinforcing bars must be properly anchored against displacement before concrete placement, by tying up to and against the FRP grid panel.

A.3. METHOD OF MEASUREMENT

FRP Reinforcing Bar will be measured by the kilogram, and the quantity shall be the number of kilograms incorporated in the completed work in accordance with the requirements of the plans and specifications. The masses of the bars will be computed using a density of 125 lb/ft^3 or 2000 kg/m^3.

APPENDIX B.

RAPID CONSTRUCTION OF CONCRETE BRIDGE DECK USING PREFABRICATED FRP REINFORCEMENT

The following paper was published in the Proceedings of the Third International Conference on FRP Composites in Civil Engineering (CICE 2006), December 13-15, 2006, Miami, FL, International Institute for FRP in Construction, pp. 151-154. The paper presents a summary of PROJECT 1: CONSTRUCTION, from which PAPER 1 of this dissertation originated.

RAPID CONSTRUCTION OF CONCRETE BRIDGE DECK USING PREFABRICATED FRP REINFORCEMENT

Fabio Matta[a,*], Antonio Nanni[a], Thomas E. Ringelstetter[b], and Lawrence C. Bank[b]

[a] Center for Infrastructure Engineering Studies, University of Missouri-Rolla

[b] Dept. of Civil and Environmental Engineering, University of Wisconsin-Madison

ABSTRACT

The development of durable structural systems for accelerated bridge construction is key to reducing the economic and social costs associated with replacement operations on a large scale. This paper reports on the field application of stay-in-place reinforcing panels, entirely made of glass fiber reinforced polymer components and specifically

* Graduate Research Assistant. Corresponding author – 220 Engineering Research Laboratory, 1870 Miner Circle, 65409-0710 Rolla, MO, USA. Tel +1 (573) 341-6661, Fax -6215, E-mail: *mattaf@umr.edu*.

developed for the rapid construction of concrete bridge decks. The salient features of the system are illustrated, along with significant research and development outcomes. The five-day construction of the cast-in-place deck and open-post rail of Bridge No. 14802301 in Greene County, MO, is documented, and the major outcomes outlined. The project demonstrates how lightweight and noncorrosive FRP reinforcement is a practical alternative to steel, with the potential of versatile structural forms that add relevant constructibility and economic advantages.

Keywords: Bridge deck; Fiber reinforced polymers; Accelerated bridge construction.

INTRODUCTION

During the last four years, increasing investments have been made to support the research and development of innovative technologies for accelerated bridge construction, primarily under the sponsorship of the Federal Highway Administration (FHWA), the American Society of State Highway and Transportation Officials (AASHTO Technology Implementation Group), and the Transportation Research Board (TRB Task Force on Accelerating Innovation in the Highway Industry). Emphasis has been placed on improving safety and minimizing traffic disruption while enhancing quality and durability. The issue arises from the urgent need of upgrading and maintaining a significant portion of the bridge inventory while facing inevitable budget restrictions. Redecking operations are rather frequent, since corrosion of steel reinforcement is a major instrument of degradation in reinforced concrete (RC) decks and safety appurtenances. In the case of off-system bridges, cost-benefit analysis, contractors know-how and equipment availability typically result in the adoption of either partial or full-depth cast-in-place (CIP) technologies. The most popular solution limits the use of prefabricated elements to standardized partial-depth precast prestressed concrete panels as structural stay-in-place (SIP) forms between the girders, with CIP concrete topping, as opposed to traditional removable plywood forms. SIP steel metal deck forms, with a full-depth CIP configuration that eliminates the problem of reflective cracks, are less attractive due to three major drawbacks: a) safety concerns due to risks of accidental damage of relatively thin metal sheets, resulting in local buckling problems under wet concrete load; b) corrosion issues under aggressive environments; c) efficient inspection of the underside of the deck is complicated.

In the project presented herein, an innovative prefabricated glass Fiber Reinforced Polymer (FRP) SIP reinforcement has been selected to construct the replacement deck of Bridge No. 14802301 in Greene County, MO. Corrosion resistant FRP reinforcement gratings and SIP form plates are integrated into very large-size modular panels. The structural form takes advantage of FRP composites tailorability and lightweight to provide improved constructibility, resulting in enhanced construction speed and safety.

PREFABRICATED STAY-IN-PLACE FRP REINFORCEMENT

Description and detailing

The FRP SIP panels are prefabricated assemblying off-the-shelf pultruded glass/vinylester components, typically used in floor grating applications in corrosive environments, into a three-dimensional grating made of two (top and bottom) layers (Figure 1).

The main load-carrying elements are 38 mm I-bars, spaced at 100 mm on-center, which run continuously in the direction perpendicular to traffic (transverse). Both shape and spacing of the I-bars have been thought to allow ease of walking over the three-dimensional assembly. Three-part cross rods, spaced at 100 mm on-center and running through pre-drilled holes in the I-bars web in the direction parallel to traffic (longitudinal), provide shrinkage and temperature reinforcement, enhance the in-plane rigidity of each reinforcing layer, and constrain the core concrete to ensure mechanical compatibility with the structural I-bars. Top and bottom reinforcing layers are integrated using two-part vertical connectors that space them at 100 mm on-center. The two components forming the connectors are shaped to be epoxy-bonded to the I-bars and then

fastened together. The formwork consist of 3.2 mm thick and 1.22 m long plates that are epoxy-bonded to the I-bars in the bottom layer.

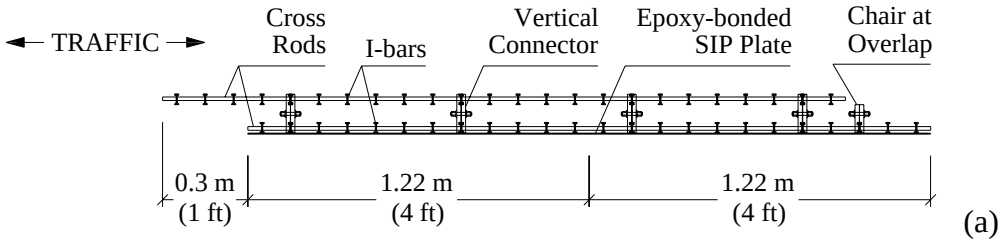

(a)

(b)

Figure 1 – FRP SIP reinforcement panels: (a) longitudinal section; and (b) close-up.

The system concept, detailing and construction procedure have been addressed to improve constructibility by introducing original solutions when needed, and constantly seeking input from practitioners. Each SIP panel has a width of 7.06 m, a typical length of 2.44 m [Figure 1(a)], and a weight of about 409 kg (23.7 kg/m^2). The width corresponds to that of the bridge deck minus 127 mm per side, to allow a traditional drip edge notch to be formed on-site. The use of large-size and lightweight panels allows easy placement of the SIP reinforcement on the bridge girders with single picks of a crane at four anchorage points. Hence, both time-consuming and labor-intensive setting/removing of plywood forms and tying of rebars are eliminated. Adjacent panels are connected in a non-mechanical fashion by means of 0.30 m overlaps, formed by

offsetting the top and bottom grating layers [Figure 1(a)], thereby preserving a degree of continuity in the longitudinal direction [Figure 1(a) and Figure 2(a)]. 3.2 mm thick strips are inserted to cover the SIP plate-to-plate butt joints in order to prevent concrete leaking during casting [Figure 2(b)]. When using steel girders, each SIP unit is anchored to the top flanges via stainless steel threaded bolts at every 2.44 m, keeping the bottom reinforcing layer in place with 6.3 mm thick FRP washers [Figure 2(c)]. Holes in the SIP plate are drilled on site. When composite action is sought between girders and deck, the panels can be supplied with pre-drilled holes with longitudinal and transverse spacing of 10 cm on-center to accommodate welded shear studs. No cambering of the panels is required to match the roadway crown, which is formed using the finishing machine. The length and layout of the end panels are designed to fit the actual bridge length and accommodate the expansion joints. Since glass FRP is easy to saw-cut, adjustments can be readily made on site [Figure 2(d)].

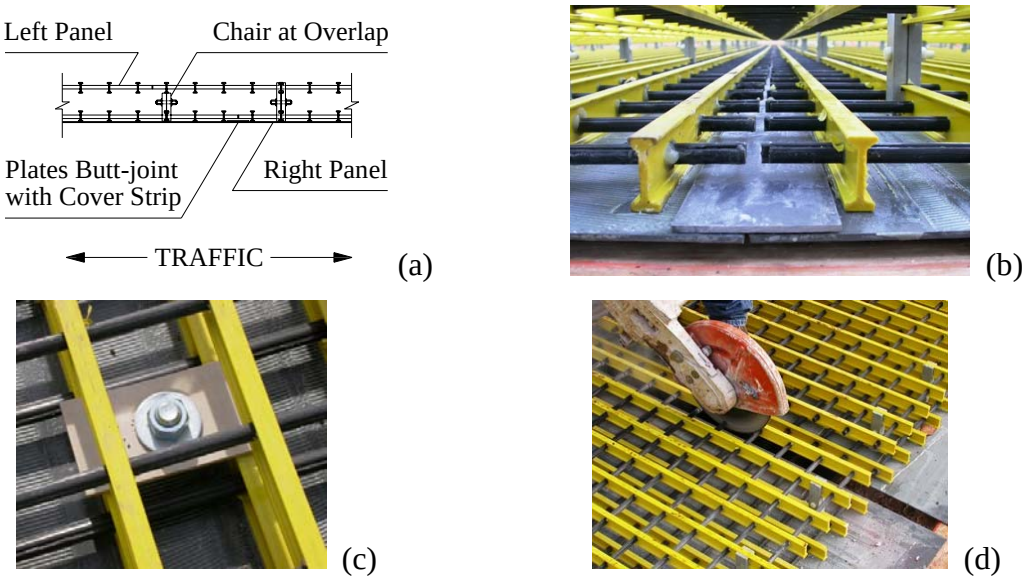

Figure 2 – Deck reinforcement detailing: (a-b) panel-to-panel connection; (c) anchoring to girder; and (d) end panels at expansion joint.

Research and development

Extensive research and development work during the last 14 years has demonstrated the structural effectiveness of pultruded FRP gratings as internal reinforcement of concrete bridge decks. Two recent pioneer construction projects have been completed in Wisconsin, USA (Bank et al. 2006, Berg et al. 2006). The solution presented herein features the last-generation system, and the first with fully-integrated reinforcement and SIP forms (Ringelstetter et al. 2006). The project Special Provisions included FRP Material Specifications, in compliance with a model specification developed for the FHWA (Bank et al. 2003). Performance Specifications were also defined for the SIP panels by imposing stress and deformation limitations to test panels when simulating typical construction loads, i.e. vertical and lateral loads, in-plane racking, vertical load on overlaps, and wet concrete load (Matta et al. 2005).

The FRP RC open post rail was designed following the ACI 440 guidelines (ACI 2006) to meet the AASHTO LRFD (AASHTO 1998) and Standard Specifications (AASHTO 2002). In the case of the LRFD provisions, where a yield-line approach is recommended to evaluate the equivalent transverse static strength, deformation compatibility was assumed to account for the lack of moment redistribution in FRP RC structures, along with conservative failure scenarios (Matta and Nanni 2006). In addition, the end posts located at the expansion joints and approach deck, where rail continuity is not provided, were designed to exceed the required crash Test Level 2 strength F_T = 120 kN.

The deck and rail design was validated through laboratory testing of full-scale deck slabs and rail post/deck connections, which was performed at key steps of the

optimization process, and confirmed the significant safety margin of the layout selected for the field implementation (Matta et al. 2005).

FIVE-DAY BRIDGE REDECKING

The old Bridge No. 14802301 (Greene County, Missouri) slab-on-girder superstructure, built in 1933, was in need of replacement because of severe corrosion-induced degradation of deck and safety appurtenances, and increased load requirements. The load rating was 3.9 t (2004), versus an original design based on a 9.1 t truck load with 30% impact factor. The new superstructure has four symmetrical spans of 11.3 m (exterior) and 10.7 m (interior) length, for a total length of 43.9 m. The cross section comprises four W610×25 steel girders spaced at 1.8 m on-center and acting non-compositely with a 178 mm thick deck. The out-to-out deck and clear roadway width are 7.3 m and 6.7 m, respectively. The girders are continuous over two spans, with a closed expansion joint at the central support.

Transition from research and development to field implementation was conducted in coordination with the manufacturers of the FRP deck and rail reinforcement, and the engineer of record. The construction operations were planned with the contractor parties to minimize the amount of time and work. Construction of the RC deck and railing from the SIP panel installation to rail casting is documented in Figure 3. The job was completed in November 2005 in five days, instead of the typical 2-3 weeks needed for similar steel reinforced bridges built by the contractor. Installation of the deck panels was finalized in six hours during the first day by six workers. During the second day, the 36 rail post cages were mounted, the deck details formed (expansion joints, chamfers,

drip edges), and the finishing machine was set. Deck casting and finishing was completed in the third day. The remaining two days were used to mount the open post concrete rail top continuous cages and the formwork, and finally casting.

(a) (b) (c)

(d) (e) (f)

(g) (h) (i)

Figure 3 – Bridge redecking operations: (a) panels installation; (b) mounting of post cages; (c) deck casting and (d) finishing; (e) mounting of top rail cages; (f) rail casting; and (g-1) finished superstructure.

CONCLUSIONS

The first application project of a novel prefabricated FRP reinforcement for rapid bridge deck construction has been presented. The use of very large-size and lightweight modular stay-in-place panels, comprising a double-layer grating with epoxy-bonded form plates and designed for improved constructibility, eliminates the need of formwork and on-site tying of reinforcing bars. The five-day redecking resulted in over 70% reduction in deck construction time, with a similar reduction in labor cost. Shape and spacing of the reinforcing profiles, devised to facilitate walking over the three-dimensional assembly, allowed an increase of about 50% in concrete placement productivity while improving safety and working conditions, as confirmed by the field workers.

A conservative cost estimate for the deck as-built is \$409/m^2 (\$38/ft^2), of which \$280/m^2 (\$26/ft^2) from the prototype FRP panels delivered to the site. The amount increases to \$483/m^2 (\$44.9/ft^2) including the cost of the open post railing (\$271/m, \$82.6/ft). The competitive potential of the proposed system is also enhanced by the durability of FRP reinforcement, with prospective increased service life and reduced maintenance costs.

5. ACKNOWLEDGMENTS

The financial support of the US DOT, the UMR UTC on Advanced Materials and NDT Technologies, and the Federal Highway Administration, thorugh the Innovative Bridge Research and Construction Program, is acknowledged. The assistance of Strongwell and Hughes Brothers, industry members of the UMR NSF I/UCRC “Repair of Buildings and Bridges with Composites” (RB^2C), is also acknowledged. Thanks are due

to Greene County, MoDOT, Great River Engineering, Hartman Construction, and Master Contractors LLC, for active support.

REFERENCES

ACI Committee 440, "Guide for the design and construction of structural concrete reinforced with FRP bars," *ACI 440.1R-06,* American Concrete Institute, Farmington Hills, MI, 2006, 44 pp.

American Association of State Highway and Transportation Officials (AASHTO), "Load and resistance factor design (LRFD) bridge design specifications," 3rd edition, AASHTO, Washington, D.C., 2004.

American Association of State Highway and Transportation Officials (AASHTO), "Standard specifications for highway bridges," 17th edition, AASHTO, Washington, D.C., 2002.

Bank, L. C., Gentry, T. R., Thompson, B. P., and Russell, J. S., "A model specification for FRP composites for civil engineering structures," *Construction and Building Materials*, V. 17, No. 6-7, 2003, pp. 405-437.

Bank, L. C., Oliva, M. G., Russell, J. S., Jacobson, D. A., Conachen, M. J., Nelson, B., and McMonigal, D., "Double layer prefabricated FRP grids for rapid bridge deck construction: case study," *Journal of Composites for Construction*, V. 10, No. 3, 2006, pp. 204-212.

Berg, A. C., Bank, L. C., Oliva, M. G., and Russell, J. S., "Construction and Cost Analysis of an FRP Reinforced Concrete Bridge Deck," *Construction and Building Materials*, V. 20, No. 8, 2006, pp. 515-526.

Matta, F., and Nanni, A., "Design of concrete railing reinforced with glass fiber reinforced polymer bars," *Proc. 2006 Structures Congress,* CD-ROM, 2006, 9 pp.

Matta, F., Nanni, A., Galati, N., Ringelstetter, T. E., Bank, L. C., Oliva, M. G., Russell, J. S., Orr, B. M., and Jones, S. N., "Prefabricated modular GFRP reinforcement for accelerated construction of bridge deck and rail system," *Proc. FHWA Accelerated Bridge Construction Conference,* FHWA, Washington, D.C., 2005, pp. 129-134.

Ringelstetter, T. E., Bank, L. C., Oliva, M. G., Russell, J. S., Matta, F., Nanni, A., "Development of a cost-effective structural FRP stay-in-place formwork system for accelerated and durable bridge deck construction," *Proc. 85th Transportation Research Board Annual Meeting*, CD-ROM #06-2218, 2006, 16 pp.

APPENDIX C.

GEOMETRIC DESIGN OF OPEN-POST RAILING PROFILE FOR BRIDGE NO. 14802301, GREENE COUNTY, MO

This Appendix presents a summary of the geometric design that addresses the functionality characteristics required for crashworthiness of the GFRP RC open-post railing used in PROJECT 1: CONSTRUCTION, from which PAPER 1 of this dissertation originated. The geometric design was discussed in a paper (Matta and Nanni 2006) that was published in the Proceedings of the 2006 ASCE Structures Congress, May 18-20, 2006, St Louis, MO, and of which the following is an extract.

Bridge railings must contain and redirect errant vehicles while preventing rollover and snagging, and allowing deceleration to a stop at a relatively short distance from the impact section. Therefore, crash testing of bridge safety appurtenances aims at assessing both the structural and geometrical crashworthiness, depending on the level of service sought (TL-1 to TL-6, being the latter the most demanding), along with the vehicle occupant risk. Based on the results of a number of full-scale crash tests performed as part of programs under the Federal Highway Administration, the American Association of State Highway and Transportation Officials, the National Cooperative Highway Research Program and individual States, Section 13 (Railings) of the AASHTO LRFD Bridge Design Specifications (AASHTO 2004) sets forth strength and geometry criteria for design.

The safety performance of an open-post concrete railing greatly depends on its geometry. With reference to Figure 1(a), critical requirements are:

- sufficient rail height *H*, and suitable profile to reduce the potential for vehicle rollover. A minimum value $H = 27$ in. is recommended for both TL-2 and TL-3;

- continuous solid rail beam with smooth and sufficient contact width, *A*, with respect to *H*, to reduce the potential for vehicle wheel, bumper or hood impact with the post. A minimum *A* / *H* ratio of 0.25 is recommended, along with specified graphical parametric criteria;

- sufficient post setback distance, *S*, with respect to combination of *A* and *H*, to reduce the potential for vehicle snagging. Parametric recommendations are provided in graphical fashion to select design alternatives that proved to perform satisfactorily.

Figure 1(a) and Figure 1(b) show the geometry of the GFRP RC MKCR designed. Compared to the profile of the original design (dashed line), A has been increased from 14 in. to 17 in., with H increased from 27 in. to 30 in. Although vertical barriers typically offer the greatest reduction in rollover potential, despite the tradeoff of increased lateral accelerations (Mak and Sicking 1990), the recommended minimum height may be inadequate, especially in case of higher service levels. This has been recently observed in the (failed) TL-3 crash test of a 27 in. GFRP RC railing [Appendix A in (Buth et al. 2003)], whereas a similar configuration with increased height performed well [Appendix B in (Buth et al. 2003)]. The post setback was kept at the original distance S = 2 in. from the rail beam contact surface, similarly to other steel RC counterparts of same or higher category, such as the Modified Corral Rail (TL-2) and 32 in. Corral Rail (TL-4) in Kansas, or the Concrete Beam and Post (TL-2) and Open Concrete Bridge Rail (TL-4) in Nebraska (FHwA 2005). Figure 1(c) and Figure 1(d) show the compliance of the

selected design with the LRFD recommendations to minimize the risk of impact on the rail post and vehicle snagging, also correcting the slightly low A / H ratio of 0.52 of the original profile. It is seen from the dark arrows that the addition of any wearing surface would further move the geometric parameters into the preferred safety domains.

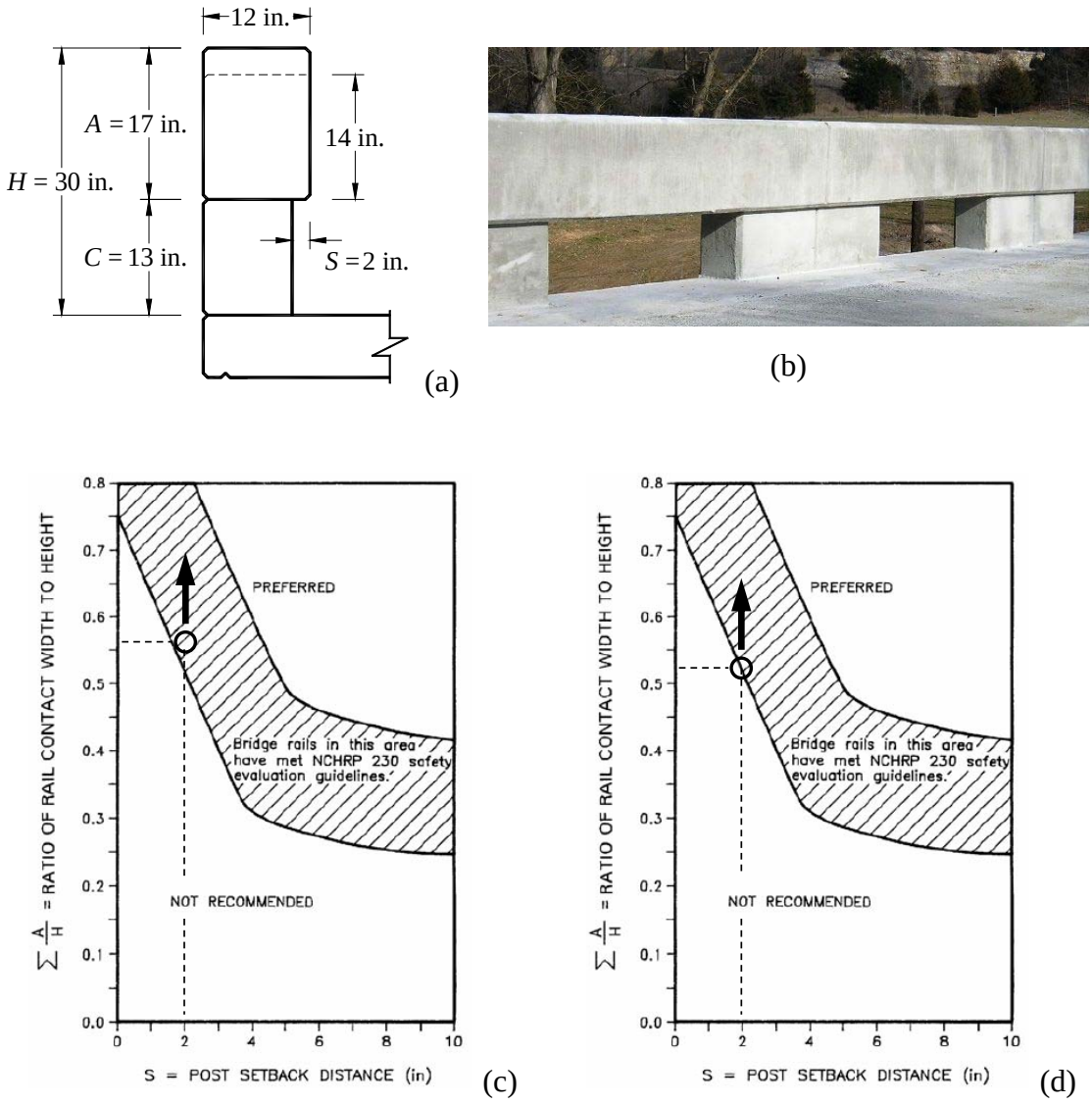

Figure 1 – Geometry of GFRP RC MKCR: (a) thru-section profile; (b) photograph of railing with post and gap opening length of 4 ft; and (c-d) compliance with AASHTO LRFD Bridge Design Specifications (circles) (AASHTO 2004).

The post and gap opening length, *P* and *G*, have been changed from the original 3 ft and 7 ft, respectively, to 4 ft each, as shown in Figure 1(b), in order to provide additional redundancy to evaluate upgrade to TL-3, as well as geometrical compatibility with the 8 ft long modular GFRP SIP reinforcing panels.

APPENDIX D.

VERIFICATION OF BOUNDARY CONDITIONS OF POST-OVERHANG SUBASSEMBLIES

The 8 ft (2.4 m) slab width in the post-deck overhang subassemblies described in PAPER 1 and shown in Figure 1 were dictated by the dimensions of the deck prefabricated reinforcement panels supplied. The boundary conditions reflect the simplest option for a meaningful test setup. A finite element study was conducted to verify that the selected slab dimensions and boundary conditions were consistent with those of an imaginary cut-out from a longer overhang, that is, a comparable displacement at the top of the 30 in. (762 mm) post is produced under a given transverse load under linear elastic conditions.

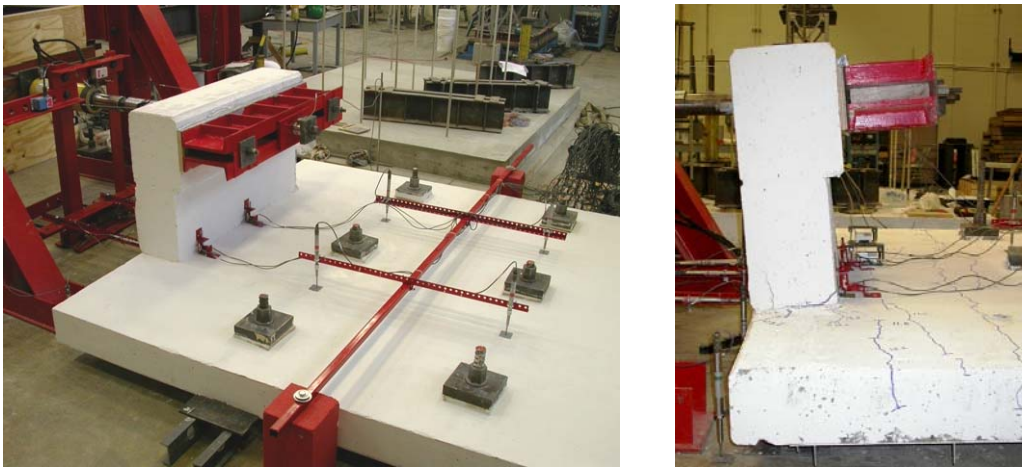

Figure 1 – Photographs of post-overhang subassembly and test setup.

Two finite element models (FEMs) were developed using a commercially available software (Strand7 2005). FEM A, illustrated in Figure 2, replicates the dimensions and approximate the symmetric boundary conditions of the tested specimen. Eight-node hexahedral (brick) elements (HEXA8) were used to model both the slab and the post. The 5 kip (22.2 kN) transverse load applied at a distance of 24 in. (610 mm) from the slab surface was rendered as uniform normal pressure on a 6 in. (152 mm) by 48

in. (1219 mm) area on the post face. Fixed boundary conditions were used at the support line at 3 ft (0.9 m) from the slab free edge. The maximum displacement at the top of the post was 0.013 in. (0.34 mm). FEM B, illustrated in Figure 3, differs from FEM A in the total slab width, increased from 8 ft (2.4 m) to 32 ft (9.8 m), that become 16 ft (4.9 m) considering symmetry. The maximum displacement at the top of the post was 0.012 in. (0.30 mm). The similarity confirmed the validity of the subassembly configuration.

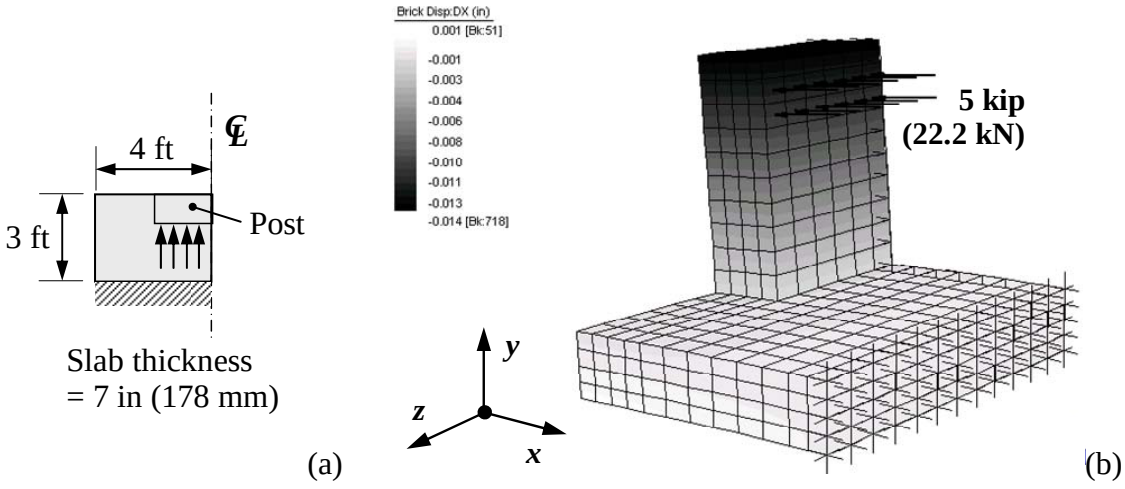

Figure 2 – FEM A: (a) schematic; and (b) contour of horizontal displacements.

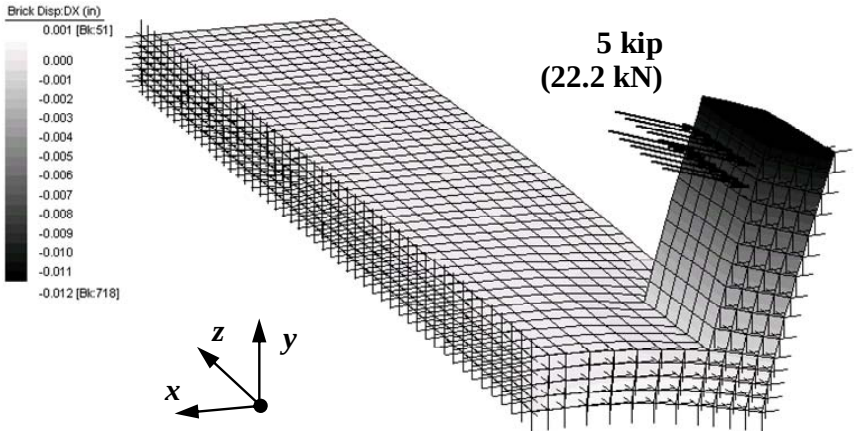

Figure 3 – FEM B: contour of horizontal displacements.

APPENDIX E.

GENERALIZED *N*-DOF NONLINEAR FINITE ELEMENT FORMULATION FOR OPEN-POST RAILING SYSTEM

The nonlinear spring used to idealize the post and its connection to the deck has a single degree of freedom (DOF) of the node *i* associated with the horizontal displacement u_i at the top of the post, as illustrated in Figure 1(a). The axial stiffness is modeled by means of the nonlinear function $k_p(u_i)$, which is analytically determined from the load-displacement model for the post-deck connection in Equation 1 of PAPER 1 of this dissertation. The effective moment of inertia of the deck cross section at the connection after cracking is computed per Equation 4, combined with Equation 5b, in PAPER 1.

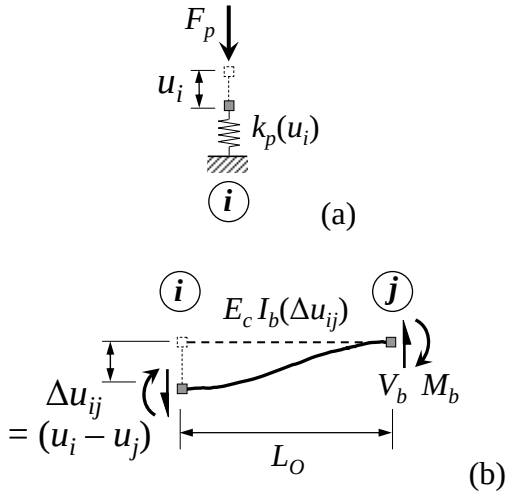

Figure 1 – Finite element formulation: (a) spring element for post; and (b) beam element along railing opening.

The idealization of the glass FRP reinforced concrete (RC) beam element along the railing opening of length L_O is shown in Figure 1(b), where E_c = modulus of elasticity of concrete, I_b = section moment of inertia of rail beam, and M_b and V_b = end moment and shear, respectively. A single DOF associated with horizontal displacement is assigned to each end node *i* and *j*, where rigid connections to the adjacent posts are assumed. Torsional effects are neglected. The 2×2 stiffness matrix is expressed as

$$\begin{cases} \mathbf{K_b}\left(\mathbf{u}\right) = \dfrac{12}{L_O^3} E_c I_b \left(\Delta u_{ij}\right) \begin{bmatrix} 1 & -1 \\ -1 & 1 \end{bmatrix} = \dfrac{2}{L_O} M_b \left(\Delta u_{ij}\right) \begin{bmatrix} 1 & -1 \\ -1 & 1 \end{bmatrix} \\ \Delta u_{ij} = u_i - u_j \end{cases}$$

where the nonlinear moment-net displacement function M_b-Δu_{ij} is computed by applying Equation 4, combined with Equation 5b, in PAPER 1 to determine the effective moment of inertia of the beam cross section after cracking.

The two critical loading scenarios for an open-post railing are illustrated in Figure 2(a) and Figure 3(a), respectively. The first, denoted as Case A, accounts for the equivalent static load F_t applied on a rail beam at the mid-section of the opening. The second, denoted as Case B, accounts for the transverse load applied directly on an intermediate post. The structure is idealized by means of the symmetric finite element model (FEM) shown in Figure 2(b) and Figure 3(b), for *Case A* and *Case B*, respectively. The post closest to the applied load is identified by the node $i = 1$, and the fixed node $i = N + 1$ identifies the post that is far enough from the applied load area to negligibly affect the maximum displacement u_1, and the end moment and shear M_b and V_b in the beam element between Node 1 and Node 2.

The vector of the horizontal displacement of the posts

$$\mathbf{u} = \begin{bmatrix} u_1 & \cdots & u_N \end{bmatrix}^T$$

is computed for a given transverse force vector of dimension N

$$\mathbf{F_t} = \begin{bmatrix} \dfrac{F_t}{2} & 0 & \ldots & 0 \end{bmatrix}^T$$

by solving the nonlinear system

$$\mathbf{u} = \mathbf{K}\left(\mathbf{u}\right)^{-1} \mathbf{F}_t ,$$

where the global stiffness matrix for the *N*-DOF post-and-beam system is assembled in the form of a typical narrowly banded matrix (half-bandwidth = 2) as

$$\mathbf{K}(\mathbf{u}) = \begin{bmatrix} K_{11}(\mathbf{u}) & K_{12}(\mathbf{u}) & 0 & \cdots & 0 \\ K_{21}(\mathbf{u}) & \ddots & \ddots & & \vdots \\ 0 & \ddots & K_{mm}(\mathbf{u}) & \ddots & 0 \\ \vdots & & \ddots & \ddots & K_{N-1,N}(\mathbf{u}) \\ 0 & \cdots & 0 & K_{N,N-1}(\mathbf{u}) & K_{N,N}(\mathbf{u}) \end{bmatrix},$$

where

$$\begin{cases} K_{11}(\mathbf{u}) = \dfrac{2}{L_O}\dfrac{\left|M_b\left(\Delta u_{12}\right)\right|}{\Delta u_{12}} + k_1\left(u_1\right) \\ k_1\left(u_1\right) = \begin{cases} k_p\left(u_1\right) & \text{for impact on rail beam (Case A)} \\ \dfrac{1}{2}k_p\left(u_1\right) & \text{for impact on post (Case B)} \end{cases} \end{cases}$$

$$K_{mm}(\mathbf{u}) = \frac{2}{L_O}\sum_{i=m-1}^{m}\frac{\left|M_b\left(\Delta u_{i,i+1}\right)\right|}{\Delta u_{i,i+1}} + k_p\left(u_m\right)$$

$$K_{m-1,m}(\mathbf{u}) = K_{m,m-1}(\mathbf{u}) = -\frac{2}{L_O}\frac{\left|M_b\left(\Delta u_{m-1,m}\right)\right|}{\Delta u_{m-1,m}}$$

with $2 \le m \le N$ and $u_{N+1} = 0$.

The model in Figure 2 may be used for the analysis of end posts when necessary, provided that the load is taken as F_t, and the specific stiffness function of the end post is incorporated. In fact, of a modified post-deck connection (for example, wider post and increased amount of reinforcement) may need to be designed with respect to that of the intermediate posts.

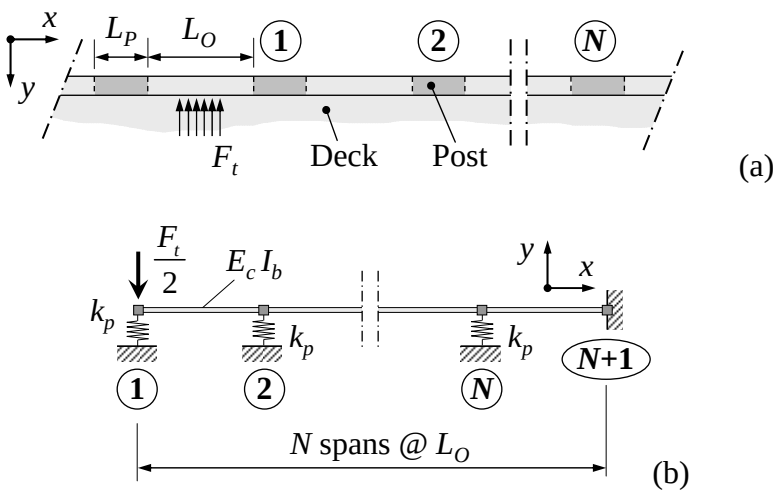

Figure 2 – Finite element analysis: (a) load Case A; (b) *N*-DOF symmetric FEM.

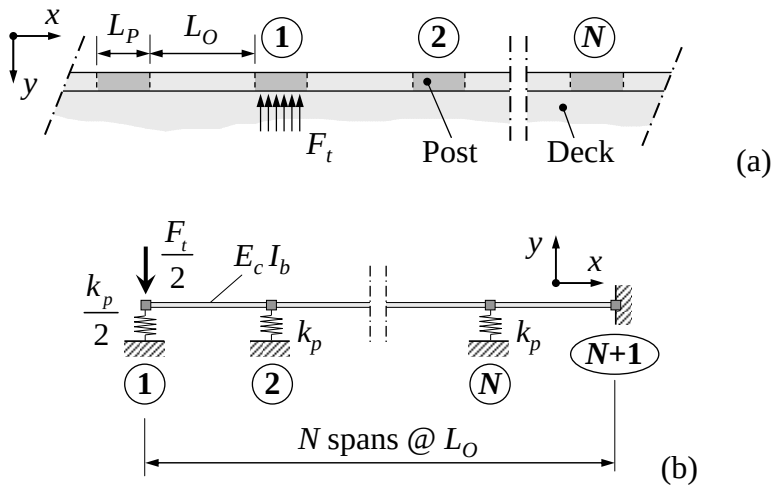

Figure 3 – Finite element analysis: (a) load *Case B*; (b) *N*-DOF symmetric FEM.

If the rail beam is capable of transferring the end moment and shear to the adjacent posts, the governing scenario is Case B. For the case of the glass FRP reinforced concrete connection and beam sections implemented in Bridge No. 14802301 in Greene County, MO, the load-displacement response at the post directly loaded,

computed using N = 4 (so that convergence of all relevant parameters is ensured), is shown in Figure 4 for opening length L_O of 4 ft, 6 ft, and 8 ft. The dashed horizontal line indicates the transverse load demand for Test Level 2 (TL-2) railings (AASHTO 2004), aimed at simulating the equivalent static load of a 4500 lb (2043 kg) pickup truck impacting at a speed of 45 mph and crash angle of 25°. The criterion applies to the open-post railings on Bridge No. 14802301.

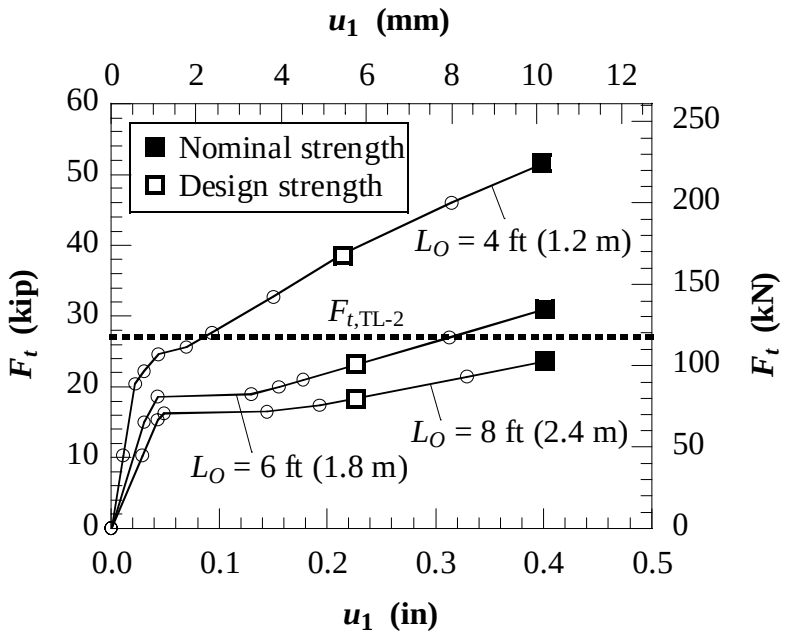

Figure 4 – Numerical load-displacement response of post-and-beam railing system.

It is also noted that the failure mode changes from diagonal tension at the post-deck connection for a 4 ft (1.2 m) to flexural failure of the rail beam at greater values of the opening length.

APPENDIX F.

RAW DATA OF QUASI-STATIC TEST ON POST-DECK CONNECTION SPECIMEN M2

This Appendix includes the raw data of the quasi-static test on the post-connection Specimen M2, whose design was implemented in Bridge No. 14802301 in Greene County, Missouri.

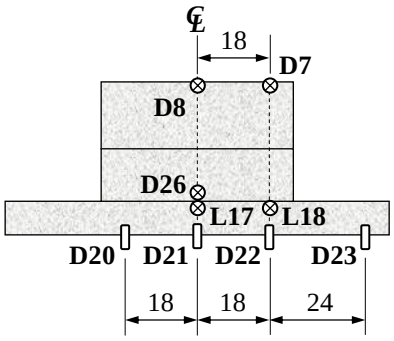

DCVT (D) and LVDT (L) displacement sensors (D7 and D8 draw-wire sensors). View from back of post.

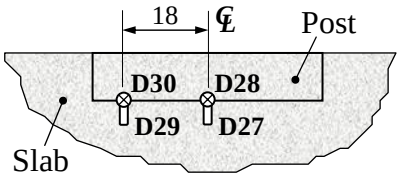

DCVT linear potentiometers for horizontal and vertical crack displacement measurement.

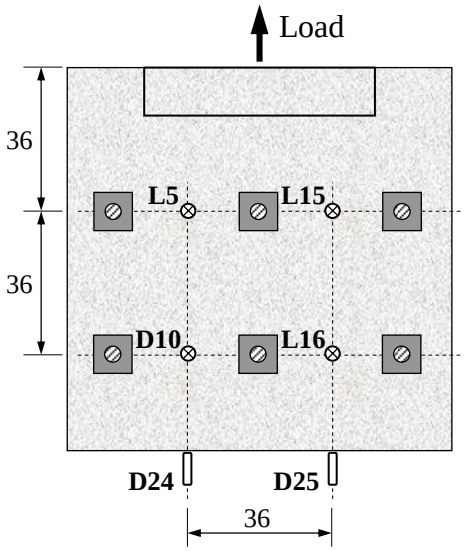

DCVT (D) and LVDT (L) displacement sensors. Plan view.

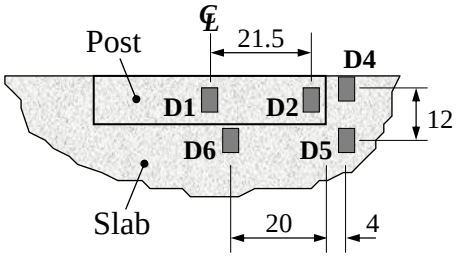

DCVT inclinometers.

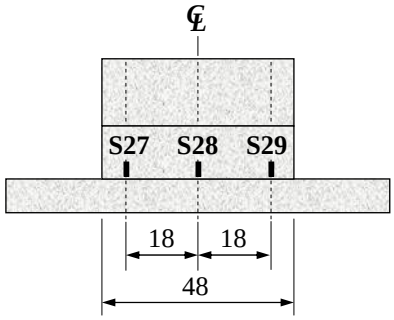

Concrete electrical-resistance strain gauges (gauge 2.4 in.). View from back of post.

Figure 1 – Schematic of instrumentation.

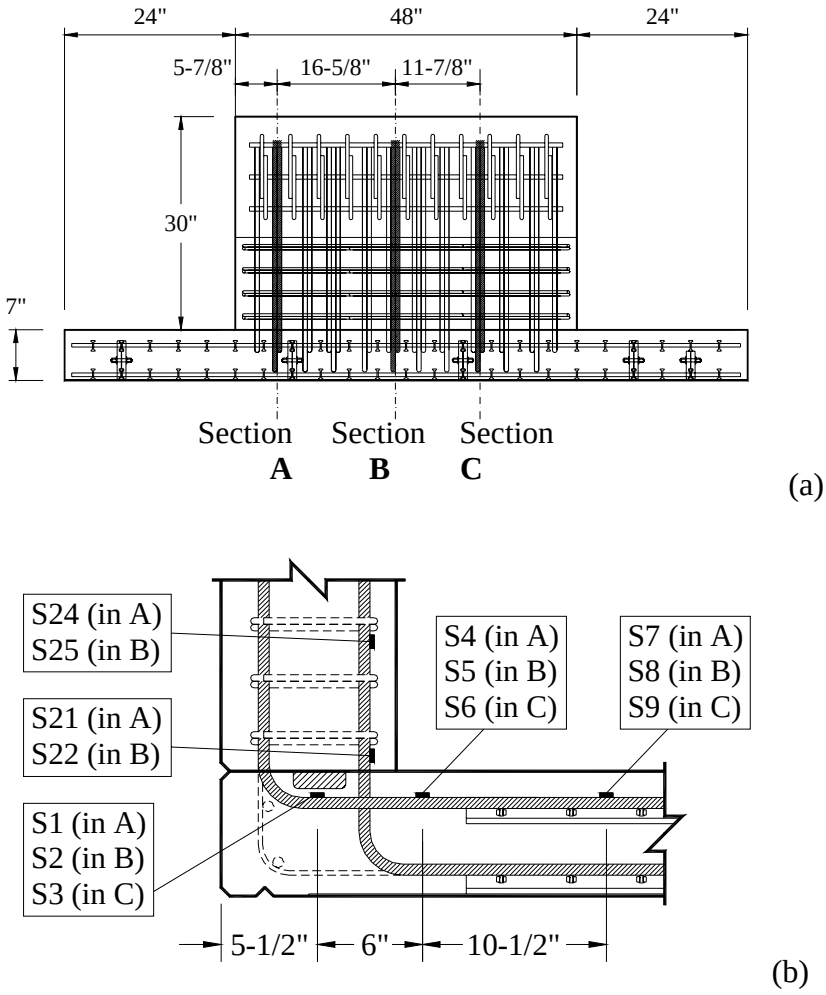

Figure 2 – Map of relevant strain gauges (S) in glass FRP bars in deck and post: (a) view from back of post; and (b) thru-connection section.

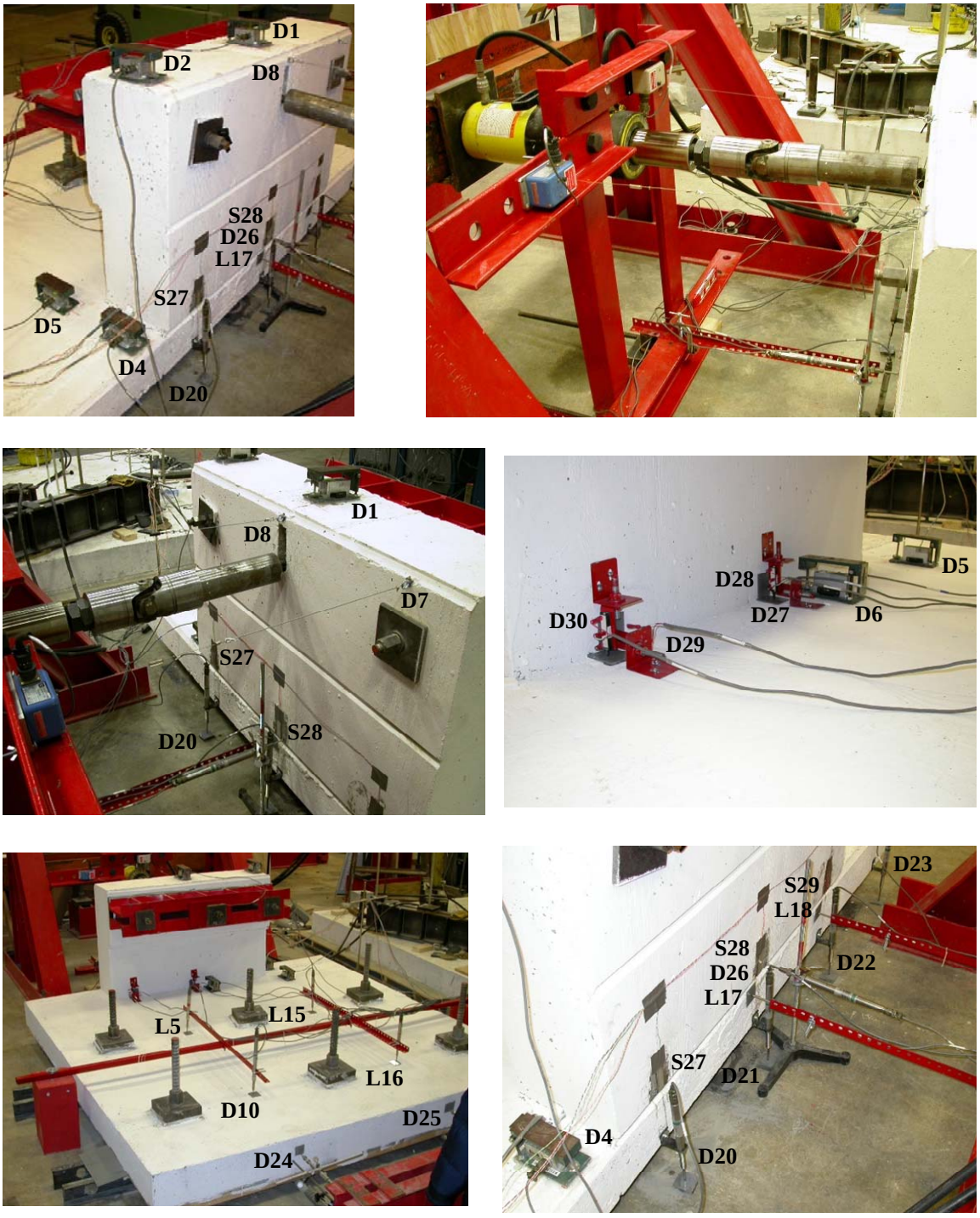

Figure 3 – Photographs of Specimen M2 setup and instrumentation: DCVT (D) sensors (displacement, crack opening, inclination), LVDT (L) sensors (displacement) and concrete electrical-resistance strain gauges (S).

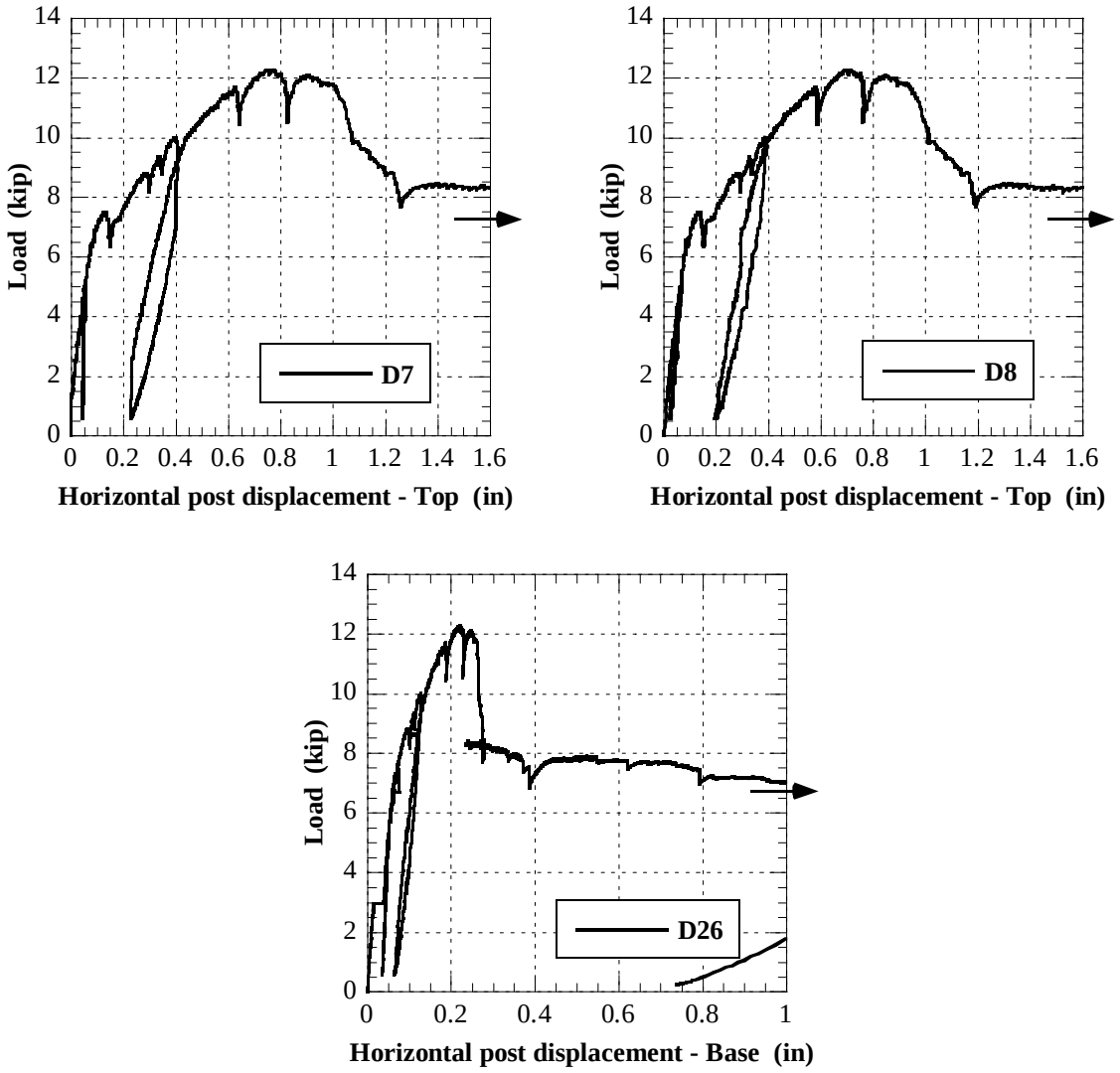

Figure 4 – Horizontal displacement of post (at top and at base).

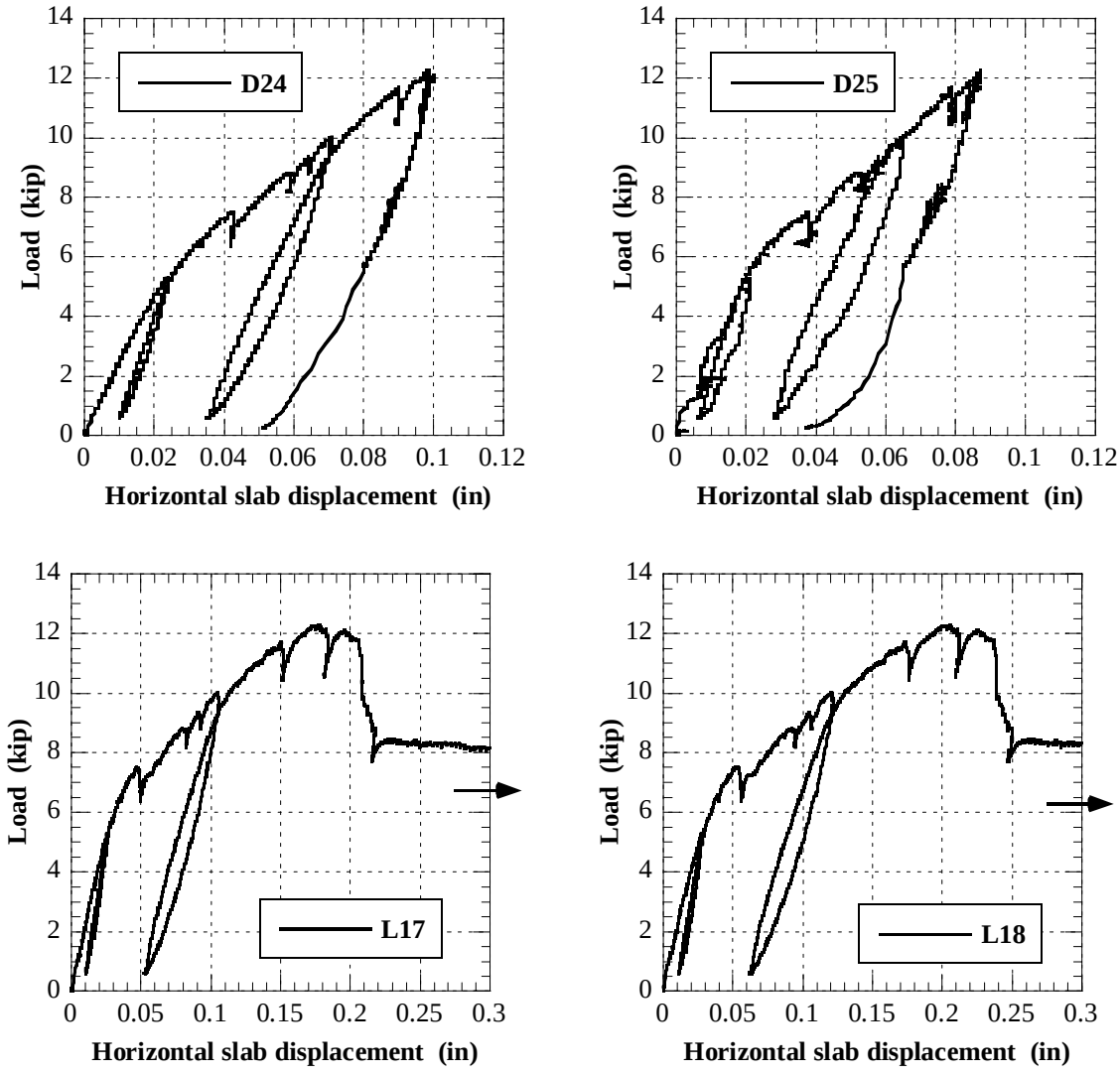

Figure 5 – Horizontal displacement of slab edge at connection (L17 and L18) and at opposite end (D24 and D25).

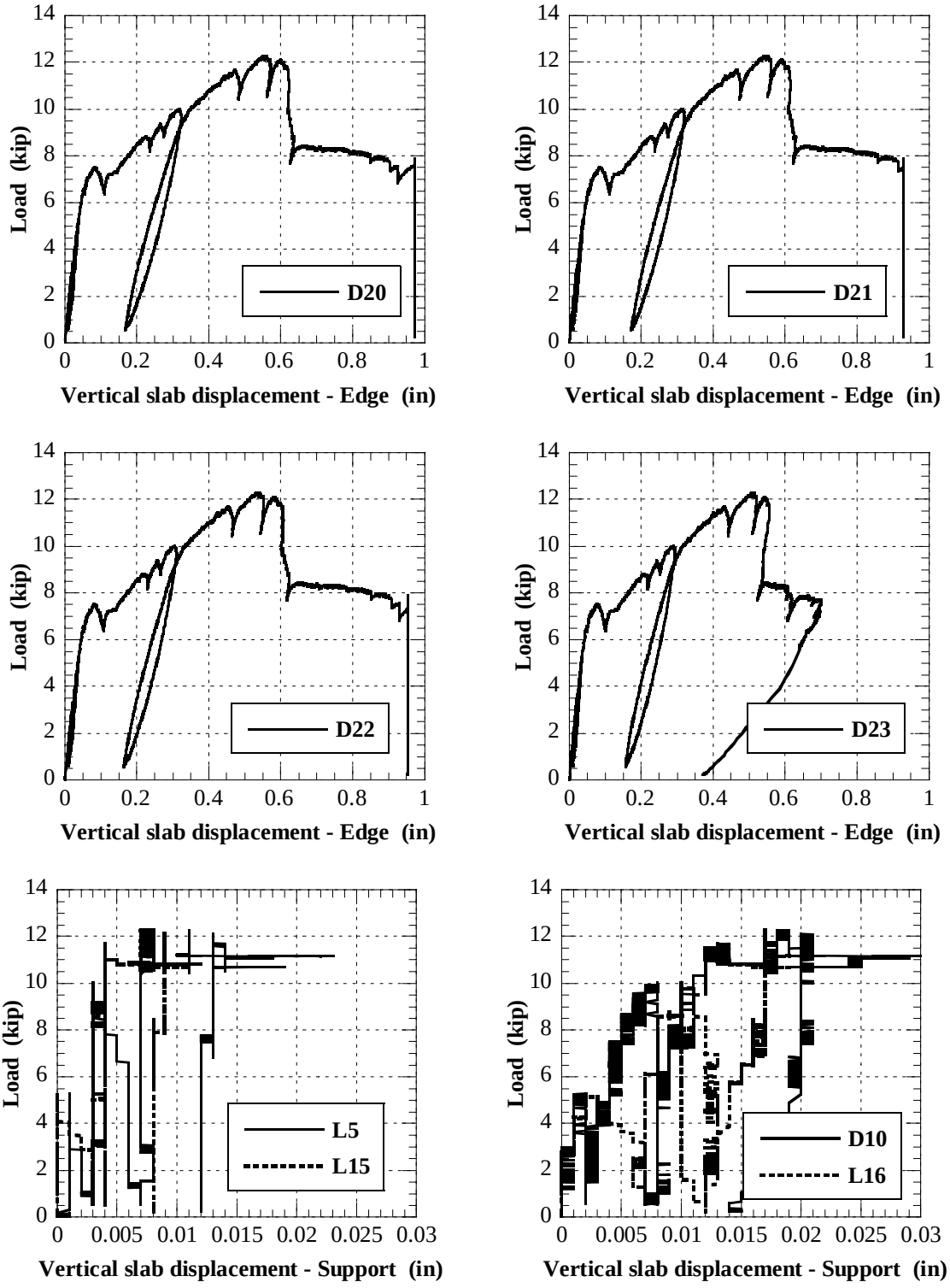

Figure 6 – Vertical displacement of slab at connection edge (D20, D21, D22 and D23) and at tie-down supports (L5, L15, L16 and D10).

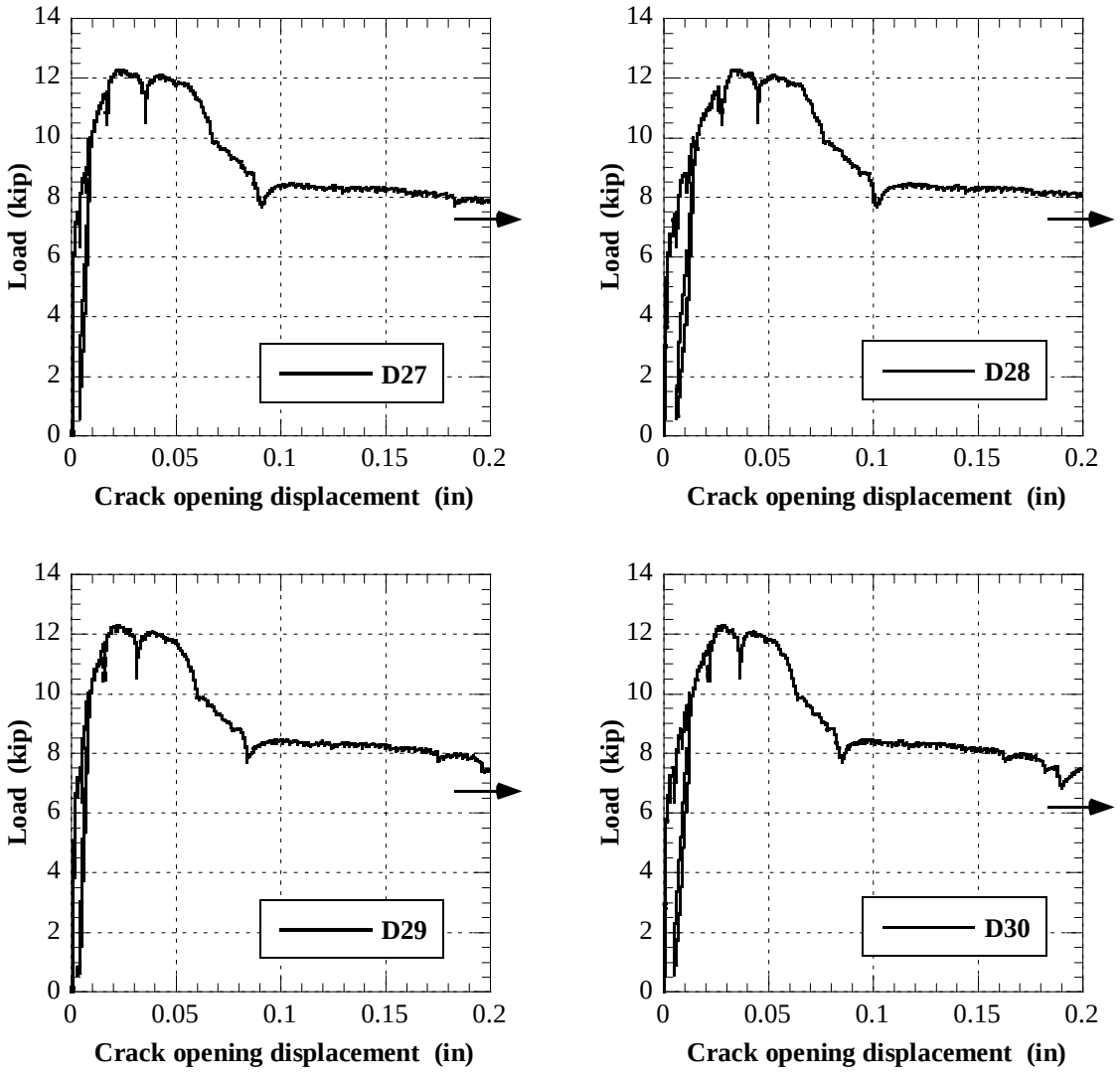

Figure 7 – Horizontal and vertical crack opening displacement at post-deck connection.

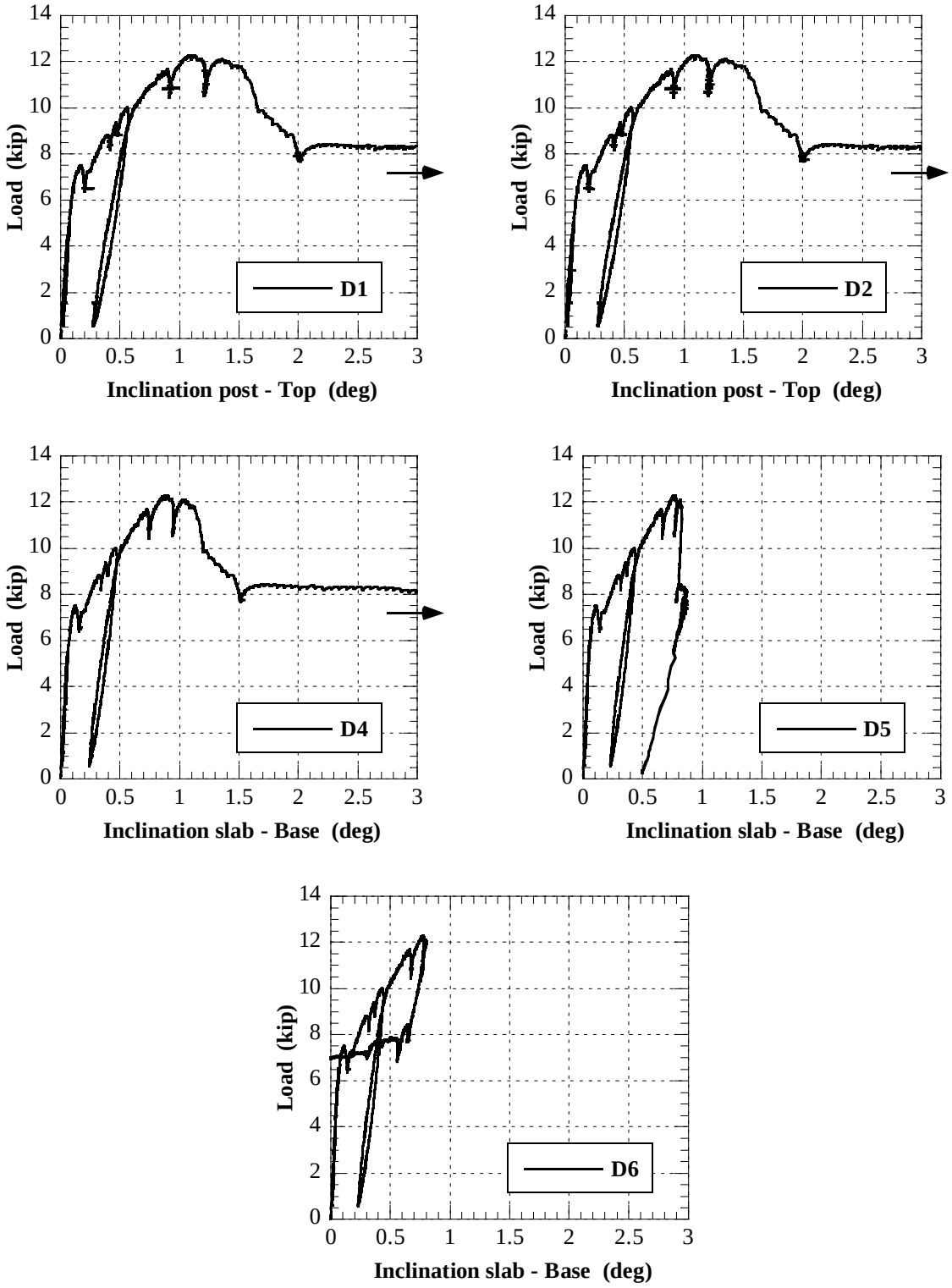

Figure 8 – Inclination of top of post (D1 and D2) and of slab at base of connection (D4, D5 and D6).

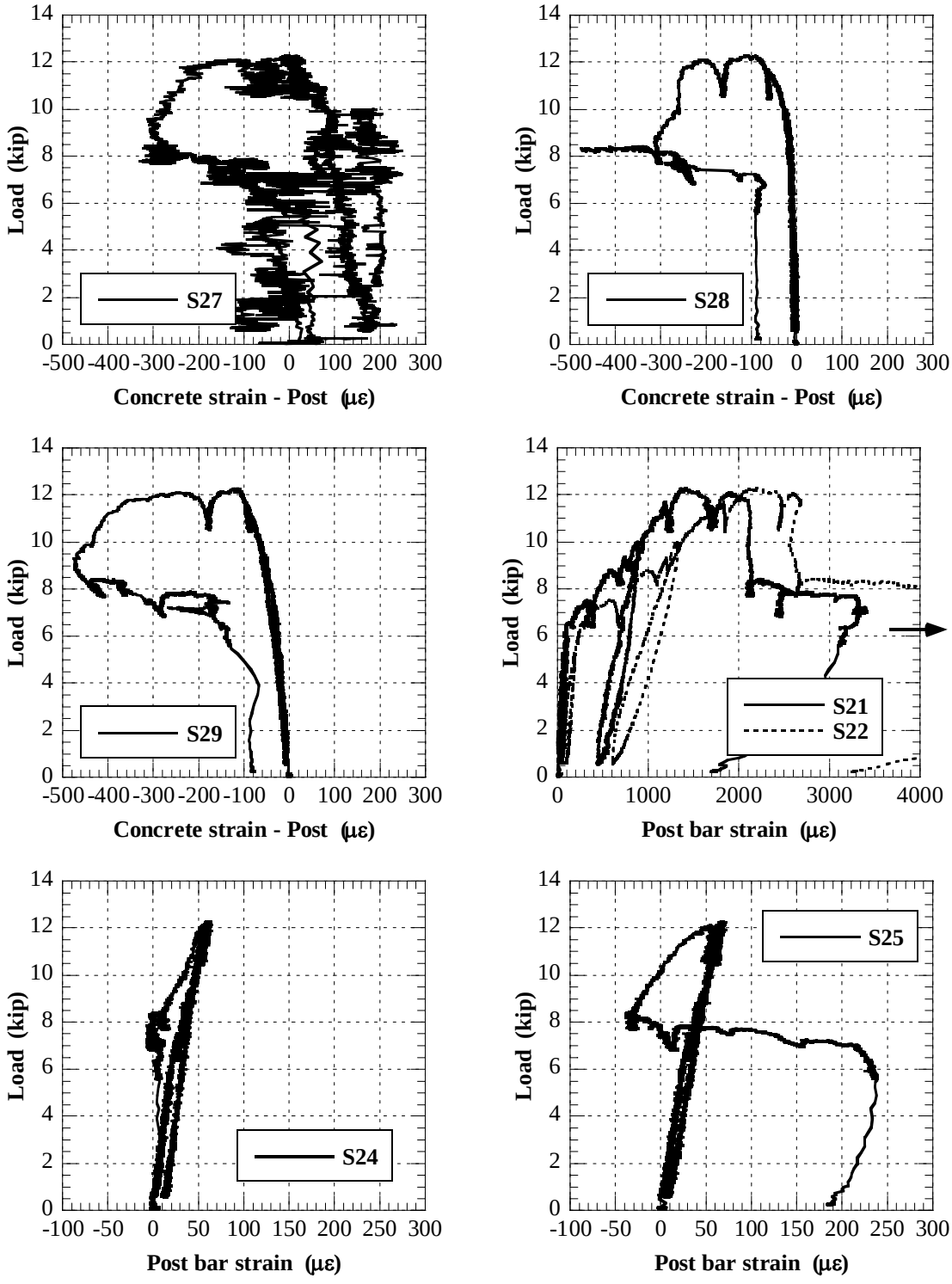

Figure 9 – Strains in concrete at base of post and in tension glass FRP bars in post.

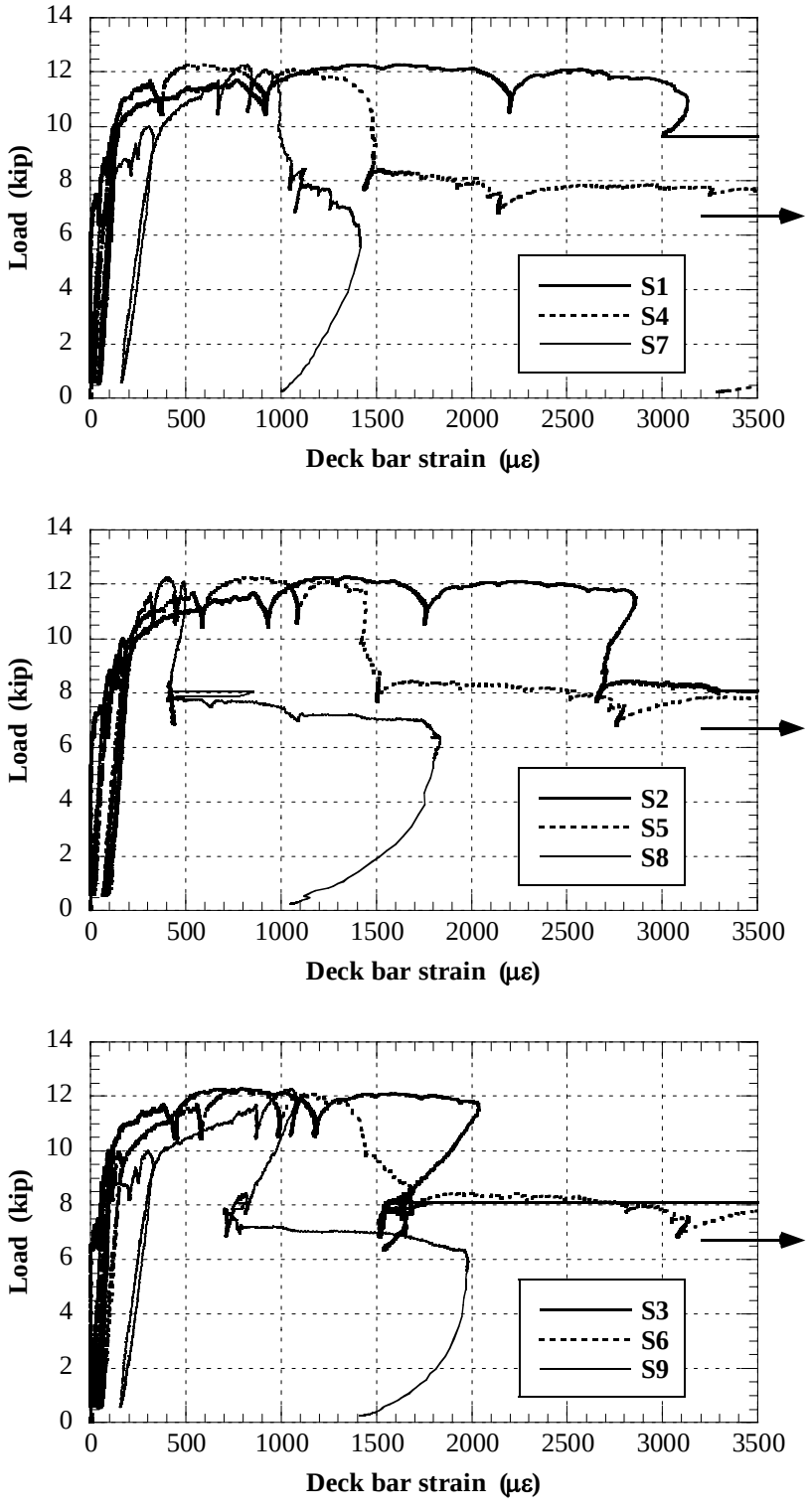

Figure 10 – Strains in tension glass FRP bars in deck at connection.

APPENDIX G.

MODULAR FRAME CONCEPT CART FOR INSPECTION OF SLAB-ON-GIRDER BRIDGE SUPERSTRUCTURE

The following paper was published in the Proceedings of the Fifth International Conference on Bridge Management (BM5), April 11-13, 2005, Guildford, Surrey, UK, Thomas Telford, pp. 187-194. The paper presents the design and construction of the steel-aluminum-FRP cart used to install the fiber optic circuit in PROJECT 3: STRUCTURAL HEALTH MONITORING, from which PAPER 3 of this dissertation originated. The paper documents the results of a strict collaboration with the Machine Technology and Precision Manufacturing class (2004) at the Rolla Technical Institute.

MODULAR FRAME CONCEPT CART FOR INSPECTION OF SLAB-ON-GIRDER BRIDGE SUPERSTRUCTURE

Fabio Matta[a,*], Max Vath[b], Nestore Galati[a], and Antonio Nanni[a]

[a] Center for Infrastructure Engineering Studies, University of Missouri-Rolla

[b] Machine Technology and Precision Manufacturing, Rolla Technical Institute

ABSTRACT

Accessibility of bridge superstructures is often a major issue for the cost-effective inspection and for the installation of health monitoring systems. Depending on the case

* Graduate Research Assistant. Corresponding author – 220 Engineering Research Laboratory, 1870 Miner Circle, 65409-0710 Rolla, MO, USA. Tel +1 (573) 341-6661, Fax -6215, E-mail: *mattaf@umr.edu*.

studies under consideration, tailored solutions may be required to best suit particular needs. This paper presents a concept cart that has been conceived, designed and built to allow a minimum of two operators to move along the whole length of the steel I-girders of a 263 m five span continuous slab-on-girder bridge. The vehicle has been equipped with a set of built-in devices, used to rapidly pass through the transverse stiffeners and cross frames, also at the bent locations. This solution allowed the successful installation of a 1.1 km fiber optic circuit for strain and temperature monitoring.

Keywords: Bridge monitoring; Fiber optics; Inspection.

INTRODUCTION

Accurate routine inspection and monitoring of bridge structures are essential to rate their condition and prioritize maintenance, rehabilitation and emergency repairs. In order to overcome the limitations of traditional inspection methods, such as visual inspection (Phares et al. 2004), extensive research is being funded to develop cost-effective in-situ health monitoring techniques (Chang and Liu 2006) for either global or local structural assessment. These methods typically require sensors be placed in contact with the structure. Accessing the desired locations may become of concern due to the complexity, variability and location of bridge superstructures. Nevertheless, accessibility represents a key factor in enabling efficient inspection and/or sensor installation operations, and may indirectly affect the performance of the monitoring system.

A wide variety of vehicle-mounted working platforms are commonly used for the purpose, as that depicted in Figure 1(a). However, alternative and creative solutions may be required to best suit particular needs: for instance, Figure 1(b) shows the inspection of in-board structural members of two paired steel arch bridges using a custom-made mobile truss cart that was moving on the roadway (Vertical Access 2003), while a robotic aerial inspection platform prototype, currently under development, is illustrated in Figure 1(c) (UC Davis and Caltrans 2003).

A modular frame concept cart for inspection of slab-on-girder bridge superstructures is presented herein. The vehicle was developed to overcome a number of issues posed by the field installation of a fiber optic circuit for distributed strain and temperature monitoring along the steel I-girders, to be performed during a diagnostic load test (Matta et al. 2005).

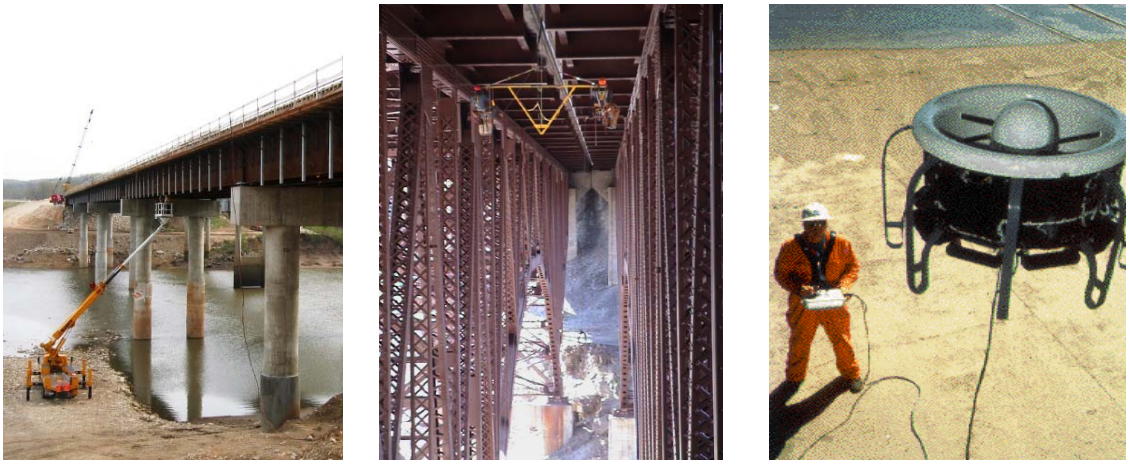

(a) (b) (c)

Figure 1 – Examples of accessibility solutions for inspection of bridge superstructure: (a) vehicle mounted platform; (b) mobile truss cart (Vertical Access 2003); and (c) aerial platform (UC Davis and Caltrans 2003).

PROBLEM STATEMENT

The bridge under investigation, shown in Figure 1(a), is numbered A6358 and it is sited on the U.S. Rt. 54/Osage River, Miller County, MO. It is a symmetric five-span continuous high performance steel (HPS) bridge with a reinforced concrete deck. The external spans are 45 m and 56 m long, respectively, while the central one has a length of 61 m, resulting in a total bridge length of 263 m. Each internal support consists of reinforced concrete bents on two circular piers having a 2 m diameter. The superstructure consists of five composite, equally spaced, HPS I-girders acting compositely with the 216 mm thick concrete deck.

A circuit made of bare fibers and sensing fibers embedded in a custom-made GFRP tape had to be installed on the web of four girders at different depths, along two

continuous spans. This required the personnel to access the desired locations along the steel girders and complete the operations with a two-week timeline. The fact that the bridge spans over the Osage River for 174 m, together with the high variability of the water level, precluded the use of a vehicle-mounted platform. This solution was adopted to mount a total of 22 reflecting prisms for automated total station deflection measurements on the first and part of the second span, in less than one working day [Figure 1(a)]. Since the concrete deck had not been cast yet, a similar approach using a platform connected with a crane to a vehicle that moved along the roadway was not practical. The solution proposed consists of a cart able to move along the whole bridge, rolling over the bottom flanges of two parallel girders. The vehicle was developed with the following goals:

- the cart needed to safely carry a crew of at least two members and all the material and equipment needed to complete the installation operations, providing a sufficiently large working surface;
- to move along the full bridge length, proper solutions had to be devised to rapidly by-pass several transverse stiffeners, either stand-alone or in combination with cross frames, as shown in the framing plan in Figure 2, and the bolted joints, while additional geometrical restrictions were enforced at the bent locations;
- the vehicle had to be easily conducted due to the presence of personnel that needed to focus on the sensor installation work;
- the cart had to be as lightweight as possible, for ease in transportation and to allow switching from a girder pair to another without the need of additional operators other than the crew;

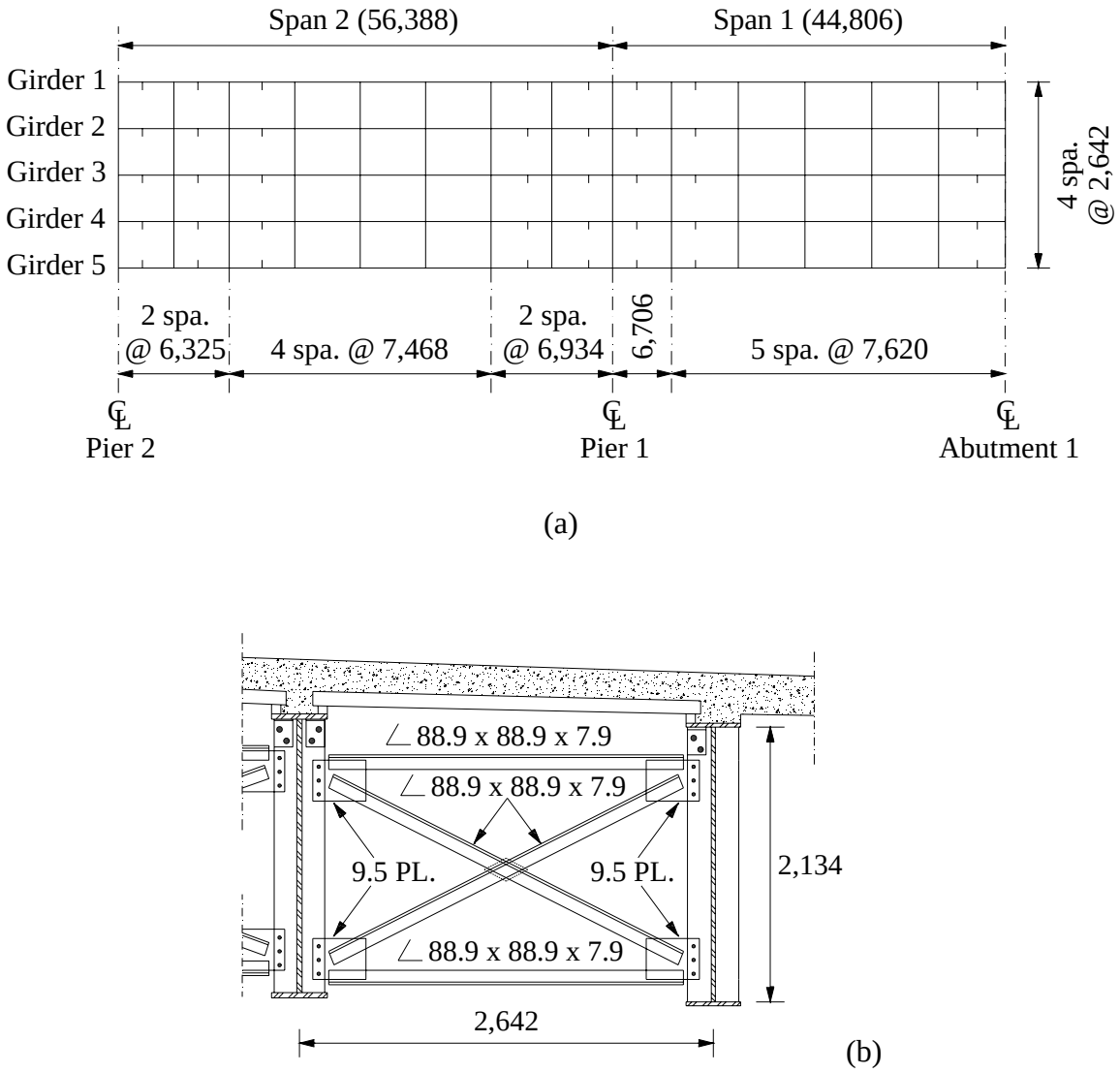

Figure 2 – Framing plan of monitored bridge spans: (a) layout; and (b) typical cross frame. Not to scale, dimensions in mm.

- providing full demountability had practical importance to ensure effective inspection of the device and economical replacement of its components;
- a modular design of the cart, with the possibility to add/subtract units as needed, was a plus to improve the flexibility in its utilization.

DESIGN AND CONSTRUCTION

The frame configuration illustrated in Figure 3 and Figure 4 was selected to meet the aforementioned requirements. The cart was designed and constructed in a collaborative effort between the University of Missouri-Rolla and the Rolla Technical Institute. Due consideration was given to ease and rapidity in construction, using commercially and readily available components and limiting the machining operations. The allowable stress design was used, with a factor of safety of 3 with respect to the yield strength, and 4 with respect to the ultimate strength, depending on the properties guaranteed by the supplier. A minimum span/deflection ratio of 250 and 100 was imposed for the frame structural members under flexure and for the flooring system, respectively, being the latter suggested by the manufacturer (Strongwell 2002).

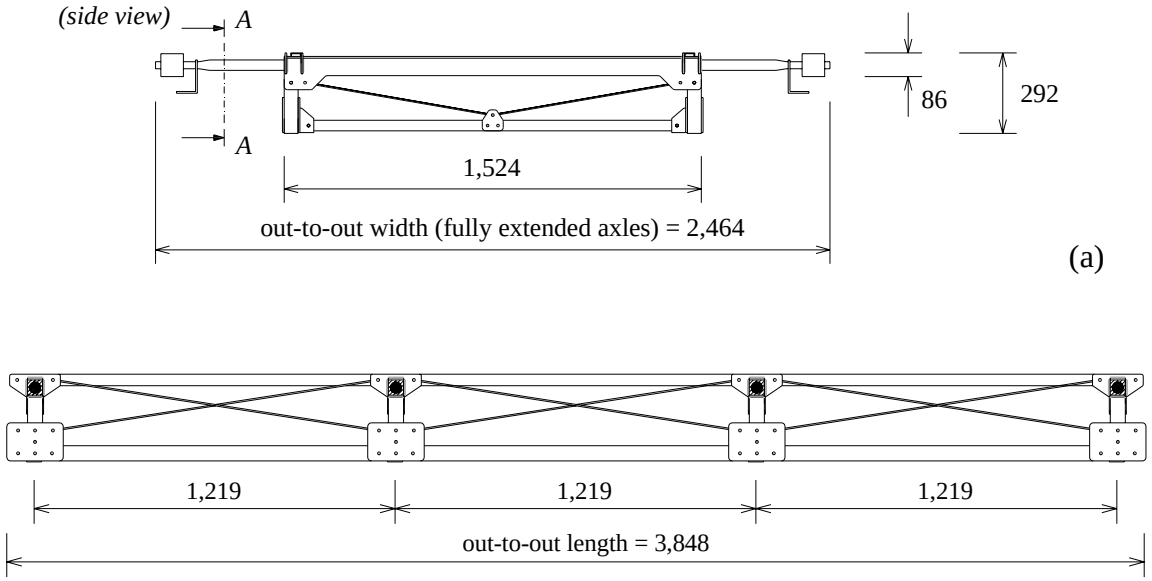

Figure 3 – Dimensions of cart framework: (a) front view; and (b) side view *A-A*. Not to scale, dimensions in mm.

Geometry

The cart frame is composed by three box-shaped 1,463 mm wide and 1,219 mm long (center-to-center) demountable modules, for a total working surface of 5.3 m^2. The overall dimensions are provided in Figure 3. The maximum height of the frame is 292 mm, of which only 86 mm laid above the bottom of the wheels. The out-to-out width with fully extended axles is 2,464 mm, and the possibility of adjusting the extension length by means of electrical actuators, as described later on, allows for utilization on other bridges.

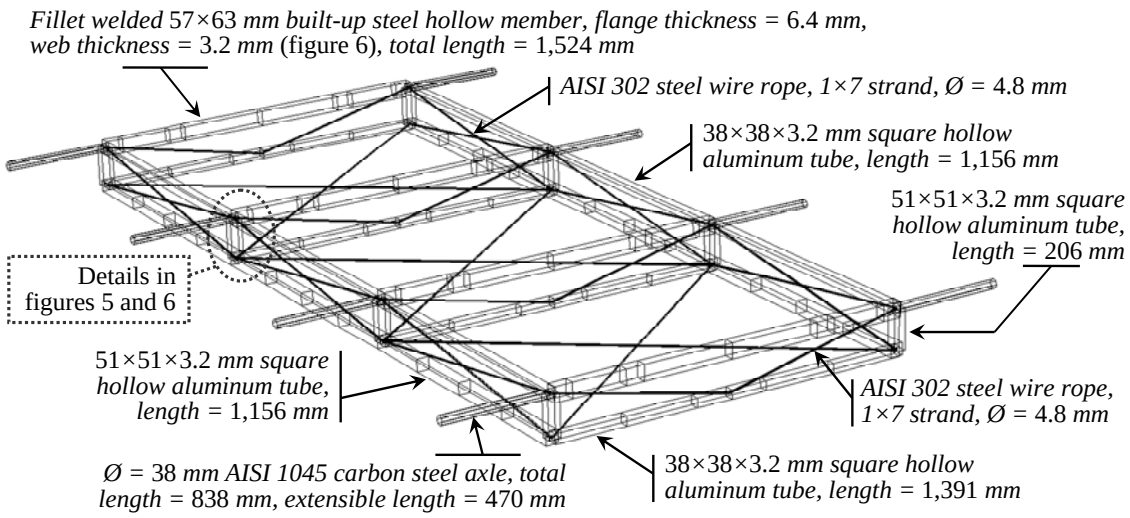

Figure 4 – Outline wireframe of modular cart structure (aluminum: IADS 6061-T6 alloy; steel: AISI 1018 low-carbon alloy unless specified).

The selected geometry was conceived to maximize the available space, since two to three crew-members were to stay on board for several hours, while meeting strict dimensional limitations. These were controlled by the position of the lower transverse

member of the cross frames, that allowed a net clearance of 102 mm above the girders bottom flange bearing the vehicle, and the clear space between the flanges, ranging between 2,083 mm and 2,235 mm. Additional geometrical restrictions were dictated by the width of the bevel sole steel plates over the elastomeric pads and by the concrete surface at the bent locations, which allowed a total horizontal and vertical net clearance of 1,727 mm and 302 mm, respectively.

Materials

A summary of the structural members making up the body of the vehicle is shown in Figure 4. Extensive use of A6061-T6 aluminum profiles was made to build the framework, in order to minimize the overall weight while providing sufficient strength, stiffness and fatigue resistance. Typical material properties are reported in Table 1. Due to weldability characteristics and to contain the maximum deflection, AISI 1018 low-carbon steel (nominal tensile and yield strength σ_u = 634 MPa and σ_y = 386 MPa, respectively) was utilized for the four transversal members containing the axles, built-up from 3.2 mm and 6.4 mm thick plates that were cut to measure and welded together. The axles were realized by machining commercially available Ø38 mm AISI 1045 carbon steel rods (nominal yield strength σ_y = 531 MPa). AISI 302 stainless steel wire rope with guaranteed breaking strength of 20.9 kN was used for all the diagonal ties.

Structural FRP pultruded panels made of glass fibers and mat, and polyester resin matrix, with a weight of 12.7 kg/m^2, were utilized as the flooring system. Single 1,524×305×51 mm planks with gritted surface were cut to measure and interlocked to form the working platforms. The load - deflection properties for the span used are

reported in Table 2 (Strongwell 2002), along with a picture of the plank assembly. The total weight of the cart was limited to 192 kg, 57% of which given by the transversal steel members and axles and 28% by the GFRP platform.

Table 1 – Typical properties of IADS 6061-T6 aluminum alloy.

Density	2,700 kg/m^3
Tensile strength, ultimate	310 MPa
Tensile strength, yield	275 MPa
Elongation at break	12-17% in 5 cm
Modulus of elasticity	69 GPa
Poisson's ratio	0.33
Fatigue strength @ $N = 5 \cdot 10^8$ (cycles)	95 MPa
Fracture toughness	29 MPa m$^{1/2}$

Table 2 – GFRP plank load-deflection design values (span = 1.52 m) (Strongwell 2002).

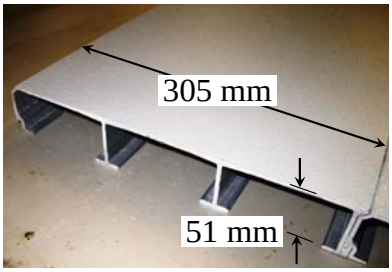

Uniform load (kN/m^2)	2.4	4.8	9.6	14.4
Deflection (mm)	3.6	7.1	14.3	>15
Concentrated load (kN/m)	0.7	1.5	2.9	4.4
Deflection (mm)	1.1	2.3	4.6	6.9

Detailing

All structural members were pin-connected with each other using Ø 9.5 mm high strength steel fasteners, thus allowing for full demountability of the framework, providing

a 3 mm spacing between each other to obtain actual hinges. Wood blocks were inserted as cores in the aluminum profiles at the fastener locations. In order to prevent loosening and backing-off in the connections during the field operations, self-locking fasteners were utilized. Figure 5 shows the detail of the mechanical joint assembly between the lateral members supporting the GFRP platform, the bottom transverse profiles, and the vertical ties connecting the working plane to the top transverse support steel members.

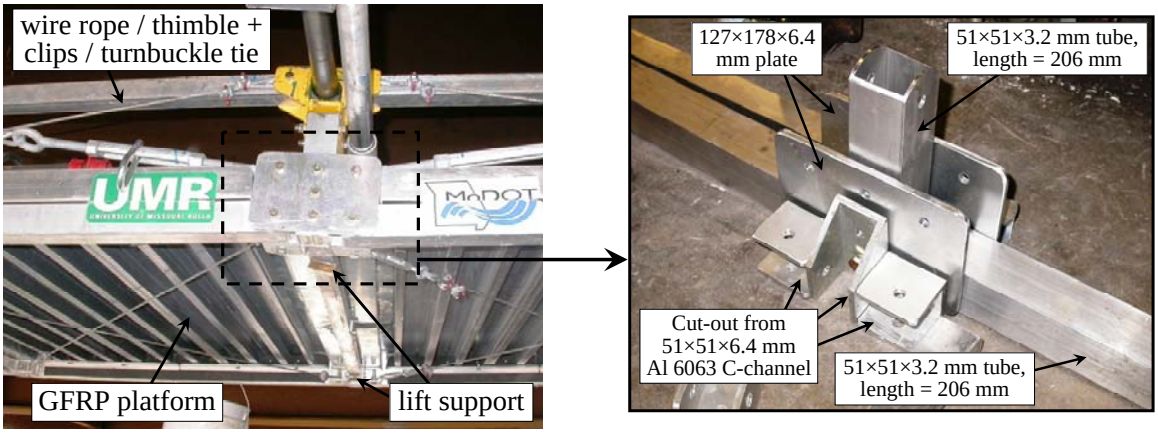

Figure 5 – Detail of bolted connection assembly (material Al 6061-T6 unless specified).

The welded built-up support steel members, which are detailed in Figure 6, contain two independent, 832 mm long Ø38 mm steel axles. Each of them passes through two 51×51×76 mm steel blocks, spaced at 210 mm, which hold the axles in place and aligned. In order to accommodate an anti-overturn 6.4 mm thick steel plate equipped with a PTFE guide damper, and a 82.5×82.5 mm polyurethane lift truck wheel with steel core and precision ball bearing, the diameter of the axles was reduced from 38 mm to 25 mm at the outer end, for a length of 159 mm, with a 38 mm taper. Each wheel was secured by means of a Ø4.8 mm ring-grip steel pin.

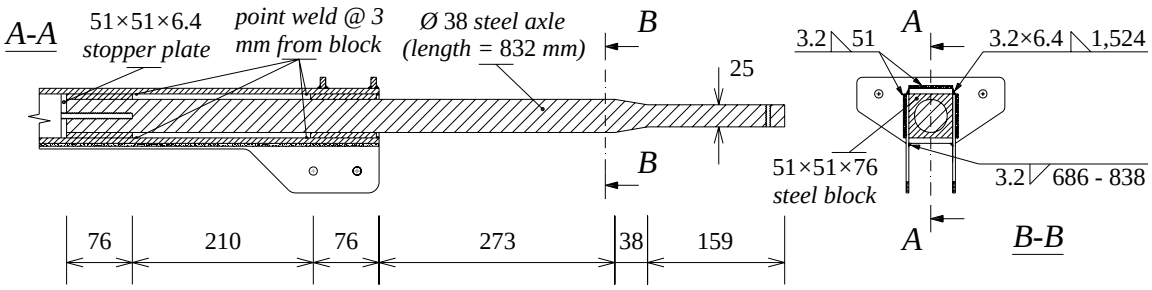

(a)

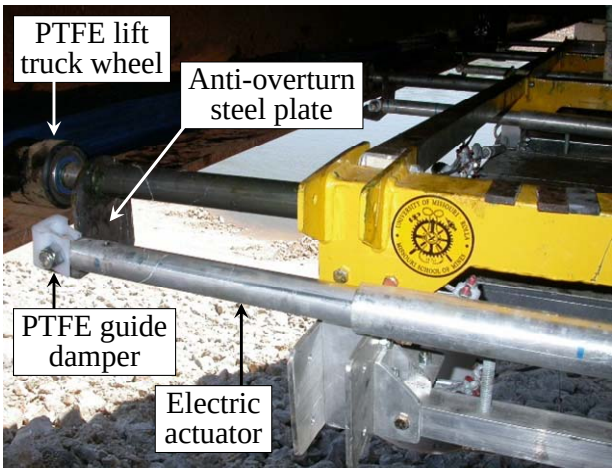

(b)

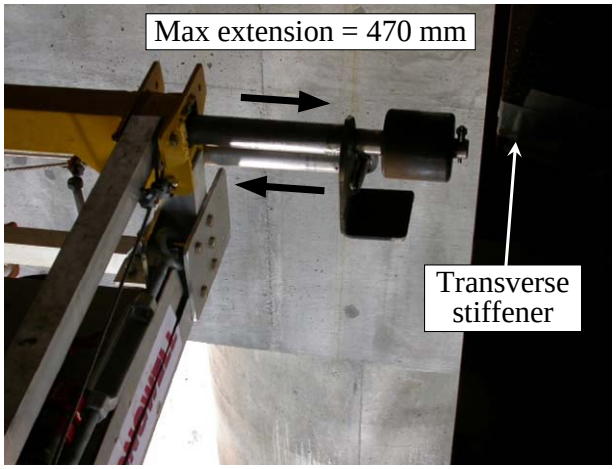

(c)

Figure 6 – Assembly of fillet welded built-up steel support member and pneumatic axles: (a) longitudinal section view (not to scale, dimensions in mm); (b) close up; and (c) obstacle by-passing during installation of optical fiber circuit under Bridge A6358.

A total of eight aluminum electric actuators were connected to Ø9.5 mm threaded rods welded onto the anti-overturn steel plates. By drilling with a 6.4 mm HEX key shaft at the free end of the actuators, the axles were allowed to slide back and forth, extending for a maximum of 470 mm on each side of the vehicle. This system enables the cart to move with four to six wheels out of eight, by retracting the wheels from the supporting flanges to by-pass the vertical stiffeners, cross frames and diaphragms at the bent locations, as shown in Figure 6(c). Properly connected ties composed of a steel wire rope, thimbles and clips, and a forged eye-and-eye turnbuckle withstand the tension reactions needed at the unsupported nodes of the frame structure. The system also provides the ability to adjust the position of the wheels when by-passing the bolted joint plates, since less than 30 mm of net space was available between the bolt nut and the edge of the flange.

In order to facilitate uplifting of the retracted axles to re-position the wheels over the flanges at the bents, two lift supports were mounted in the bottom transverse profiles. They consist of Ø13 mm steel HEX bolts with threaded length of 102 mm, which pass through a filleted 31×31×51 mm aluminum block inserted into the hollow tube, and with a 38×38×3.2 mm square plate welded at the outer end (Figure 5): using a ratchet wrench, it was possible to rapidly lift the cart bearing on the concrete surface. When outside the bent locations, this was done using a system of chains secured either at the cross braces or at the stiffener/top flange web gaps, together with a falling chain hooked to the transverse built-up member. Further development of the concept cart should provide the ability to by-pass obstacles independently of anchorage areas. A viable option may be devising a portable frame to be connected to the supported transverse members, and

equipped with a web-strap puller/hoist hooked to the unsupported member with retracted axles to be lifted.

Double-L built-up aluminum profiles, placed between the GFRP planks and the longitudinal support tubes, were used to prevent horizontal movement of the working platform, interposing adhesive backed rubber layers to reduce vibrations and improve the comfort.

CONCLUSIONS

Design and construction of a modular frame concept cart for inspection of slab-on-girder bridge superstructures has been presented and detailed. The vehicle, equipped with built-in devices for by-passing the stiffeners and cross frames, was needed to install a fiber optic circuit along two spans of a 263 m five-span HPS bridge. The field operations consisted of moving along the spans preparing the bonding surface, then coming back installing the sensors (Figure 7), and finally setting up the circuit.

(a) (b) (c)

Figure 7 – Field operations using modular frame cart: (a) cart between two girders; (b) along second span; and (c) installation of sensors from cart working platform.

The inspection vehicle was efficiently conducted by one operator, while no delay was brought to the field work. As a reference, it was possible to complete the optical fibers installation on two girders along a 56 m span in five and a half hours. Four girders were successfully instrumented, for a total circuit length of 1,159 m.

ACKNOWLEDGMENTS

The financial support received from the Missouri Department of Transportation (MoDOT) and from the University Transportation Center (UTC) on Advanced Materials and NDT Technologies is gratefully acknowledged. The authors wish to thank Strongwell Corporation for the donation of the GFRP planks.

REFERENCES

Phares, B. M., Washer, G. A., Rolander, D. D., Graybeal, B. A., and Moore, M., "Routine highway bridge inspection condition documentation accuracy and reliability," *Journal of Bridge Engineering*, V. 9, No. 4, 2004, pp. 403-413.

Chang, P. C., and Liu, S. C., "Recent research in nondestructive evaluation of civil infrastructures," *Journal of Materials in Civil Engineering*, V. 15, No. 3, 2003, pp. 298-304.

Vertical Access, 2003, Project Profile, URL: http://www.vertical-access.com/download/catskill_bridges.pdf, accessed July 2007.

UC Davis, and Caltrans, Advanced Highway Maintenance and Construction Technology (AHMCT). URL: http://www.ahmct.ucdavis.edu/other/o_struc.htm, accessed October 2003.

Matta, F., Bastianini, F., Galati, N., Casadei, P., and Nanni, A., "In-situ load testing of Bridge A6358, Osage Beach, MO," *Report UTC RI04-006 (Part 1)* for the Missouri Department of Transportation, University Transportation Center on Advanced Materials and NDT Technologies, University of Missouri-Rolla, 75 pp.

Strongwell Corp., Fiberglass flooring and decking systems – Design manual, CD-ROM, 2002.

APPENDIX H.

RAW DATA FROM DIAGNOSTIC LOAD TEST OF BRIDGE NO. A6358, OSAGE BEACH, MO

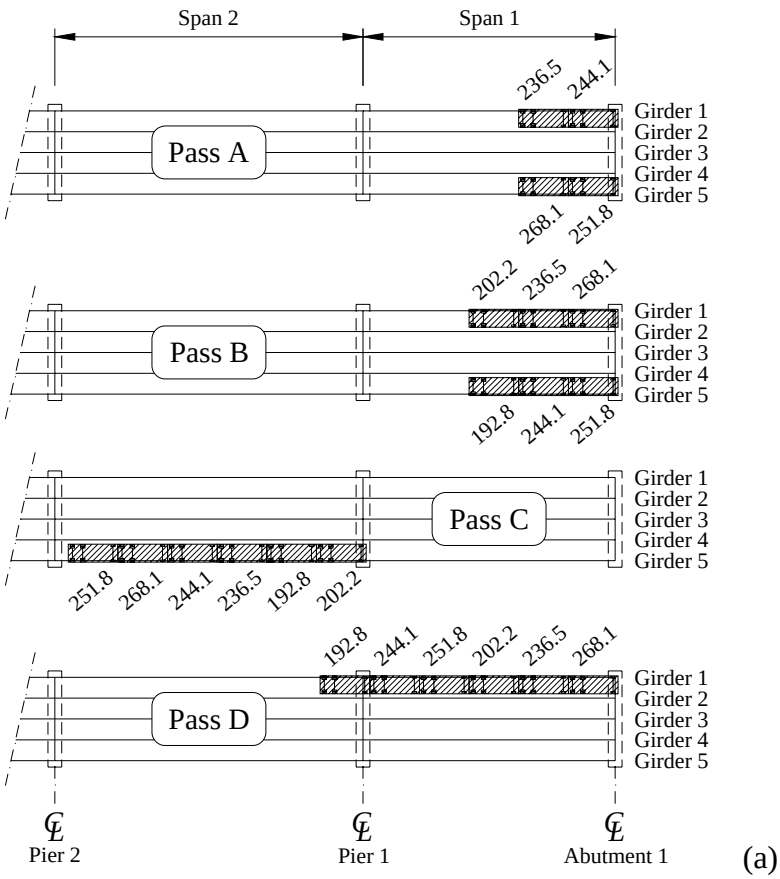

Figure 1 – Schematic of diagnostic load test passes: (a) plan view; and (b) side view.

(a)

(b)

(c)

(d)

Figure 2 – Photographs of load test passes: (a) Pass A; (b) Pass B; (c) Pass C, and (d) Pass D.

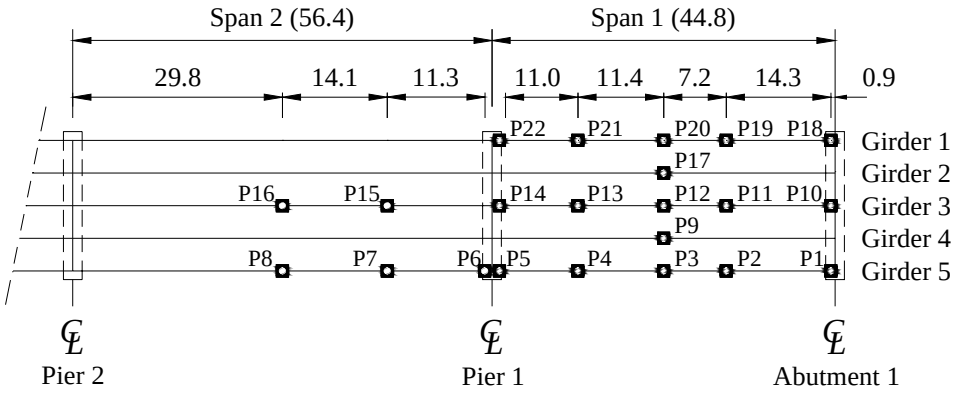

(a)

(b)

(c)

Figure 3 – ATS setup: (a) schematic of location of reflecting prisms; (b) photograph of targets along Girder 5; and (c) photograph of test setup. Note reflection on targets.

Table 1 – Deflection measurements with automated total station system.

Distance from Abutment 1 (ft)	Pass A (in)	Pass B (in)	Pass C (in)	Pass D (in)
Girder 1				
3.0	-5.56E-02	-6.41E-02	-1.26E-02	-1.55E-01
50.0	-4.99E-01	-8.29E-01	-2.11E-01	-1.37E+00
73.5	-4.79E-01	-8.48E-01	-1.95E-01	-1.50E+00
111.0	-2.20E-01	-4.57E-01	-1.23E-01	-9.85E-01
143.0	1.34E-03	-1.57E-02	1.08E-02	-1.26E-01
Girder 2				
73.5	-4.19E-01	-7.47E-01	5.76E-02	-9.57E-01
Girder 3				
3.0	-1.64E-02	-4.34E-02	4.98E-02	-3.03E-02
50.0	-3.67E-01	-6.03E-01	2.20E-01	-4.57E-01
73.5	-3.84E-01	-6.55E-01	2.79E-01	-5.18E-01
111.0	-2.18E-01	-3.80E-01	2.34E-01	-3.27E-01
143.0	3.94E-05	-2.16E-02	6.14E-02	-2.62E-02
188.0	1.59E-01	2.23E-01	-3.82E-01	1.82E-01
234.5	1.75E-01	2.44E-01	-6.56E-01	1.86E-01
Girder 4				
73.5	-5.26E-01	-7.62E-01	3.38E-01	-2.36E-01
Girder 5				
3.0	-4.68E-02	-4.90E-02	7.24E-02	2.30E-02
50.0	-5.97E-01	-7.35E-01	5.19E-01	1.26E-01
73.5	-5.23E-01	-7.05E-01	7.16E-01	1.88E-01
111.0	-3.06E-01	-4.20E-01	5.90E-01	1.21E-01
143.0	2.99E-03	-2.47E-02	9.46E-02	2.07E-02
151.0	4.40E-02	4.31E-02	-7.43E-02	6.61E-03
188.0	1.38E-01	1.67E-01	-1.11E+00	-6.39E-02
234.5	1.37E-01	1.38E-01	-1.85E+00	-1.08E-01

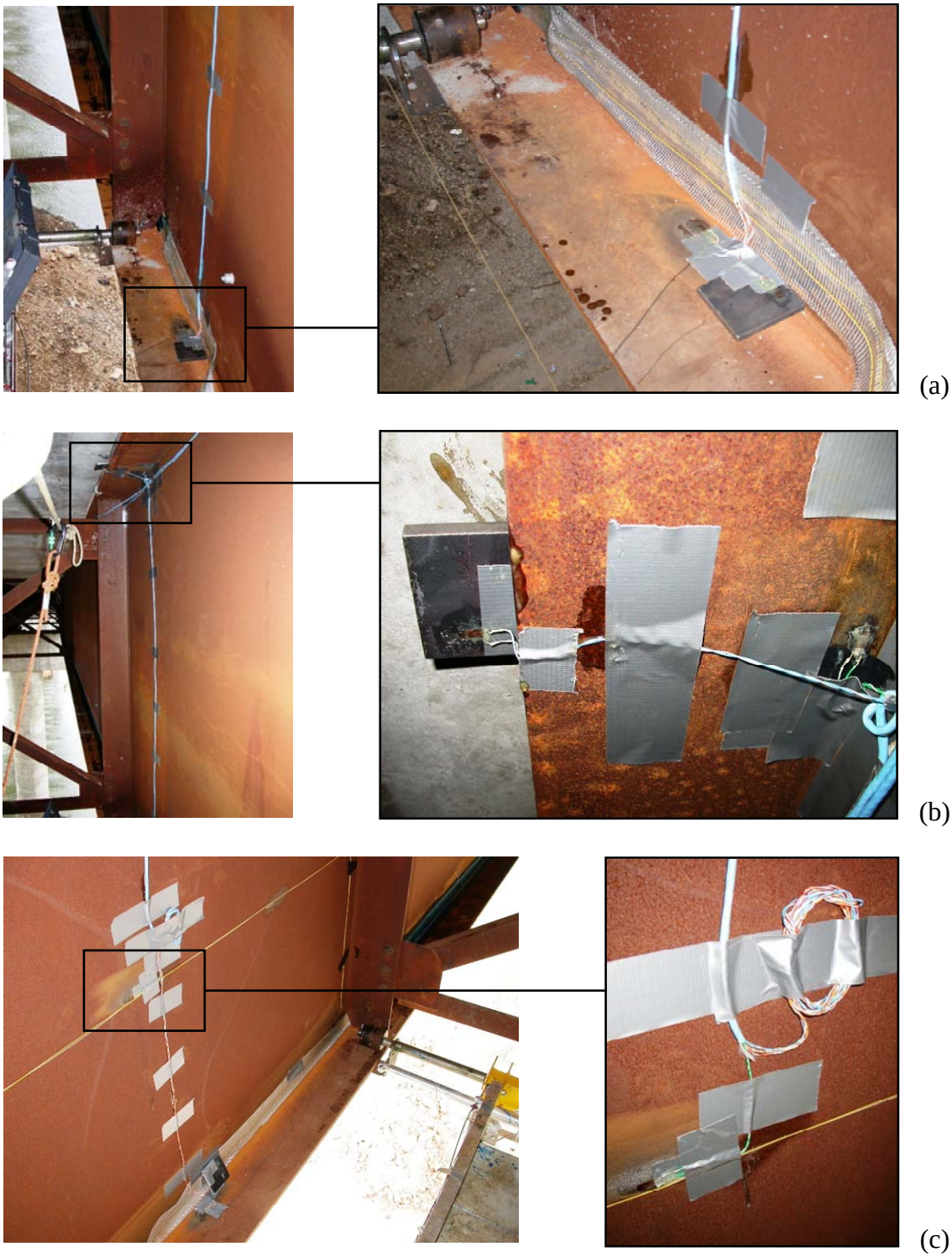

Figure 4 – Photographs of bonded and unbonded strain gauges on Girders 1 and 2: (a) Girder 1, bottom flange; (b) top flange; and (c) Girder 2, bottom flange and Location II.

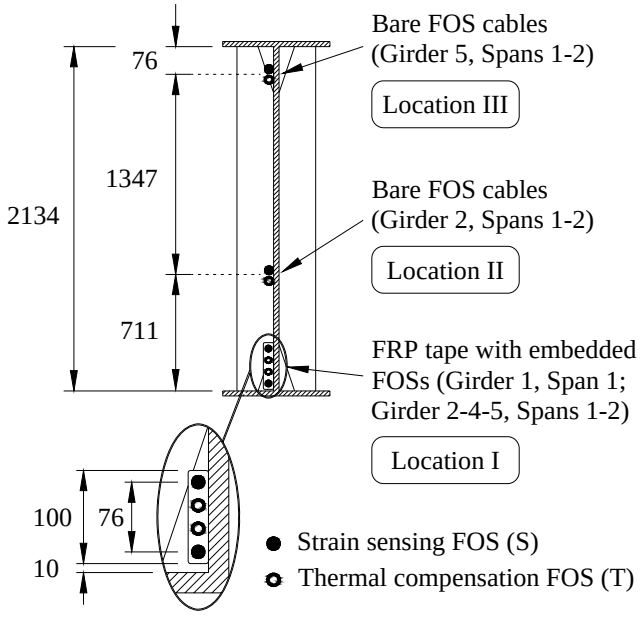

(a)

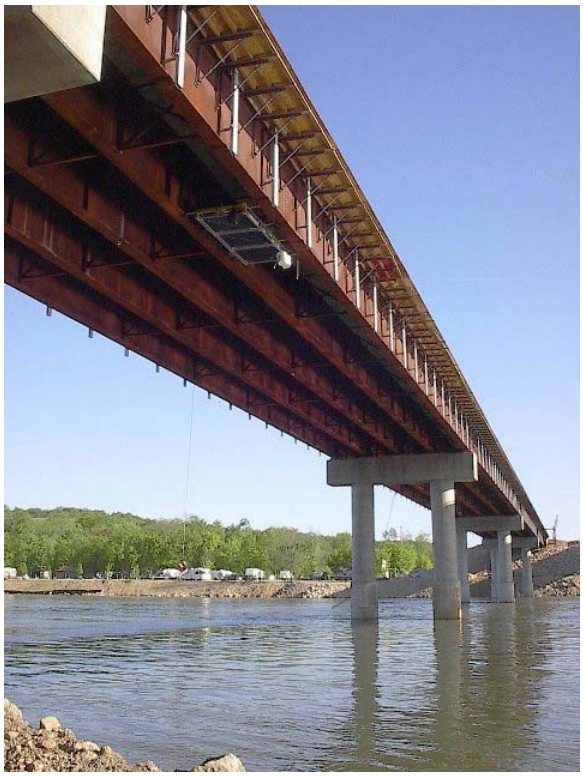

(b)

(c)

(d)

Figure 5 – Installation of optical fiber circuit: (a) schematic of sensor location; (b) cart on Girders 1 and 2, Span 2; (c) sensors on Girder 2; and (d) sensors on Girder 5.

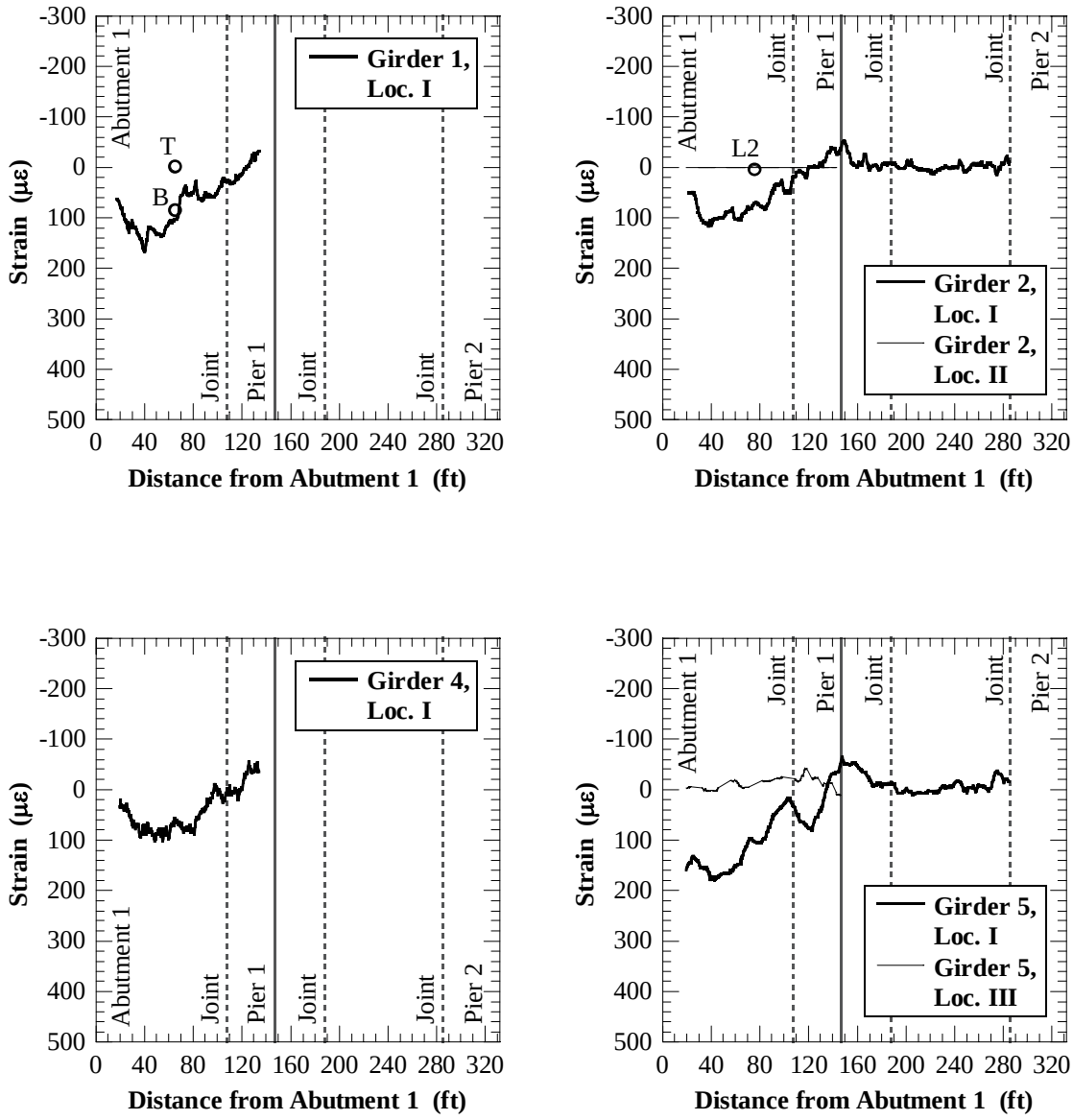

Figure 6 – Strain profiles at Pass A. Circles indicate strain gauge readings (B = bottom flange, T = top flange, L2 = Location II in Girder 2).

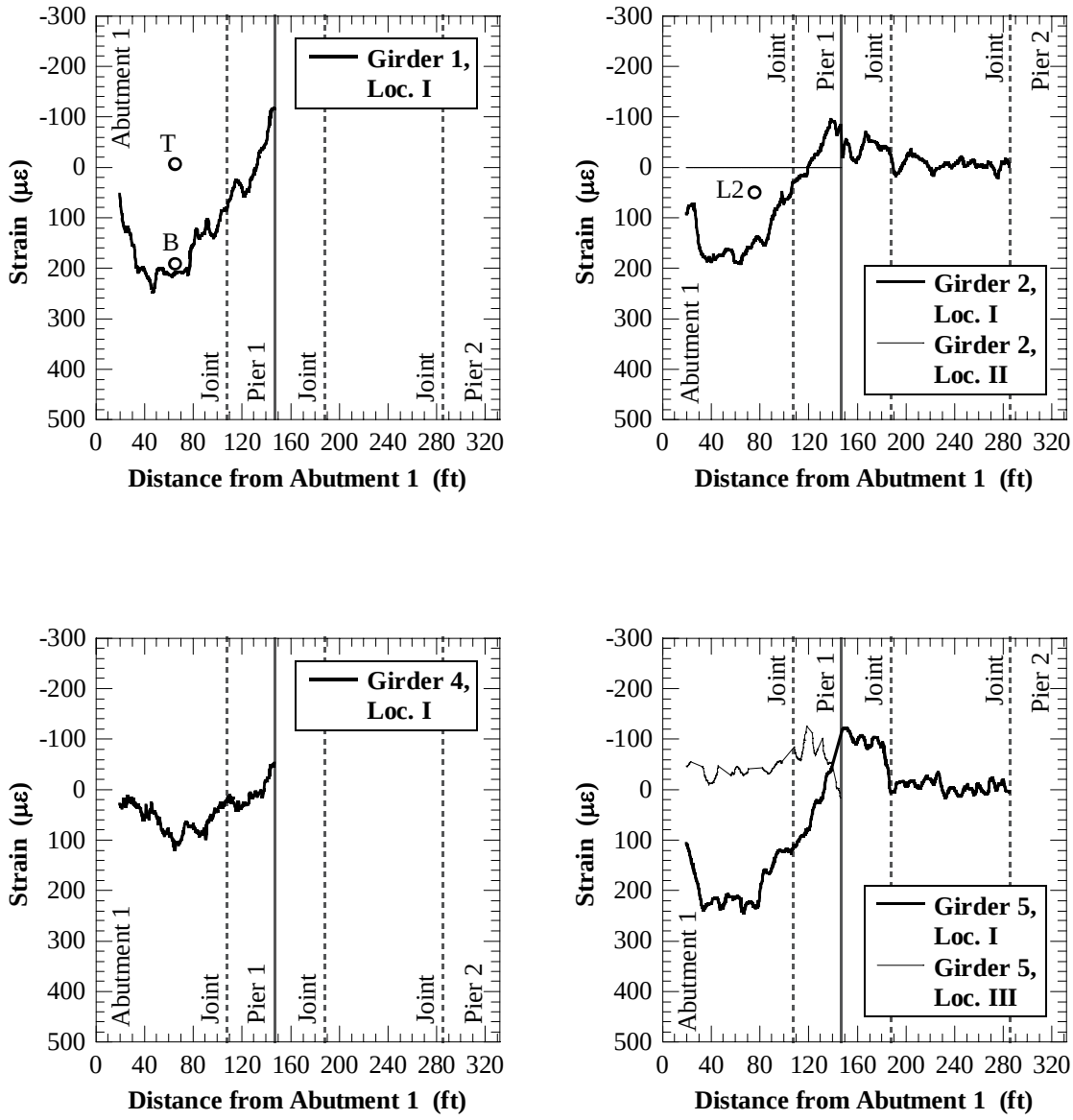

Figure 7 – Strain profiles at Pass B. Circles indicate strain gauge readings (B = bottom flange, T = top flange, L2 = Location II in Girder 2).

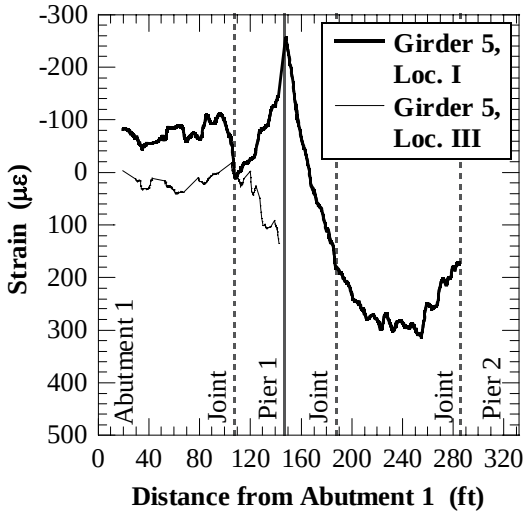

Figure 8 – Strain profiles at Pass C.

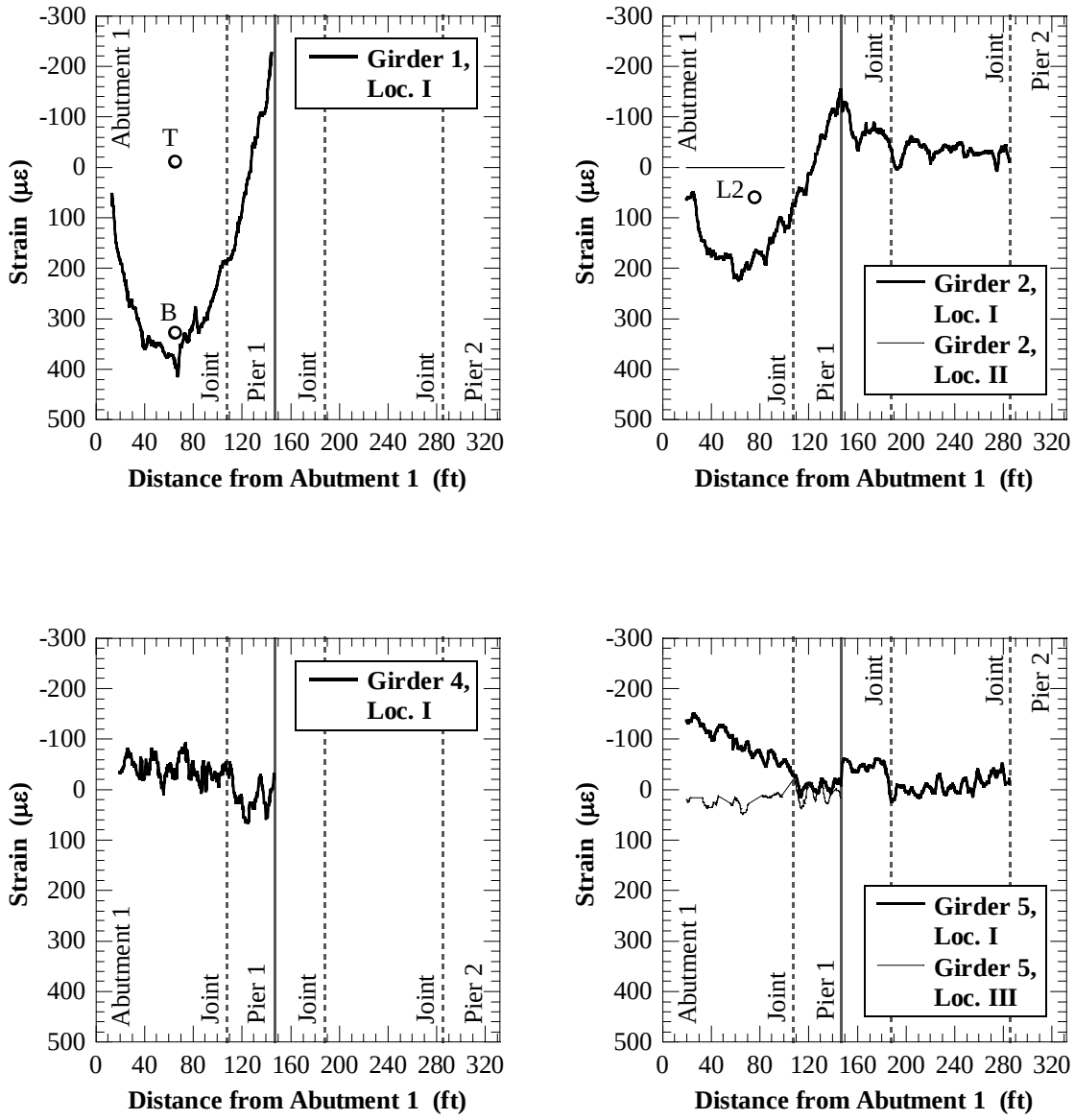

Figure 9 – Strain profiles at Pass D. Circles indicate strain gauge readings (B = bottom flange, T = top flange, L2 = Location II in Girder 2).

APPENDIX I.

PUBLICATIONS

The following publications have been authored or co-authored throughout the duration of the doctoral studies (manuscripts currently in review are not included):

A. ARCHIVAL JOURNALS

1. Matta, F., Karbhari, V. M., and Vitaliani, R., "Tensile Response of Steel/CFRP Adhesive Bonds for the Rehabilitation of Civil Structures," *Structural Engineering and Mechanics*, V. 20, No. 5, 2005, pp. 589-608.

2. Matta, F., Rizzo, P., Karbhari, V. M., and Lanza di Scalea, F., "Acoustic emission damage assessment of steel/CFRP bonds for rehabilitation," *Journal of Composites for Construction*, V. 10, No. 3, 2006, pp. 265-274.

3. Ringelstetter, T. E., Bank, L. C., Oliva, M. G., Russell, J. S., Matta, F., and Nanni, A., "Cost-effective, structural stay-in-place formwork system of fiber-reinforced polymer for accelerated and durable bridge deck construction," *Transportation Research Record*, No. 1976, 2006, pp. 183-189.

B. CONFERENCE PROCEEDINGS

1. Matta, F., Karbhari, V. M., Tinazzi, D., and Vitaliani, R., "Static and fatigue behavior of steel/CFRP adhesive bonds for the rehabilitation of metallic bridges," *Proc. 2nd National Symposium on Mechanics of Masonry Structures Strengthened with FRP-Materials*, December 6-8, 2004, Venice, Italy, Libreria Internazionale Cortina, pp. 411-420 (invited paper for post-symposium "FRP Materials in Metallic Structures").

2. Bastianini, F., Matta, F., Galati, N., and Nanni, A., "A Brillouin smart FRP material and a strain data post processing software for structural health monitoring through laboratory testing and field application on a highway bridge," *Proc. SPIE*, V. 5765, 2005, International Society for Optical Engineering, pp. 600-611.

3. Matta, F., Vath, M., Galati, N., and Nanni, A., "Modular frame concept cart for inspection of slab-on-girder bridge superstructure," *Proc. 5th International Conference on Bridge Management*, April 11-13, 2005, Guildford, Surrey, UK, Thomas Telford, pp. 187-194.

4. Matta, F., Galati, N., Nanni, A., Ringelstetter, T. E., Bank, L. C., and Oliva, M. G., "Pultruded grid and stay-in-place form panels for the rapid construction of bridge decks," *Proc. Composites 2005 Convention and Trade Show*, September 28-30, 2005, Columbus, OH, American Composites Manufacturers Association, CD-ROM, 9 pp.

5. Matta, F., Nanni, A., Galati, N., Ringelstetter, T. E., Bank, L. C., Oliva, M. G., Russell, J. S., Orr, B. M., and Jones, S. N., "Prefabricated modular GFRP reinforcement for accelerated construction of bridge deck and rail system," *Proc. FHWA Accelerated Bridge Construction Conference*, December 14-16, 2005, San Diego, CA, Federal Highway Administration, pp. 129-134.

6. Ringelstetter, T. E., Bank, L. C., Oliva, M. G., Russell, J. S., Matta, F., and Nanni, A., "Development of a cost-effective structural FRP stay-in-place formwork system for

accelerated and durable bridge deck construction," *Proc. 85th Transportation Research Board Annual Meeting*, January 22-26, 2006, Washington, DC, Transportation Research Board, CD-ROM #06-2218, 16 pp.

7. Matta, F., and Nanni, A., "Design of concrete railing reinforced with glass fiber reinforced polymer bars," *Proc. 2006 ASCE Structures Congress*, May 18-20, 2006, St. Louis, MO, CD-ROM, American Society of Civil Engineers, 9 pp.

8. Matta, F., Galati, N., Bastianini, F., Casadei, P., and Nanni, A., "Distributed strain and non-contact deflection measurement in multi-span highway bridge", *Proc. Structural Faults & Repair 2006 (SF+R 2006)*, June 13-15, 2006, Edinburgh, UK, ECS Publications, CD-ROM, 11 pp.

9. Bastianini, F., Matta, F., Galati, N., and Nanni, A., "Distributed strain measurement in steel slab-on-girder bridge via Brillouin Optical Time Domain Reflectometry," *Proc. 3rd International Conference on Bridge Maintenance, Safety and Management (IABMAS'06)*, July 16-19, 2006, Porto, Portugal, Taylor & Francis, 8 pp.

10. Bastianini, F., Matta, F., Rizzo, A., Galati, N., and Nanni, A., "Overview of recent bridge monitoring applications using distributed Brillouin fiber optic sensors," *Proc. 2006 NDE Conference on Civil Engineering*, August 14-18, 2006, St. Louis, MO, American Society for Nondestructive Testing, pp. 269-276.

11. Matta, F., Nanni, A., Ringelstetter, T. E., and Bank, L. C., "Rapid construction of concrete bridge deck using prefabricated FRP reinforcement," *Proc. Third International Conference on FRP Composites in Civil Engineering (CICE 2006)*, Dec. 13-15, 2006, Miami, FL, USA, International Institute for FRP in Construction, pp. 151-154.

12. Matta, F., Nanni, A., Galati, N., and Mosele, F., "Size effect on shear strength of concrete beams reinforced with FRP bars," *Proc. 6th International Conference on Fracture Mechanics of Concrete and Concrete Structures (FraMCoS-6)*, June 17-22, 2007, Catania, Italy, Taylor & Francis, 8 pp.

C. TRADE AND PROFESSIONAL MAGAZINES

1. Matta, F., Nanni, A., Ringelstetter, T., Bank, L., Nelson, B., Orr, B., and Jones, S., "Don't cross that bridge until we fix it! – Pultruded FRP reinforcement for bridge repair," *Composites Manufacturing Magazine*, American Composite Manufacturing Association (ACMA), V. 22, No. 8, 2006, pp. 18-23, 57 (cover story).

2. Barefoot, G., and Matta, F., "Rapid bridge deck construction with FRP reinforcing grids," *JEC Composites Magazine*, V. 33, 2007, pp. 47-49.

D. TECHNICAL REPORTS

1. Matta, F., Bastianini, F., Galati, N., Casadei, P., and Nanni, A., "In-situ load testing of Bridge A6358, Osage Beach, MO," *Report UTC RI04-006 (Part 1)* for Missouri

Department of Transportation, University Transportation Center on Advanced Materials and NDT Technologies, University of Missouri-Rolla, 2005, 75 pp.

2. Matta, F., Vath, M., Galati, N., and Nanni, A., "Design and construction of hybrid aluminum/steel/FRP bridge inspection vehicle," *Report CIES 07-66* for Missouri Department of Transportation, Center for Infrastructure Engineering Studies, University of Missouri-Rolla, 2006, 22 pp.

3. Galati, N., Matta, F., and Nanni, A., "Uniform air pressure load test of precast wall panel," Report for Construction Research Laboratory, Inc. (Miami, FL), University of Miami and University of Missouri-Rolla, 2006, 30 pp.

4. Marianos, W. N. Jr, Chen, G., Galati, N., and Matta, F. (2006), "Investigation of cause of cracked stringer on the Blanchette Bridge," *Report RI05-036* for Missouri Department of Transportation, Center for Infrastructure Engineering Studies, University of Missouri-Rolla, 2006, 54 pp.

5. Nanni, A., Matta, F., and Galati, N., "Externally post-tensioned CFRP system for deflection control of reinforced concrete slabs – Volume I: design and analysis," *Report CAE 06-01* for Samsung Corporation – Engineering & Construction Group, University of Miami, 2006, 92 pp.

6. Gremel, D., Koch, R., Nanni, A., and Matta, F., “Externally post-tensioned CFRP system for deflection control of reinforced concrete slabs – Volume II: installation guide,” *Report CAE 06-02* for Samsung Corporation – Engineering & Construction Group, University of Miami, 2006, 27 pp.

E. THESES AND DISSERTATIONS

1. Matta, F., “Innovative solutions in bridge construction, rehabilitation, and structural health monitoring,” Ph.D. dissertation, Department of Civil, Architectural, and Environmental Engineering, University of Missouri-Rolla, Rolla, USA, 240 pp.

APPENDIX J.

PRESENTATIONS

The following presentations have been delivered as part of the technology transfer programs throughout the duration of the doctoral studies:

1. “RTI/UMR research projects,” Rolla Technical Institute (RTI) Board of Education Meeting, Rolla Technical Center, October 14, 2004, Rolla, MO.

2. “Rehabilitation of Farm Road Bridge No. 14802301, Greene County, MO – Project presentation,” project showcase at University of Missouri-Rolla Structures Laboratory, April 13, 2005.

3. “FRP for internal concrete reinforcement in bridges: innovative applications,” Missouri Society of Professional Engineers (MSPE) – Ozark Chapter meeting, May 5, 2005, Springfield, MO (invited 1 PDH presentation).

4. “Identification of performance characteristics of concrete railings with pultruded FRP reinforcement,” National Science Foundation Industry/University Cooperative Research Center (I/UCRC) “Repair of Buildings and Bridges with Composites” – Plenary meeting, June 9, 2005, Rolla, MO.

5. “Prefabricated modular GFRP reinforcement for accelerated construction of bridge deck and rail system,” US Federal Highway Administration (FHwA) Accelerated Bridge Construction Conference, December 15, 2005, San Diego, CA.

6. “Rapid construction of FRP reinforced bridge deck in Greene County, MO,” 96th Annual Conference of the Transportation Engineers Association of Missouri (TEAM), March 23, 2006, Branson, MO (invited 1/2 PDH presentation).

7. “Design of concrete railing reinforced with glass fiber reinforced polymer bars,” American Society of Structural Engineers (ASCE) Structures Congress, May 19, 2006, St. Louis, MO.

8. “Five-day construction of FRP reinforced concrete deck and rail for Bridge 14802301, Greene County, MO,” 23rd International Bridge Conference, June 13, 2006, Pittsburgh, PA (invited 1/2 PDH presentation for Special Interest Session “FRP Composites – Advancements in Bridge Construction”).

9. “Design, construction and field validation of the Southview Bridge in Rolla, Missouri,” 23rd International Bridge Conference, June 13, 2006, Pittsburgh, PA (on behalf of authors).

10. “Shear strength of large size GFRP reinforced concrete beams,” National Science Foundation Industry/University Cooperative Research Center (I/UCRC) “Repair of Buildings and Bridges with Composites” – Plenary meeting, June 22, 2006, Rolla, MO.

BIBLIOGRAPHY

ACI Committee 440, "Guide for the design and construction of structural concrete reinforced with FRP bars," *ACI 440.1R-06*, American Concrete Institute, Farmington Hills, MI, 2006, 44 pp.

ACI Committee 440, "Prestressing concrete structures with FRP tendons," ACI 440.4R-04, American Concrete Institute, Farmington Hills, MI, 2004, 35 pp.

American Association of State Highway and Transportation Officials (AASHTO), "Load and resistance factor design (LRFD) bridge design specifications," 3rd edition, AASHTO, Washington, D.C., 2004.

American Association of State Highway and Transportation Officials (AASHTO), "Standard specifications for highway bridges," 17th edition, AASHTO, Washington, D.C., 2002.

Bank, L. C., "Composites for construction: structural design with FRP materials," John Wiley & Sons, Hoboken, NJ, 2006, 560 pp.

Benmokrane, B., El-Salakawy, E., Desgagné, G., and Lackey, T., "FRP bars for bridges," *Concrete International*, V. 26, No. 8, 2004, pp. 84-90.

Benmokrane, B., El-Salakawy, E., El-Ragaby, A., and Lackey, T., "Designing and testing of concrete bridge decks reinforced with glass FRP bars," *Journal of Bridge Engineering*, V. 11, No. 2, 2006, pp. 217-229.

Bradberry, T. E., "Fiber-reinforced-plastic bar reinforced concrete bridge decks," *Proc. 80th Annual Transportation Research Board Meeting*, Jan. 9-13, 2001, Washington, D.C., CD-ROM #01-3247.

Brillouin, L., "Diffusion de la lumière et des rayons X par un corps transparent homogéne - Influence de l'agitation thermique," *Annales de Physique*, V. 17, 1922, pp. 88-122.

Buth, C. E., Williams, W. F., Bligh, R. P., Menges, W. L., and Haug, R. R., "Performance of the TxDOT T202 (MOD) bridge rail reinforced with fiber reinforced polymer bars," *Report FHWA/TX-03/0-4138-3*, Texas Transportation Institute, 2003, 100 pp.

Canadian Standards Association (CSA), "Canadian highway bridge design code," *CAN/CSA-S6-06*, CSA, Mississauga, Ontario, Canada, 2006, 788 pp.

Federal Highway Administration, California Department of Transportation, "Bridge rail guide 2005," FHwA - Caltrans, 2005, 227 pp.

Hirsch, T. J., "Analytical evaluation of Texas bridge rails to contain buses and trucks," *Report FHWA/TX-78/9-230-2*, Texas Transportation Institute, 1978, 92 pp.

Jiang, T., Grzebieta, R. H., and Zhao, X. L., "Predicting impact loads of a car crashing into a concrete roadside safety barrier," *International Journal of Crashworthiness*, V. 9, No. 1, 2004, pp. 45-63.

Katsumata, H., Kobatake, Y., and Takeda, T., "A study on the strengthening with carbon fiber for earthquake-resistant capacity of existing concrete columns," *Proc. Ninth World Conference on Earthquake Engineering (9WCEE)*, August 2-9, 1988, Tokyo – Kyoto, Japan, V. VII, pp. 517-522.

Kaw, A. K., "Mechanics of composite materials," 1st edition, CRC Press, Boca Raton, FL, 1997, 329 pp.

Komatsu, K., Fujihashi, K., and Okutsu, M., "Application of optical sensing technology to the civil engineering field with optical fiber strain measurement device (BOTDR)," *Proc. SPIE*, V. 4920, 2002, pp. 352-361.

Mak, K. K., and Sicking, D. L., "Rollover caused by concrete safety-shaped barrier," *Transportation Research Record*, No. 1258, 1990, pp. 71-81.

Matta, F., and Nanni, A., "Design of concrete railing reinforced with glass fiber reinforced polymer bars," *Proc. 2006 ASCE Structures Congress*, May 18-20, 2006, St. Louis, MO, CD-ROM, 9 pp.

Matta, F., Nanni, A., Galati, N., Ringelstetter, T. E., Bank, L. C., Oliva, M. G., Russell, J. S., Orr, B. M., and Jones, S. N., "Prefabricated modular GFRP reinforcement for accelerated construction of bridge deck and rail system," *Proc. FHWA Accelerated Bridge Construction Conference*, Federal Highway Administration, December 14-16, 2005, San Diego, CA, pp. 129-134.

Matta, F., Nanni, A., Ringelstetter, T. E., and Bank, L. C., "Rapid construction of concrete bridge deck using prefabricated FRP reinforcement," *Proc. Third International Conference on FRP Composites in Civil Engineering (CICE 2006)*, Dec. 13-15, 2006, Miami, FL, USA, pp. 151-154.

Meier, U., "Brückensanierungen mit hochleistungs-faserverbund-werkstoffen (Bridge repair with high performance composite materials)," *Material und Technik*, V. 4, 1987, pp. 125-128.

Missouri Department of Transportation (MoDOT), "Bridge design manual," MoDOT, Jefferson City, MO, 2002.

Mufti, A., Banthia, N., Benmokrane, B., Boulfiza, M., and Newhook, J., "Durability of GFRP composite rods," *Concrete International*, V. 29, No. 2, Feb. 2007, pp. 37-42.

Nanni, A., "North American design guidelines for concrete reinforcement and strengthening using FRP: principles, applications and unresolved issues," *Construction and Building Materials*, Vol. 17, No. 6-7, 2003, pp. 439-446.

Nanni, A., "CFRP strengthening – New technology becomes mainstream," *Concrete International*, V. 19, No. 6, 1997, pp. 19-23.

Nanni, A., "Innovation in structural engineering: strengthening with composites and in-situ load testing," *Proc. 2nd fib Congress*, Naples, Italy, June 5-8, 2006, 12 pp.

Nanni, A., and Faza, S., "Designing and constructing with FRP bars: an emerging technology," *Concrete International*, V. 24, No. 11, 2002, pp. 53-58.

Phelan, R. S., Vann, W. P., and Bice, J., "FRP reinforcing bars in bridge decks – Field instrumentation and short-term monitoring," *Report FHWA/TX-06/9-1520-4*, Texas Tech University, Aug. 2003, 51 pp.

Polivka, K. A., Faller, R. K., Rohde, J. R., Reid, J. D., Sicking, D. L., and Holloway, J. C., "Safety performance evaluation of the Nebraska Open Bridge Rail on an inverted tee bridge deck," *Report TRP-03-133-04*, Midwest Roadside Safety Facility (MwRSF), University of Nebraska-Lincoln, Jan. 2004, 94 pp.

Ringelstetter, T. E., Bank, L. C., Oliva, M. G., Russell, J. S., Matta, F., and Nanni, A., "Cost-effective, structural stay-in-place formwork system of fiber-reinforced polymer for accelerated and durable bridge deck construction," *Transportation Research Record*, No. 1976, 2006, pp. 183-189.

Ross, H. E., Sicking, D. L., Zimmer, R. A., and Michie, J. D., "Recommended procedures for the safety performance evaluation of highway features," *NCHRP Report 350*, National Academy Press, Washington, D.C., 1993.

Strand7 Pty Ltd., "Using Strand7 – Introduction to the Strand7 finite element analysis system," Strand7 Pty Ltd., Sydney, Australia, 2005, 292 pp.

Teng, J. G., Chen, J. F., Smith, S. T., and Lam, L., "FRP strengthened RC structures," John Wiley & Sons, Chichester, UK, 2002, 266 pp.

VITA

Fabio Matta was born in Vicenza, Italy, on October 27, 1975. In October 2003, he received his M.S. in Civil Engineering, with final grade of 110 out of 110, from the University of Padova, Padova, Italy. He spent the full Academic Year 2002-2003 as a Visiting Student at the Department of Structural Engineering at the University of California, San Diego, USA, to conduct research for his M.S. thesis through an Education Abroad Program scholarship. From November 2003 to February 2004 he conducted research at the Department of Structural and Transportation Engineering at the University of Padova with the support of a scholarship awarded by Metalmeccanica Fracasso, S.p.A.

From March 2004 to June 2004 he was a Visiting Scholar at the Center for Infrastructure Engineering Studies at the University of Missouri-Rolla, USA, where he was appointed Graduate Research Assistant in August 2004. From October 2006 to May 2007 he was a Visiting Researcher at the NSF Industry/University CRC "Repair of Buildings and Bridges with Composites" at the University of Miami, Florida, USA, with the support of three scholarships awarded by the National University Transportation Center on Advanced Materials and Non-destructive Testing Technologies. In August 2007, he received his Ph.D. in Civil Engineering from the University of Missouri-Rolla.

He has published conference and archival journal papers, research reports to sponsors, and trade magazine articles, focusing on the use of advanced materials for bridge construction, rehabilitation of metallic and reinforced concrete structures, and on structural health monitoring. As part of his Ph.D. work, he led a team with partners from academia, industry, practice, and local administrations, in the design and accelerated construction of an FRP reinforced concrete bridge, and was recognized as runner-up for the 2006 ASCE/CERF Pankow Award for Innovation, and finalist for the 2006 CIF NOVA Award for Outstanding Innovation in Construction. He is a member of the American Concrete Institute (ACI), the American Society of Civil Engineers (ASCE), Engineers Without Borders (EWB-USA), the International Concrete Repair Institute (ICRI), and the Society for the Advancement of Materials and Process Engineering (SAMPE). He serves as an Associate Member on the ACI Committee 440, Fiber Reinforced Polymer Reinforcement. He is a certified Professional Engineer in Italy.